AD_____

Award Number: W81XWH-12-1-0517

TITLE: The role of NG2 glial cells in ALS pathogenesis

PRINCIPAL INVESTIGATOR: Jeffrey D. Rothstein MD, PhD

CONTRACTING ORGANIZATION: Johns Hopkins University,
Baltimore, MD 21205

REPORT DATE: October 2013

TYPE OF REPORT: Annual

PREPARED FOR: U.S. Army Medical Research and Materiel Command
Fort Detrick, Maryland 21702-5012

REPORT DOCUMENTATION PAGE

Form Approved
OMB No. 0704-0188

1. REPORT DATE	2. REPORT TYPE	3. DATES COVERED
October 2013	Annual Report	30 September 2012-29 September 2013

4. TITLE AND SUBTITLE
The role of NG2 glial cells in ALS pathogenesis

5a. CONTRACT NUMBER

5b. GRANT NUMBER
W81XWH-12-1-0517

5c. PROGRAM ELEMENT NUMBER

6. AUTHOR(S)
Jeffrey D. Rothstein MD, PhD
Betty Diamond

E-Mail: jrothstein@jhmi.edu

5d. PROJECT NUMBER

5e. TASK NUMBER

5f. WORK UNIT NUMBER

7. PERFORMING ORGANIZATION NAME(S) AND ADDRESS(ES)
Johns Hopkins University,
Baltimore, MD 21205

8. PERFORMING ORGANIZATION REPORT NUMBER

9. SPONSORING / MONITORING AGENCY NAME(S) AND ADDRESS(ES)
U.S. Army Medical Research and Materiel Command
Fort Detrick, Maryland 21702-5012

10. SPONSOR/MONITOR'S ACRONYM(S)

11. SPONSOR/MONITOR'S REPORT NUMBER(S)

12. DISTRIBUTION / AVAILABILITY STATEMENT
Approved for Public Release; Distribution Unlimited

13. SUPPLEMENTARY NOTES

14. ABSTRACT

A growing body of evidence suggests that glial cells are critical for the support of normal neuronal function, and in particular astrocyte and oligodendroglial dysfunction may contribute to a number of neurodegenerative diseases, including ALS. One important function of glial cells is to transport nutrients from capillaries to neurons. Much of the nutritional support is in the form of glucose; however our lab and others have provided strong evidence that lactate support from *oligodendrocytes* via monocarboxylate transporters (MCTs) is a major contributor to neuronal metabolism and survival in vivo. Preliminary data from our laboratory indicates that genetic knockdown or pharmacological inhibition of glial specific monocarboxylate transporter 1 (MCT1) leads to loss of spinal cord motor neurons in vitro and in vivo. In addition, our lab and others recently showed in SOD1 mutant mice NG2+ cells, the progenitor cells for oligodendrocytes, upregulate NG2 and show enhanced proliferation in the ventral horn gray matter where motor neurons die. In addition, NG2+ cells formed large numbers of newly generated immature, non-myelinating oligodendroglia, but no astrocytes or neurons. Finally, when we specifically protected oligodendrocyte injury in the SOD1 animal model by deleting mutant SOD1 in NG2+ cells, we were able to delay disease onset by >126 days- many months longer than any other genetic ablation approach to date. We hypothesize that NG2 glial cells play a significant role in ALS pathogenesis. In particular, we are testing how human NG2 glial cells derived from ALS patient iPS cells will impact human motor neurons, also derived from human iPS cells.

15. SUBJECT TERMS
ALS, NG2 cell, myelin, therapy, oligodendroglia

16. SECURITY CLASSIFICATION OF:			17. LIMITATION OF ABSTRACT	18. NUMBER OF PAGES	19a. NAME OF RESPONSIBLE PERSON
a. REPORT	b. ABSTRACT	c. THIS PAGE			USAMRMC
U	U	U	UU	38	19b. TELEPHONE NUMBER *(include area code)*

Table of Contents

The role of human ALS iPSC-derived NG2 glia on human motor neuron survival: Strong implication of NG2 glia in ALS pathogenesis

Jeffrey D. Rothstein MD. PhD, Johns Hopkins University

Specific Aim 1: Differentiation and characterization of NG2 glia derived from ALS patient-specific iPS cells with A4V SOD1 mutation.

1. Differentiation of ALS-iPS cells to NG2+ glial cells.

To differentiate the Control-iPS and A4V-iPS cells to NG2+ glial cells (oligodendeocyte progenitor cells, OPCs), they were first differentiated to neural progenitor cells (NPCs) by using two protocols. The first one used was the most established protocol, via embryoid body (EB) formation, and the efficiency of rosettes/neural tube formation was compared between control and A4V-iPS cells. For these studies, two lines of control iPS cells, and 2 lines of A4V-iPS cells and one A4V-carrier line were used. The cells generated rosettes/neural tube structures which expressed NPC markers (Figure 1A), Pax6 and Sox1. There was no significant difference in the efficiency of neural tube formation (Figure 1B). As recent studies showed that inhibition of SMAD pathway enhances NPC induction, we used this method to increase and enhance NPC generation. After about 12 days of neural induction in the presence of BMP and TGFβ pathway inhibitors, LDB and SB, high efficiency of NPC generation was observed from both control and A4V iPS cell lines. No differences in NPC differentiation efficiency was seen between control and A4V lines (Figure 1C and 1D). As immunocytochemistry did not show differences in NPC differentiation efficiency using two protocols, qPCR was not performed to determine neural progenitor marker expression at mRNA level.

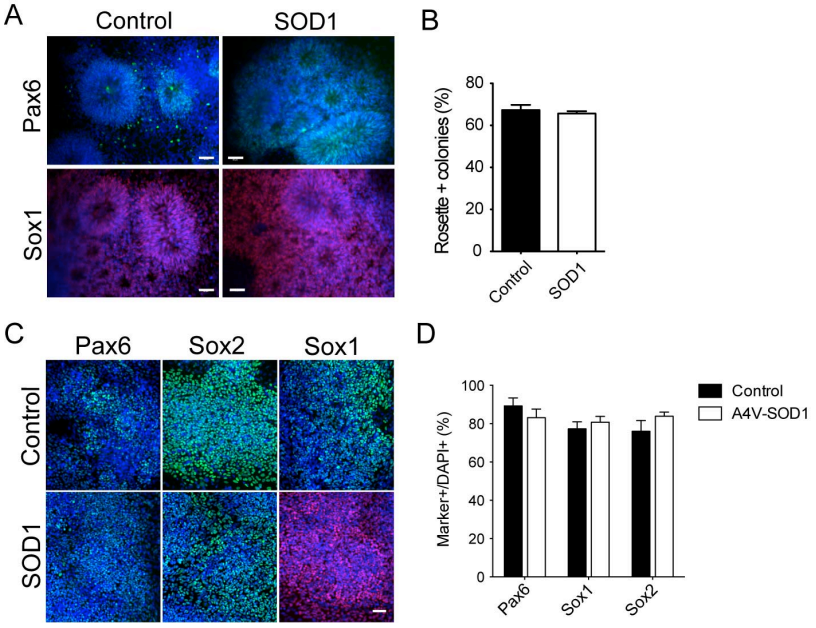

Figure 1. Neural progenitor cell differentiation from control and A4V-iPS cells. (A & B) NPCs were induced via EB formation. EB were cultured for 5 days and then attached for neural induction. After 10-12 days, rosettes and neural tubes were generated. Cells were stained for Pax6 and Sox1 expression. The differentiation efficiency was defined as rosettes/neural tube+ colonies out of total colonies. (C&D) NPCs were induced by inhibition of SMAD pathways. The iPS cells were treated with LDN and SB for 7 days, and induced for NPC generation. After 12 days of induction, most cells expressed NPC marker, Pax6, Sox1 and Sox2. No differences in NPC differentiation efficiency (NPC marker+/total cell) was observed. Size bar, 50um.

To generate NG2+ glial cells (OPCs), NPCs were further differentiated to pre-OPCs and OPCs, outlined in Figure 2, which showed reliable cell morphology and cell marker expression. Pre-OPCs were determined by their expression of Olig2 and NKX2.2 (Figure 3). The majority of colonies showed Olig2+, NKX2.2+, and Olig2+/NKX2.2+ cells, however the percentage of each marker expression varied among colonies.

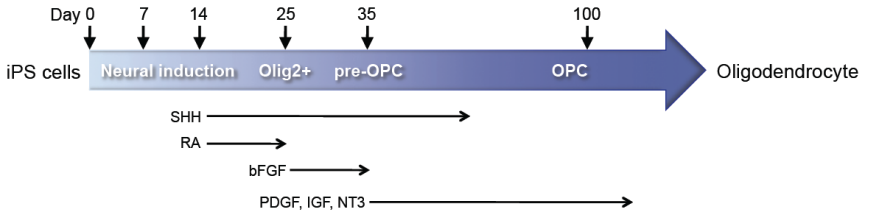

Figure 2. Time line of OPC differentiation from iPS cells. SHH, sonic hedgehog; RA, retinoitic acid; bFGF, basic FGF; PDGF, platelet-derived growth factor; IGF, insulin-like growth factor; NT2, neurotrophin 3.

To further differentiate pre-OPCs to OPCs, the spheres were cultured in the presence of PDGF, IGF and NT3. This is the most time consuming step, which takes at least 2 months. After about 120d differentiation, spheres were attached and cells migrated out from the spheres. Some had typical OPC morphology (figure 4A), bipolar and tripolar. More importantly, they expressed NG2, Olig2 and PDGFaR (figure 4B), all the OPC markers, indicating they are authentic OPCs.

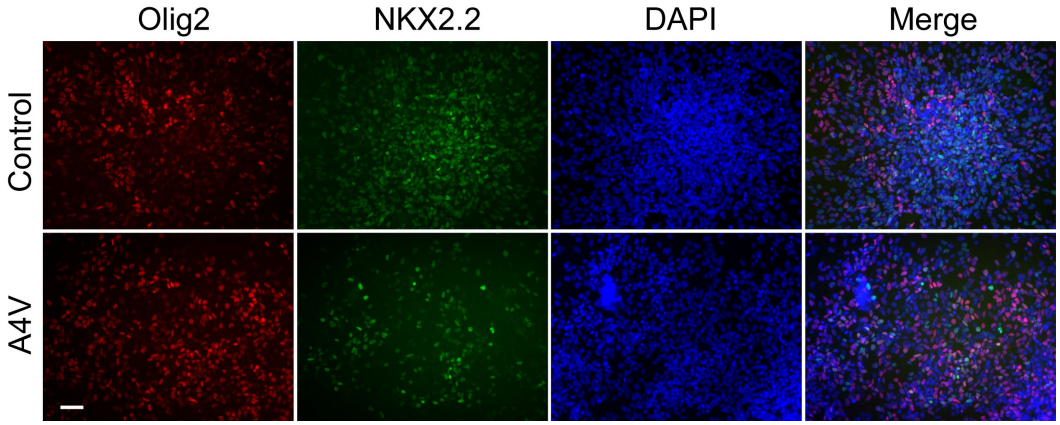

Figure 3. Pre-OPC generation by control and A4V-iPS cells. Spheres were attached around d35 and stained for marker expression 2-3 days later. Both control and A4V lines showed Olig2+/NKX2.2-, Olig2-/NKX2.2+, and Olig2+/NKX2.2+ cells. The positive cell number varies between colonies. Representative picutres were from 018 Control line and 013 A4V-line. Size bar, 50um.

2. Characterization of NG2+ glial cells.

To further characterize NG2+ glial cells, we first purified the cells using FACS. We took advantage of their cell membrane expression of PDGFaR, and labeled the cells with PE conjugated anti-CD140a (anti-PDGFaR), then sorted the cells (Figure 5A). The sorted cells showed NG2 and Olig2 expression (Figure 5B) after being cultured. After being treated with T3, some cells changed their bipolar and tripolar morphology to multiple process-bearing cells. These cells started to show O4 expression (Figure 5C and 5D). Slowly, the O4+ cells started to express the mature oligodendrocyte marker, MBP (Figure 5D). After at least about one month, there were some MBP+ oligodendrocytes with multiple processes and membranous structures (Figure 5E & 5F).

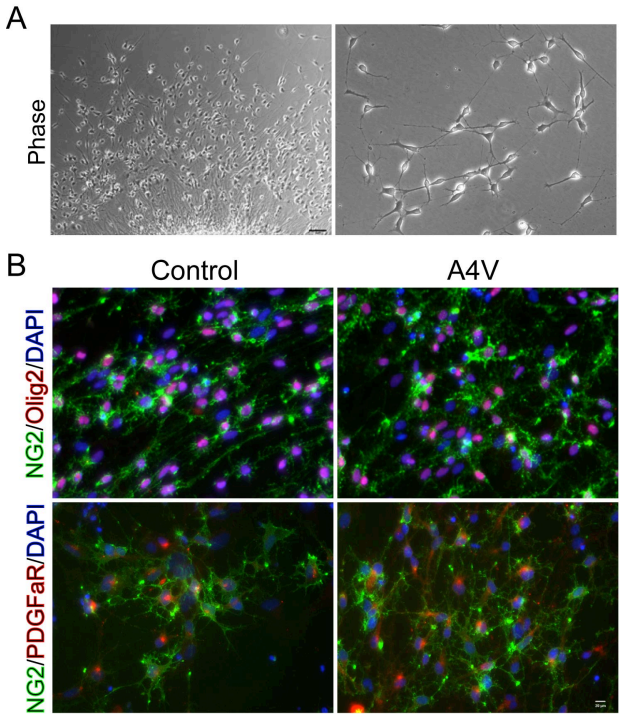

Figure 4. OPC differentiation from control and A4V-iPS cells. After about differentiation d120, oligospheres were attached and allowed the cells migrate out. (A) Some cells showed bipolar and tripolar morphology. (B) Immunocytochemistry analysis of OPC marker expression. The libe cells were stained for NG2 (green) expression, and then the cells were fixed and permeablized, followed by Olig2 (red) or PDGFaR (red) staining. Nuclei were stained with DAPI. Note the colocalization of NG2 and Olig2, or NG2 and PDGFaR.

To determine whether $SOD1^{A4V}$ expression affect OPC gene expression, we did gene profiling analysis using Human Exon 1.0 ST Array (Affymetrix). As shown in Figure 6, principle component analysis showed that $SOD1^{A4V}$ expression probably interferes with gene expression based on PC1. In addition, A4V-patients and A4V-carriers may also have different gene expression profiles as suggested by PC2 analysis. However, more biological and technical repeats are needed to make final conclusions.

Currently, we carrying out additional oligodendrocyte differentiations of A4V-carriers, A4V-patients iPS cells, and we are going to increase biological and technical repeats to for the gene profiling study. The FACSoring purified OPCs will be also used further in proliferation and differentiation analysis in the presence and absence of human neurons.

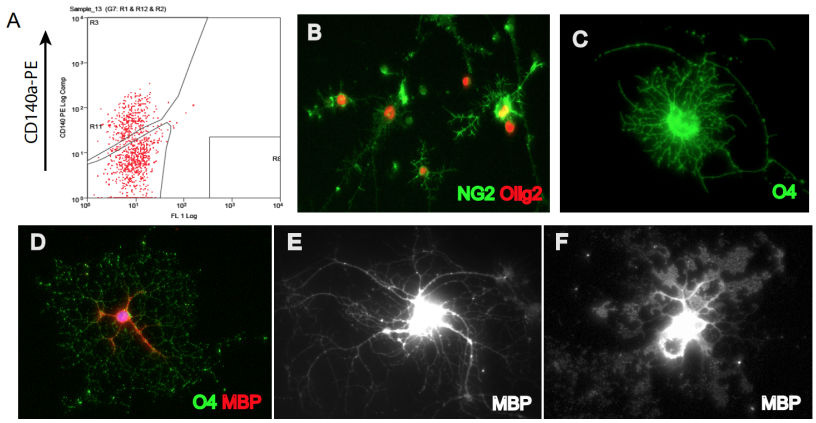

Figure 5. Differentiation of FACSed OPCs to mature oligodendrocytes. (A) OPCs were FACSed by their expression of PDGFaR (CD140a). (B) Sorted OPCs were cultured and expressed NG2 and Olig2. (C & D) O4 (green) expression by pre-oligodendrocytes differentiated from sorted OPCs. (D, E &F) mature MBP+ oligodendrocytes were differentiated from FACSed OPCs.

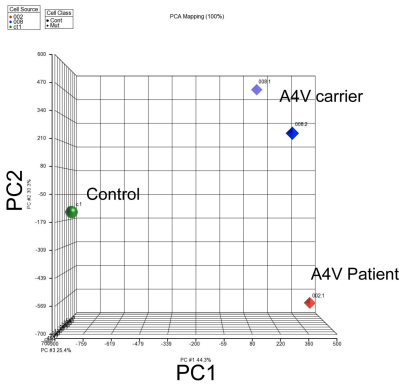

Figure 6. Principle component analysis on human OPCs. Control, A4V carrier and A4V patient specific OPCs were differentiated and purified by FACS based on their cell membrane expression of PDGFaR. Human exon array analysis was performed to compare their gene expression. Principle component analysis showed that A4V-carrier (blue, duplicate) and A4V patient (red) were separated from the healthy control (green) based on PC1.

Specific Aim 2: Effects of NG2 cells with A4V SOD1 mutation on the survival of human motor neurons derived from patient-specific iPS cells.

1. *Differentiation and purification of motor neurons.*

To differentiate control and A4V-11SOD1 iPSCs to motor neurons, the cells were differentiated to NPCs first and then to motor neuron. Motor neurons were defined by their expression of Hb9 or Islet1/2 (figure 7).

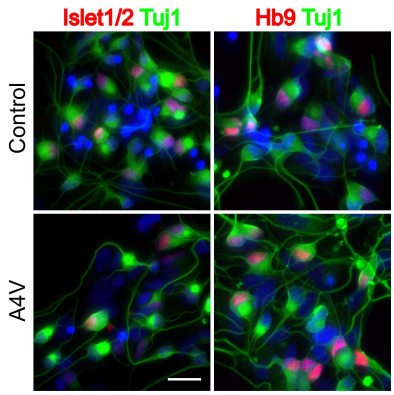

Figure 7. Motor neuron differentiation from A4V-iPS cells. Neural progenitor cells was induced in the presence of inhibition of SMAD pathway, followed by motor neuron differentiation. At differentiation day 32, Tuj1+ (green) neurons expressed motor neuron markers Hb9 (red) and Islet 1 (red). Size bar, 20um.

Given that during differentiation, neural progenitor or neuronal progenitors can give rise to new motor neurons. It is known that Hb9 expression is down regulated when motor neurons reach certain maturity. Therefore, it is necessary to use purified motor neurons in the coculture to limit the effects from newborn neurons or avoid the possible over estimation of neurotoxic effects due to the down regulation of Hb9. As shown in figure 7, differentiated motor neurons at differentiation day 32 expressed Islet1/2 and Hb9. To purify motor neurons, we took advantage of the expression of Hb9 by motor neurons during their development/genesis and transduce the cells with Lentivirus encoding Hb9-RFP as shown in published literature. Three days after transduction, some cells started to express RFP as determined under the fluorescence microscope. More RFP+ cells were observed after a few more days. After about 5 days of transduction, not only neuron-like cells (with neuron morphology), but also some cells with flat morphology showed RFP expression. Given that the size of many flat cells are larger than that of neurons, during FACSorting, we separated those RFP+ cells to two populations based on their relative cell size. This is majorly based on the side scatter, the granule contents inside the cells, which still cannot separate them exclusively. Further culture of sorted RFP+

cells showed that all of them had RFP expression (figure 8 B and C). Big size cell population consisted mainly of non-neuron cells without Hb9 expression. In contrast, small size cell population consisted of neurons expressing Tuj1 (figure 8B), but also small percentage (lower than 10%) of flat cells without neuron morphology. In addition, not all of the Tuj1+ neurons expressed Hb9. It is possible that the motor neurons were more maturing and turned Hb9 expression down, or the promoter is leaky. Although FACSed RFP+ small size cells are not pure motor neurons, this still can give enriched motor neurons for down stream experiments.

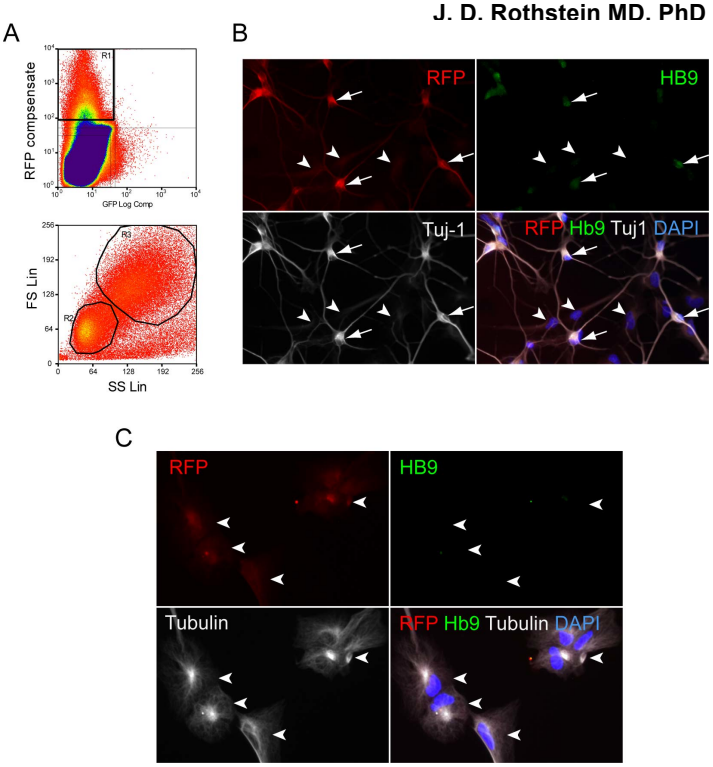

Figure 8. Purification of human motor neurons. To purify motor neurons, mixed neurons derived from iPS cells were transduced using Hb9-RFP Lentivirus. RFP+ cells were FACSed 5 days after transduction and cultured for another 3 days before immunocytochemistry staining. (A) FACSorting of RFP+ cells. RFP+ cells (upper panel) were separated into two populations based their size (lower panel). (B) Small size RFP+ cell population culture. All the cells expressed RFP+ neurons with Tuj1 expression (white), while not all the cells had Hb9 expression (green). (C) Large size RFP+ cell population culture. The majority of the large size cells had flat morphology and had tubulin expression. None of these cells expressed Hb9. Nuclei were stained with DAPI.

2. Co-culture of human oligospheres and human mixed neurons.

Given unexpected encountered limitations of motor neuron purification, further optimization of motor neuron purification will be performed. In the mean time, we explored whether human OPCs expressing $SOD1^{A4V}$ are toxic to human neurons by co-culture of oligospheres and neurons. Interestingly, after about 3 weeks of coculture, more beaded axons were seen in the coculture with $SOD1^{A4V}$ oligospheres compared to those with control oligospheres or neuron culture alone (figure 9). It has been reported that expressing of mutant SOD1, even wild type SOD1, by astrocytes is toxic to mouse motor neurons. Therefore, further analyses will be carried out using FACS purified human NG2+ glia and enriched human motor neurons.

In the coculture of human oligospheres and human neurons, OPCs have been observed to migrate out from the spheres as seen in seeded oligosphere cultures in the absence of neurons. In the presence of neurons, oligodendrocytes were differentiated as indicated by their expression of MBP and they interacted with axons (figure 10). This very preliminary study suggested that human oligodendrocyte can myelinate human neuron axons in the dish, although the efficiency was not high. Further analyses will be performed/repeated by using enriched motor neurons and purified OPCs to study human OPC proliferation and differentiation.

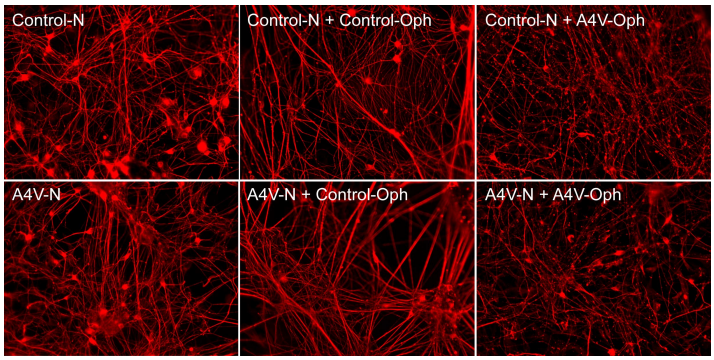

Figure 9. Axon degeneration in cocultures of human oligospheres and human neurons. Human Oligospheres were cocultured with human mixed neurons for about three weeks. Neurons were labeled by their expression of Tuj1 (red). Note beaded axons in the coculture with $SOD1^{A4V}$ oligospheres.

3. *Co-culture of mouse OPCs overexpressing SOD1^{G93A} and human neurons.*

3.1 Overexpression of SOD1^{G93A} in mouse OPCs enhanced OL differentiation, but has no effects on OPC proliferation and cell death during oligodendrocyte differentiation, in the absence of neurons.

As differentiation of human OPCs from control and A4V-iPSCs takes a long time (longer than 4 months) and there are many factors/culture conditions that need to be optimized, in the mean time, we evaluated mouse NG2 glia cells over-expressing G93A human SOD1 alone or in the presence of human neurons with and without A4V mutation. The reasons to use mouse G93A-NG2 cells are: 1) highly pure NG2 glia can be isolated from NG2-DsRed animals using FACS, and 2) the cells differentiate to mature oligodendrocytes (OLs) in a short time (5-6 days in the presence of T3).

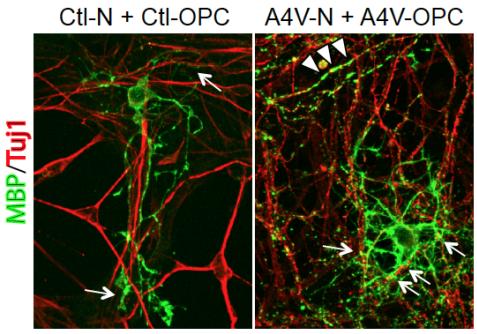

Figure 10. co-culture of human oligodendrocytes and human neurons. Human oligospheres were cocultured with human neurons. After 3 weeks of coculture, MBP (green) and Tuj1 (red) expression were determined by immunofluorescence staining. Arrows indicate the interaction of oligodendrocyte processes with axons. Arrowheads indicate possible myelination.

To evaluate whether the overexpression of SOD1^{G93A} has effects on NG glia proliferation, differentiation and cell death during differentiation, EdU incorporation assay, efficiency of OL differentiation in the presence of T3, and TUNEL assay were performed respectively. No significant differences were observed in proliferation after a short pulse of EdU (Figure 10) and cell death during OL differentiation (figure 11) between WT-NG2 and G93A-NG2 based on three independent experiments respectively. However, the presence of G93A-SOD1 slightly, but significantly enhanced OL differentiation (Figure 12). No differences in OL morphology have been seen between WT-OL and G93A-OL (Figure 12). In addition, under unstressed condition, no ubiquitin+ aggregates were observed in G93A overexpressing cells. Furthermore, to further evaluate whether overexpression of G93A SOD1 on OPC and oligodendrocyte survival under stressed conditions, the cells were treated with H2O2, but no differences of cell death between WT and SOD1 were observed (data not shown).

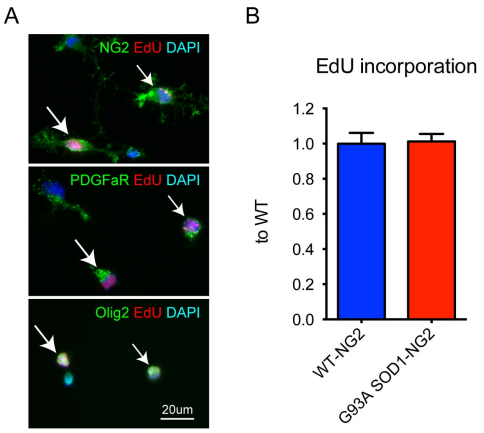

Figure 11. Overexpression of G93A SOD1 by mouse OPCs had no effects on cell proliferation. FACSed mouse NG2-DsRed cells were pulse traced with EdU for three hours and then Click-iT assay was used to determine EdU incorporation. (A) OPCs expressing NG2, PDGFaR or Olig2 (all in green) had EdU incorporation (red, arrows). Nuclei were stained with DAPI. (B) Quantification of EdU+ cells. EdU+ cells were by counted and divided by the total DAPI+ cells. Data was normalized to WT control. No differences in EdU incorporation have been seen between WT and G93A expressing OPCs ($P>0.05$, student t test).

3.2 Overexpression of G93A SOD1 enhances mouse oligodendrocyte differentiation, and possibly induce oligodendrocyte death in the presence of human neurons.

As overexpression of G93A SOD1 apparently enhanced NG2 glia differentiation to oligodendrocytes in the absence of neurons, we next asked whether the presence of neurons +/- mutant SOD1 affect mouse SOD1^{G93A} NG2 differentiation. To do that, sorted NG2 glia with and without G93A SOD1 were co-cultured with human neurons derived from iPSCs with and without A4V-SOD1, and then the cells were treated with T3. After 5-6 day differentiation, mature OLs were determined by their expression of MBP, and neurons were determined by Tuj1 expression. MBP+ mature OLs were generated in all co-cultures, while the staining intensity was much higher in the co-cultures with either SOD1-NG2 or A4V-neurons (Figure 13A). All four groups had punctate MBP+ cells, however, in the co-cultures with G93A SOD1-NG2 glia the number of punctate MBP+ OLs was significant higher (Figure 13B). Interestingly, some punctate MBP+ cells had condensed nuclear staining, indicating they are dying/dead cells (Figure 13C). These data strongly suggest that neurons with mutant SOD1 enhance SOD1-NG2 glia differentiation to OLs, and these cells probably die after they differentiated.

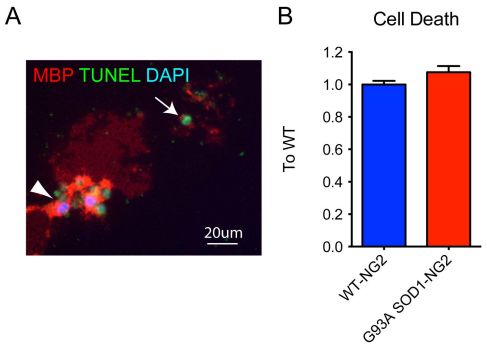

Figure 12. Overexpression of G93A SOD1 in mouse oligodendrocytes did not cause cell death during oligodendrocyte differentiation. (A) FACSed NG2-DsRed OPCs were differentiated to mature oligodendrocytes (MBP+) by T3 treatment. TUNEL assay was used to determine cell death after 5 day differentiation (dead cells are shown in green). (B) Quantification of dead cells. TUNEL+ cells were counted and divided by DAPI+ cells. Data was normalized to WT. (P>0.05, student t test)

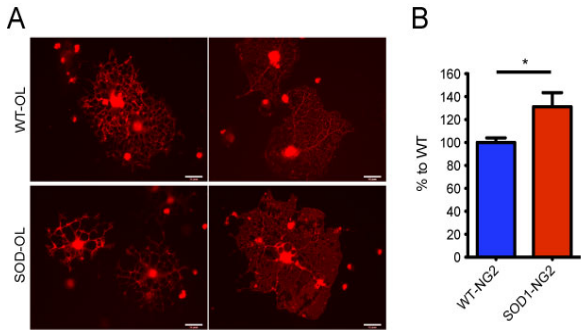

Figure 13. Overexpression of G93A SOD1 in mouse NG2 glia enhances oligodendrocyte differentiation. FACSed NG2-DsRed differentiated to oligodendrocytes in the presence of T3. (A) Mature OLs were determined by MBP expression (red). No obvious morphological differences in MBP+ cells have been noticed between the two groups. (B) Cell counting showed more MBP+ OLs were generated by G93A SOD1-NG2 cells (P<0.05, three independent experiments).

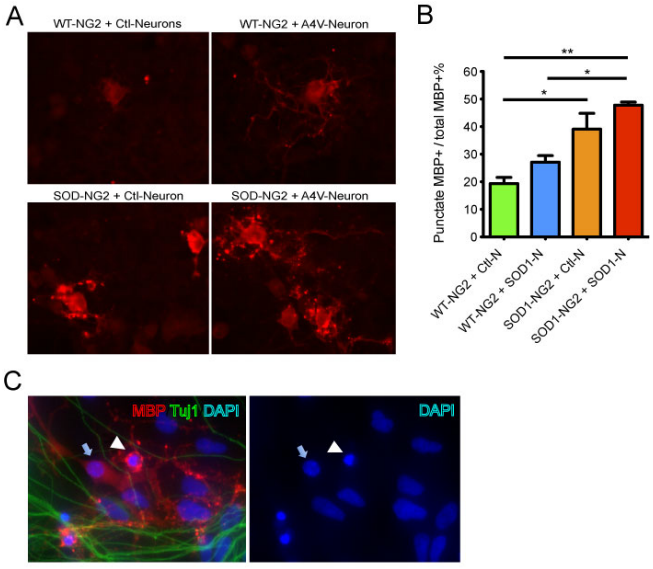

Figure 14. Expression of mutant SOD1 in NG2 glia enhances OL differentiation and cell death in the presence of neurons with mutant SOD1. (A) Co-culture of NG2 glia with and without G93A SOD1 and human neurons derived from iPSCs with and without A4V-SOD1. MBP+ (red) OLs were generated in all co-cultures and some cells showed punctate MBP staining. (B) Cell counting shows more punctate MBP+ cells have been generated in the co-culture with G93A SOD1-NG2 with control (Ctl-N) (P<0.05) and A4V-neurons (SOD-N) (P<0.01). (C) A representative picture shows a punctate MBP+ OL with a condensed nucleus (DAPI, blue, arrowhead), indicating it is a dying/dead cell. The other MBP+ cells next to the punctate one had smooth MBP staining and nice nuclear staining (arrow).

3.3 Overexpression of G93A SOD1 affects Wnt and Notch signaling pathways during mouse oligodendrocyte differentiation in the presence of neurons.

As it is known that Notch and Wnt signaling pathways play a role during oligodendrocyte differentiation and overexpression of G93A SOD1 enhanced oligodendrocyte differentiation in the presence of

neurons, we then determined whether these two pathways were interfered in differentiating oligodendrocytes expressing G93A SOD1. Mouse specific Notch and Wnt PCR array analyses were performed using the cross species co-cultures. Our very preliminary study showed that indeed oligodendrocytes with overexpression of G93A SOD1 had different gene expression profiles compared to WT no matter if they were cocultured with control or A4V-neurons (figure 14). This study suggests that overexpression of G93A SOD1 probably interferes with oligodendrocyte differentiation.

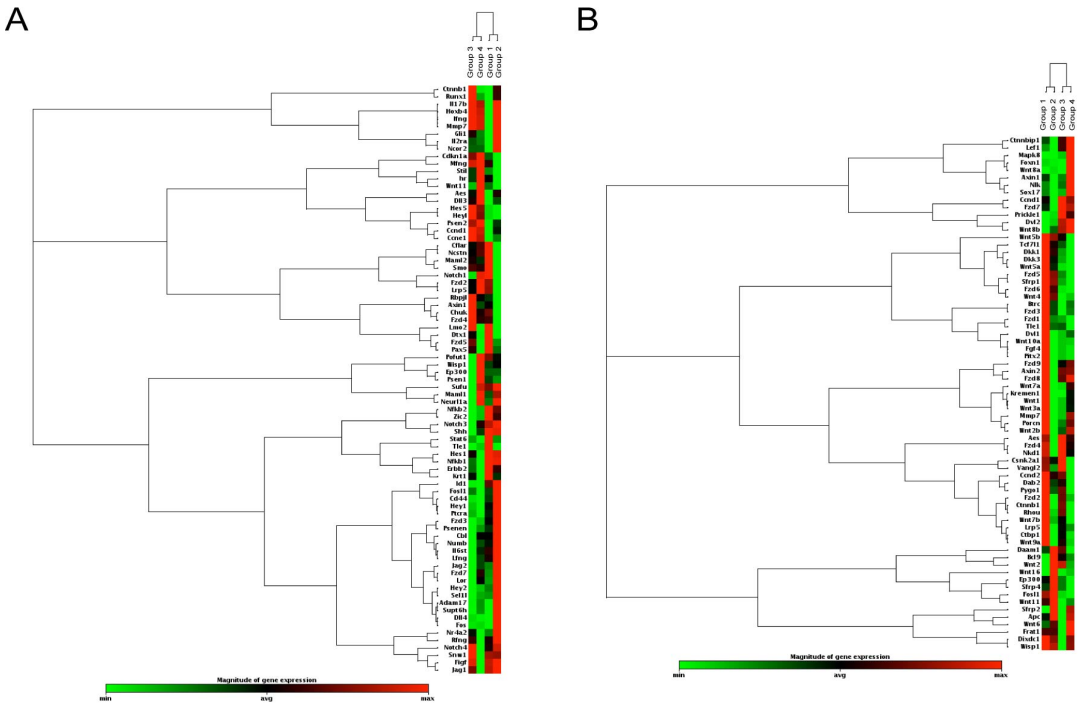

Figure 15. PCR array analyses on mouse Notch and Wnt signaling pathway. (A) Notch signaling pathway. (B) Wnt signaling pathway.

3.4 Does mouse oligodendrocyte overexpressing G93A induce human neuron death?

To evaluate the effects of NG2 glia with and without mutant SOD1 on the survival of motor neurons with and without A4V mutation, Hb9+ cells were counted in the co-cultures. No significant differences have been seen in one experiment (Figure 7). However, it is hard to make the conclusion that NG2 glia with and without mutant SOD1 have no or less effects on motor neuron survival because, 1) newborn motor neurons/neurons exist in the culture, 2) It is not clear whether A4V SOD1 has effects on motor neuron differentiation/survival in the absence of NG2 glia. In addition, the co-cultures consist of not only motor neurons, but also other types of neurons, neuronal progenitors and neural progenitors, therefore we cannot exclude their effects in the study.

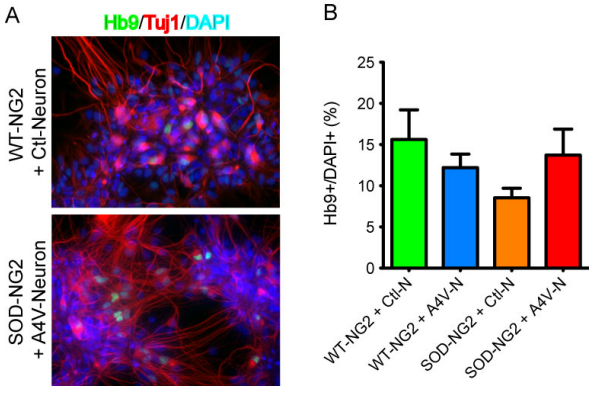

Figure 16. Motor neuron counts were not changed in the co-cultures of NG2 glia and neurons with and without mutant SOD1. (A) Mouse NG2 glia with and without G93A SOD1 were co-cultured with human control and A4V-neurons. Neurons and motor neurons were determined by the expression of Tuj1 (red) and Hb9 (green) after 5 days. Nuclei were stained with DAPI. (B) No significant differences in motor neuron numbers have been observed between each group (One-way ANOVA) in this experiment.

Progress towards on planned Milestones:

We achieved planned progress on all our orginal milestones for Year 1:

- Differentiate NG2+ glial cells and oligodendrocytes from human iPS cells: ***COMPLETED***
- Characterize the differentiated cells at different stages of differentiation (immuno and RT-PCR): ***COMPLETED***
- Perform gene array analysis on differentiated NG2+ cells and oligodendrocytes: ***COMPLETED***

Key Research Accomplishments:

1. First successful differentiation of control and ALS mutant SOD1 iPS cells to NG2+ cells
2. First characterization of human ALS NG+/OPC iPS cells:
    a. Differentiation of OPC to mature oligodendroglial form ALS and control iPS cell
    b. First gene profile of ALS mutant SOD1 OPC iPS cells
3. First analysis of ALS NG2+ cell effet con the survival of cultured human motor neurons.
    a. First description of degeneration of motor neurons in the presence of mutant human OPC cells

Reportable Outcomes

1. Creation of ALS NG2 and oligodendroglial iPS cell

2. Discovery that human ALS oligodendroglial lead to degeneration of motor neurons

3. First model system to study human ALS oligodendroglia for both pathophysiology and drugs target screening

Conclusion:

Human ALS oligodendroglia appear to cause the axon degeneration of human ALS motor neurons , invitor. This proves the studies published this year (Kang et al, Nat. Neuroscience 2013) derived form the ALS mouse model and from human post mortem tissue are correct—oligodendroglial appear to be actively causing ALS cell death.

References (Relevant publications toward Aim Progress):

None

Appendix: Relevant published articles:

1. Lee, Y., B. M. Morrison, et al. (2012). "Oligodendroglia metabolically support axons and contribute to neurodegeneration." **Nature 487**(7408): 443-448

2. Kang SH, Li Y, Fukaya M, Lorenzini I, Cleveland DW, Ostrow LW, Rothstein JD, Bergles DE. Degeneration and impaired regeneration of gray matter oligodendrocytes in amyotrophic lateral sclerosis. **Nat Neurosci**. 2013;16(5):571-9.

3. Morrison BM, Lee Y, Rothstein JD. Oligodendroglia: metabolic supporters of axons. **Trends Cell Biol**. 2013.

ARTICLE

doi:10.1038/nature11314

Oligodendroglia metabolically support axons and contribute to neurodegeneration

Youngjin Lee[1]*, Brett M. Morrison[1]*, Yun Li[1], Sylvain Lengacher[2], Mohamed H. Farah[1], Paul N. Hoffman[1], Yiting Liu[1], Akivaga Tsingalia[1], Lin Jin[1], Ping-Wu Zhang[1], Luc Pellerin[3], Pierre J. Magistretti[2] & Jeffrey D. Rothstein[1,4,5]

Oligodendroglia support axon survival and function through mechanisms independent of myelination, and their dysfunction leads to axon degeneration in several diseases. The cause of this degeneration has not been determined, but lack of energy metabolites such as glucose or lactate has been proposed. Lactate is transported exclusively by monocarboxylate transporters, and changes to these transporters alter lactate production and use. Here we show that the most abundant lactate transporter in the central nervous system, monocarboxylate transporter 1 (MCT1, also known as SLC16A1), is highly enriched within oligodendroglia and that disruption of this transporter produces axon damage and neuron loss in animal and cell culture models. In addition, this same transporter is reduced in patients with, and in mouse models of, amyotrophic lateral sclerosis, suggesting a role for oligodendroglial MCT1 in pathogenesis. The role of oligodendroglia in axon function and neuron survival has been elusive; this study defines a new fundamental mechanism by which oligodendroglia support neurons and axons.

Oligodendroglia promote rapid conduction of action potentials by ensheathing central nervous system (CNS) axons with myelin. Oligodendrocyte diseases, such as multiple sclerosis and leukodystrophies, have demonstrated demyelination and axon degeneration at autopsy[1,2]. Mouse models of oligodendrocyte injury, including proteolipid protein 1 (*Plp1*)-null mice[3] and *Cnp* (also known as *Cnp1* and *CNPase*) mutant mice[4], demonstrate axon loss without considerable demyelination, suggesting that oligodendroglia support axon survival through a myelin-independent mechanism, possibly as a result of insufficient axonal energy support[5]. Myelinated axons are only exposed to extracellular energy substrates at the nodes of Ranvier, and therefore may require specialized transport of energy metabolites from myelinating oligodendroglia to meet their high metabolic needs. The identity of these metabolites is unclear, but our study suggests that lactate may be essential and its transport dependent on MCT1 (Supplementary Fig. 1).

MCT1, along with the transporters MCT2 and MCT4, transport monocarboxylic acids (that is, lactate, pyruvate and ketone bodies), and localize to the CNS[6]. Neurons express MCT2, and glia express both MCT1 and MCT4 (refs 7, 8), although MCT1 is the dominant glial transporter in the brain[9]. Recently, MCT1 was localized to oligodendroglia and MCT2 to axons of the corpus callosum and cerebellar white matter by immunohistochemistry[10]. *In vitro* astrocytes produce lactate through aerobic glycolysis[11,12], and lactate alone can support neurons in the absence of glucose, presumably through MCT2 localized to neurons. This hypothetical energy transfer was termed the astrocyte–neuron lactate shuttle[13]. Support for lactate-based neuronal support has come from both *in vitro* and *in vivo* models[14,15]; however, the physiological role for lactate in the non-stressed, uninjured CNS is largely unknown. We now report that oligodendroglia are an important site of MCT1 expression in the brain and spinal cord and are the principal metabolic supplier of lactate to axons and neurons.

Oligodendroglia injury is well established in demyelinating diseases[16], but the supply of energy metabolites to axons could also be crucial in other neurological diseases. In this study, we investigated amyotrophic lateral sclerosis (ALS), a fatal neurological disease characterized clinically by progressive weakness and pathologically by cortical and spinal motoneuron degeneration. Although the pathogenesis of motoneuron degeneration is unknown, it is mediated partly by surrounding astroglia and microglia[17]. A recent study suggests that grey matter oligodendroglia may be injured in ALS[18], and we propose that reduced expression of MCT1 is one mechanism by which oligodendroglia produce neurotoxicity in ALS.

MCT1 localizes to oligodendroglia *in vivo*

Astrocytes[8,19,20], ependymocytes, endothelial cells[19,21] and recently oligodendroglia[10] have inconsistently been demonstrated to express MCT1. This variability is due to limitations in antibody specificity and/or affinity, along with differences in the species and age of samples analysed. To overcome this technical challenge, we produced two lines of bacterial artificial chromosome (BAC) transgenic mice carrying the tdTomato fluorescent reporter for cellular localization and *in vivo* expression level of *MCT1* messenger RNA in the CNS and peripheral organs (Fig. 1 and Supplementary Figs 2–4). Results are shown for the highest expressing line, although cellular localization was identical for the second line (data not shown). Enrichment of *MCT1* mRNA was found within fluorescence-activated cell sorted (FACS) tdTomato-positive cells (Fig. 1a, group ii), verifying the specificity of the reporter. Expression was similar in perinatal mice, although reporter expression around blood vessels was increased (data not shown). MCT1 BAC mice were crossed with MOBP–eGFP and GLT1–eGFP BAC reporter mice[22], which express enhanced green fluorescent protein (eGFP) driven by the oligodendrocyte-specific myelin-associated oligodendrocyte protein (MOBP) and astrocyte-specific glutamate transporter 1 (GLT1, also known as

[1]Department of Neurology, The Johns Hopkins University, 855 North Wolfe Street, Rangos 248, Baltimore, Maryland 21205, USA. [2]School of Life Sciences, Brain Mind Institute, Ecole Polytechnique Federale de Lausanne (EPFL), Station 19, CH-1015 Lausanne, Switzerland. [3]Department of Physiology, University of Lausanne, 7 Rue du Bugnon, CH-1005 Lausanne, Switzerland. [4]Department of Neuroscience, The Johns Hopkins University, 855 North Wolfe Street, Rangos 270, Baltimore, Maryland 21205, USA. [5]The Brain Science Institute, The Johns Hopkins University, 855 North Wolfe Street, Rangos 270, Baltimore, Maryland 21205, USA.
*These authors contributed equally to this work.

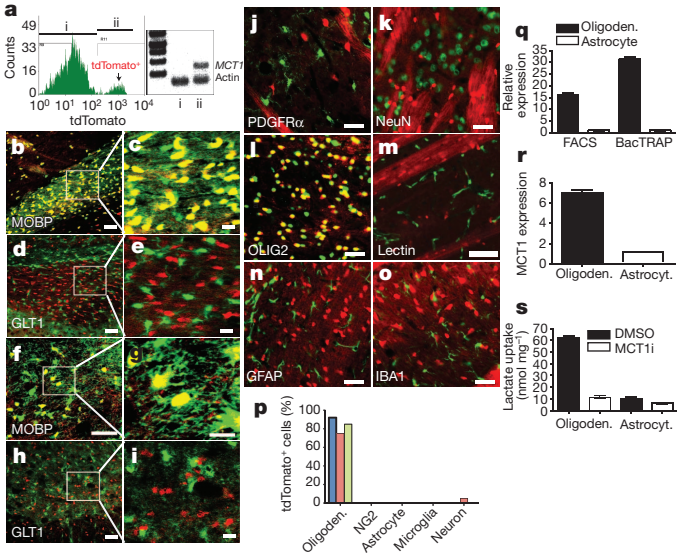

Figure 1 | MCT1 expressed primarily within oligodendroglia in the CNS. **a**, Histogram and rtPCR for *MCT1* mRNA from FACS-sorted cells with (ii) or without (i) tdTomato expression. **b**–**e**, Corpus callosum of MCT1–tdTomato reporter mice crossed with MOBP–eGFP (**b**, **c**) or GLT1–eGFP (**d**, **e**) BAC mice. **f**–**i**, Spinal cord of MCT1– tdTomato reporter mice crossed with MOBP–eGFP (**f**, **g**) or GLT1–eGFP (**h**, **i**) BAC mice. Scale bars, 50 μm (low power, left) and 14 μm (high power, right). **j**–**o**, MCT1–tdTomato reporter mouse brain immunostained with cell-specific markers. Scale bars, 12.5 μm (except 50 μm for lectin). **p**, Percentage of tdTomato cells co-labelled with CNS cell markers in the spinal cord (blue), cortex (red) and corpus callosum (green). **q**, **r**, rtPCR of *MCT1* mRNA isolated from oligodendroglia and astroglia by FACS and BacTRAP techniques (**q**) and human oligodendroglioma (M03.13) and astrocytoma (U87) cell lines (**r**; means of four replicates). **s**, Lactate transport and blockade by selective MCT1 inhibitor (MCT1i) in oligodendroglioma and astrocytoma ($n = 4$). DMSO, dimethylsulphoxide. Error bars denote s.e.m.

SLC1A2), respectively. *MCT1* mRNA was almost exclusively localized to oligodendroglia in the brain and spinal cord (Fig. 1 and Supplementary Fig. 3), with greater than 70–80% co-localization in the spinal cord, cortex and corpus callosum (Fig. 1p). Rare neuronal populations expressed MCT1 (Supplementary Fig. 4), although none in retinal ganglion cells (Supplementary Fig. 2k) or spinal cord motoneurons (Supplementary Fig. 4o, p). Surprisingly, there was virtually no expression of *MCT1* mRNA within adult CNS astrocytes (Fig. 1 and Supplementary Fig. 3), nor was it found in NG2 cells, endothelial cells or microglia (Fig. 1). Most MCT1 BAC-positive cells co-labelled with an oligodendroglia lineage marker, oligodendrocyte transcription factor 2 (OLIG2; Fig. 1l)[23], and few other CNS cells expressed tdTomato (Fig. 1p).

MCT1 protein also co-localized with myelinating oligodendroglia, as MCT1 immunoreactivity co-localized with myelin basic protein (MBP) and the oligodendrocyte-specific marker 2′,3′-cyclic-nucleotide 3′-phosphodiesterase (CNP) in rodent and human brain (Supplementary Fig. 5). MCT1 protein was closely aligned with axons (Supplementary Fig. 5h–j), but not astroglia, axonal nodes or paranodes (Supplementary Fig. 5k–p). *In vitro*, NG2 cells and primary oligodendroglia both expressed the MCT1–tdTomato reporter (Supplementary Fig. 6a–f), as do primary astrocyte cultures (Supplementary Fig. 6g–l)[24], which may account for the discrepancies in MCT1 localization in the literature.

The cell specificity and enrichment of native *MCT1* mRNA was further evaluated by FACS and BAC translating ribosome affinity purification (BacTRAP) techniques. *MCT1* mRNA, quantified by real-time PCR with reverse transcription (real-time RT–PCR) of acutely isolated mouse brain mRNA from FACS and BacTRAP astrocytes and oligodendroglia, was expressed at 16-fold (FACS) and 31-fold (BacTRAP) higher levels in mature oligodendroglia than in astrocytes (Fig. 1q). MCT1 expression (Fig. 1r) and functional lactate transport (Fig. 1s) were also detected and enriched in oligodendrocyte tumour cells (that is, oligodendroglioma) as compared with astrocyte tumour cells (that is, astrocytoma). Although not detectable by either the MCT1–tdTomato BAC reporter mice or immunohistochemistry, FACS and BacTRAP experiments suggest that astrocytes express very low levels of *MCT1* mRNA *in vivo*; although it is clear that MCT1 expression and lactate transport is much greater in oligodendroglia than astrocytes. Astrocytes *in vivo* express the MCT4 lactate transporter (Yo.L., unpublished observations)[25,26], suggesting that this transporter may have a more important role in astrocytes than MCT1.

Neuronal survival *in vitro* requires MCT1

Similar to *in vivo*, *MCT1* mRNA is primarily localized to oligodendrocyte-lineage cells, immunostained with OLIG2, in postnatal organotypic spinal cord cultures (Supplementary Fig. 7). To investigate whether downregulation or inhibition of MCT1 produces neuron death, organotypic spinal cord cultures were treated with antisense oligonucleotides (ASO) or a specific MCT1 transport inhibitor (MCT1i; Supplementary Fig. 7i)[27]. After three weeks of treatment, only 67% ± 6.7 (mean ± s.e.m.) of motoneurons survived in the ASO group ($P < 0.01$, Fig. 2a, b), and 66% ± 5.9 in the MCT1i group ($P < 0.05$, Fig. 2c). Thus, genetic or pharmacological reduction of MCT1 led to motoneuron death.

If the function of MCT1 is to export lactate from oligodendroglia and provide energy metabolites to neurons, then neurons exposed to glucose-free media or stimuli that increase neuronal activity should be particularly vulnerable. Motoneurons in organotypic spinal cord slice cultures were resistant to short periods (2 h) of glucose deprivation,

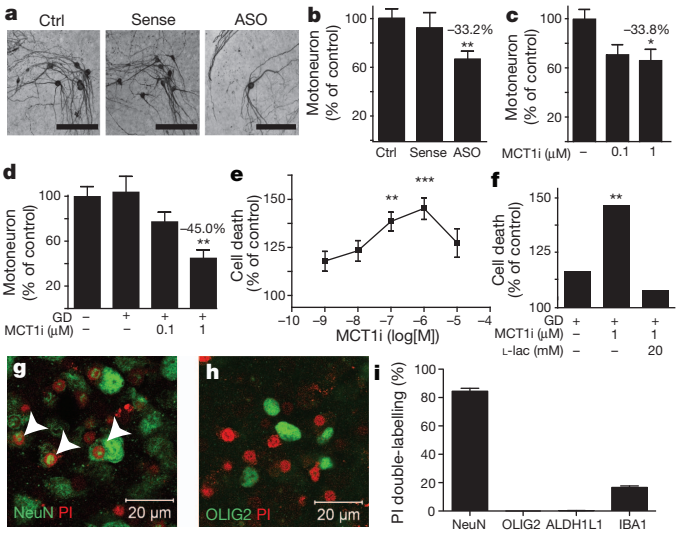

Figure 2 | MCT1 required for neuronal survival *in vitro*. **a**–**d**, Photomicrographs (**a**) and quantification (**b**–**d**) of motoneurons in spinal cord slice cultures treated with media only (ctrl; $n = 105$), MCT1 sense oligonucleotides ($n = 55$), or MCT1 ASO ($n = 101$) for 3 weeks (**b**), after 3 weeks of treatment with MCT1i (**c**; $n = 68$, 30 and 26 sections for columns 1–3, respectively), or 2 h of glucose deprivation (GD) with or without MCT1i (**d**; $n = 83$, 90, 68 and 70 sections for columns 1–4, respectively). **e**, **f**, Propidium iodide uptake in slice cultures treated with 2 h glucose deprivation plus MCT1i (**e**; $n = 79$, 14, 14, 39, 45 and 10 sections for control, 10^{-9}, 10^{-8}, 10^{-7}, 10^{-6} and 10^{-5} MCT1i, respectively) or 2 h glucose deprivation with or without MCT1i and 20 mM lactate (**f**; $n = 15$ for all groups). **g**, **h**, Propidium iodide uptake in slices treated with glucose deprivation and MCT1i, labelled with a neuronal (**g**; NeuN, co-localized cells marked with arrowheads) or an oligodendroglia (**h**; OLIG2) marker. Scale bars, 20 μm. **i**, Percentage of propidium iodide-labelled cells co-localizing with cell-specific markers ($n = 11$, 10, 10 and 11 sections for NeuN, OLIG2, ALDH1L1 (an astrocyte marker) and IBA1, respectively). Error bars denote s.e.m. $^*P < 0.05$; $^{**}P < 0.01$.

presumably owing to the presence of glycogen stores in astrocytes[28]. Simultaneous exposure to glucose deprivation and MCT1i led to concentration-dependent motoneuron loss, as measured by counts of neurofilament-containing neurons in the ventral horn ($P < 0.01$, Fig. 2d), and overall cell death, as measured by propidium iodide uptake ($P < 0.001$, Fig. 2e). Propidium iodide uptake occurred mainly within neurons ($P < 0.001$, Fig. 2g, i and Supplementary Fig. 7) and occasionally within IBA1-positive microglia (Fig. 2i and Supplementary Fig. 7). Much of the propidium iodide uptake in microglia is probably due to phagocytosing dead cells; however, limited microglia death cannot be excluded. Importantly, there was no death of oligodendrocyte-lineage cells or astrocytes after glucose deprivation and treatment with MCT1i (Fig. 2h, i and Supplementary Fig. 7). Other neurons were also vulnerable to glucose deprivation and MCT1i treatment, as considerable propidium iodide uptake was seen in the dorsal horn of the spinal cord and in organotypic cultures from neocortex (Supplementary Fig. 7). MCT1i- and glucose deprivation-induced neurodegeneration was completely prevented by supplementing media with 20 mM L-lactate ($P < 0.01$, Fig. 2f), confirming that the toxicity in cultures was due to reduced lactate release from oligodendroglia, not blockage of lactate uptake on neurons or oligodendroglia. Cell death was also produced by co-treatment of organotypic spinal cord cultures with MCT1i and either glutamate or the GABA (γ-aminobutyric acid) antagonist, bicuculline, both of which depolarize neurons in slice cultures ($P < 0.05$, Supplementary Fig. 8)[29,30]. Because glutamate is also a substrate of metabolism, we confirmed that cell death was dependent on neuron depolarization by blocking cell death with the AMPA (α-amino-3-hydroxy-5-methyl-4-isoxazole propionic acid) and kainate receptor antagonist 6-cyano-7-nitroquinoxaline-2,3-dione (CNQX) (Supplementary Fig. 8). In summary, neurons *in vitro* are vulnerable to inhibitors of MCT1 lactate transport. Toxicity is potentiated by removing glucose or increasing the metabolic activity of neurons, and is prevented by supplying exogenous lactate.

Downregulation of MCT1 *in vivo* is motoneuron toxic

To downregulate MCT1 *in vivo*, we produced a lentivirus that expressed GFP and *MCT1* short hairpin RNA (shRNA) driven by the cytomegalovirus (CMV) and H1 promoters, respectively (lenti-shRNA). Lenti-shRNA downregulated MCT1 protein both in cultured cells and cervical spinal cord *in vivo* (Fig. 3a). The amount of downregulation *in vivo* is underestimated by western blot because only a fraction of oligodendroglia are transfected by virus. Controls included injection of a lentivirus expressing GFP only (lenti-GFP) and contralateral injections of virus media. Both of the lentiviruses (lenti-shRNA and lenti-GFP) effectively transduced oligodendroglia and astrocytes (Fig. 3b, c). Four weeks after cervical spinal cord injection of lenti-shRNA, 56% ± 5.7 ($n = 10$, $P < 0.05$) of motoneurons near the injection site survived relative to contralateral media injection, whereas injection of lenti-GFP had no significant effect (Fig. 3, $P > 0.05$). In addition, numerous pathological axonal swellings, immunoreactive for the neurofilament marker SMI-32, resulted from lenti-shRNA treatment (Fig. 3g). As expected, motoneuron death in lenti-shRNA-injected spinal cords produced microglial activation, which was not seen using the lenti-GFP control (Fig. 3h, i). Thus, subacute downregulation of MCT1 focally in the spinal cord is sufficient to produce motoneuron death.

Heterozygous *MCT1*-null mice develop CNS axonopathy

MCT1 shRNA treatment was neurotoxic, and we postulated that reducing expression of *MCT1* in a null mouse would also produce neurodegeneration. Complete absence of MCT1 is embryonically lethal, but heterozygous-null mice ($MCT1^{+/-}$), with ~50% reduction in MCT1, breed and mature normally with no gross phenotypic abnormalities. The mice eventually developed an axonopathy in the brain and spinal cord by 8 months of age, with axon swellings

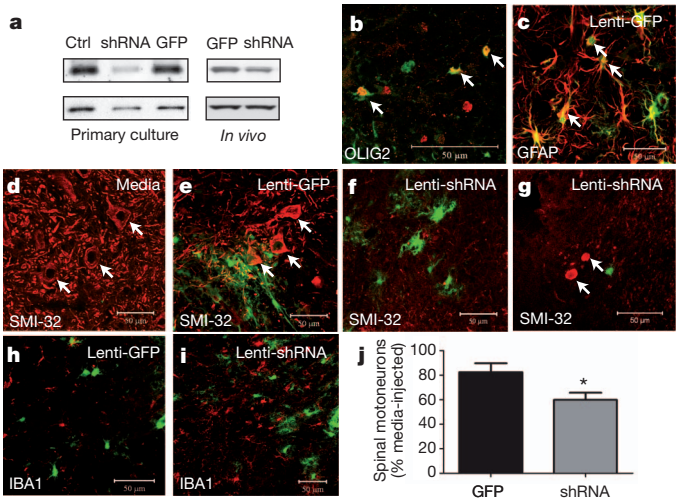

Figure 3 | Lentiviral *MCT1* shRNA is toxic to motoneurons. **a**, Lenti-shRNA (shRNA) downregulates MCT1 in primary astrocyte cultures and *in vivo* compared with untreated (ctrl) or lenti-GFP control (GFP). **b**, **c**, OLIG2 (**b**) and glial fibrillary acidic protein (GFAP; **c**) in lenti-GFP-injected spinal cords. **d**–**f**, Non-phosphorylated neurofilament (SMI-32) (red) in spinal cords injected with media (**d**), lenti-GFP (**e**), or lenti-shRNA (**f**). Arrows indicate motoneurons. **g**, SMI-32 labels aberrant axonal swellings in lenti-shRNA-injected spinal cords. **h**, **i**, IBA1-positive microglia in spinal cords injected with lenti-GFP (**h**) and lenti-shRNA (**i**). Scale bars, 50 μm. **j**, Quantification of cervical spinal motoneurons injected with lenti-GFP ($n = 8$) or lenti-shRNA ($n = 10$), relative to contralateral media injection. Error bars denote s.e.m. $^*P < 0.05$.

visualized by both light and electron microscopy (Fig. 4 and Supplementary Fig. 9). Notably, axon pathology in these mice is similar to *Cnp*-null mice[31], SOD1 transgenic mice as a model of ALS[32], and to patients with ALS[33]. Despite the axonopathy and activation of astrocytes, microglia and NG2-positive cells (Fig. 4 and

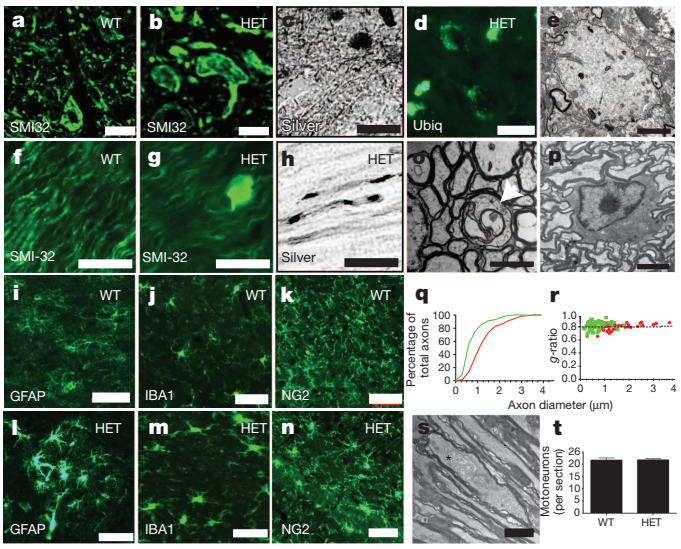

Figure 4 | Heterozygous *MCT1*-null mice develop widespread axonopathy. **a**–**d**, Spinal cords of wild-type (WT) and $MCT1^{+/-}$ (HET) mice, immunostained for non-phosphorylated neurofilament (SMI-32) (**a**, **b**), silver-stained (**c**), or immunostained for ubiquitin (**d**). **e**, Electron microscopy of axonal spheroid in spinal cord. **f**–**h**, Optic nerves of wild-type and $MCT1^{+/-}$ mice immunostained for SMI-32 (**f**, **g**) or silver-stained (**h**). **i**–**n**, GFAP (**i**, **l**), IBA1 (**j**, **m**), and NG2 (**k**, **n**) in wild-type (**i**–**k**) and $MCT1^{+/-}$ (**l**–**n**) mice. **o**, **p**, Degenerating axon (**o**; arrow) and intact oligodendrocyte (**p**) in optic nerve. **q**, **r**, Axon diameter (**q**) and *g*-ratio (**r**) in $MCT1^{+/-}$ (green line/dots; $n = 158$) and wild-type (red line/dots; $n = 78$) mice. **s**, Distended mitochondrion (asterisk) in $MCT1^{+/-}$ optic nerve. **t**, Number of spinal motoneurons per section from wild-type and $MCT1^{+/-}$ mice ($n = 7$ for each group). Scale bars, 20 μm (**a**–**d**, **f**–**h**), 2 μm (**e**, **o**, **s**), 50 μm (**i**–**n**) and 6 μm (**p**). Error bars denote s.e.m.

Supplementary Fig. 9), there was no change in overall myelination in *MCT1*$^{+/-}$ mice (Supplementary Fig. 9a–f), suggesting that the pathology was not secondary to oligodendrocyte injury.

In the optic nerve, a pure sample of CNS axons the function of which is partly dependent on lactate[34], large and intermediate sized degenerating axons were observed in *MCT1*$^{+/-}$ mice (Fig. 4o). Overall, 1.74 ± 0.06% of optic nerve axons from *MCT1*$^{+/-}$ mice showed morphologic features of degeneration, including swellings, enlarged mitochondria and reduced axon diameter, which were not seen in age-matched littermate control mice (Fig. 4 and Supplementary Fig. 9). Notably, oligodendrocyte morphology (Fig. 4p) and number were not changed, nor was myelination as represented by normal *g*-ratios (the ratio between the diameter of the inner axon and the total out diameter) (Fig. 4r), and intact myelin in non-degenerating axons (Supplementary Fig. 9), again suggesting that axonal degeneration was not due to oligodendrocyte damage or demyelination. Thus, despite only having a partial reduction in MCT1 expression (Supplementary Fig. 9j), adult *MCT1*$^{+/-}$ mice demonstrate widespread CNS axonopathy. Given the low percentage of axons affected, it is not surprising that this axonopathy did not produce a behavioural phenotype, loss of motoneurons (Fig. 4s), or obvious injury to retinal ganglion cells (Supplementary Fig. 9t, u) in *MCT1*$^{+/-}$ mice. In summary, *MCT1*$^{+/-}$ mice develop axon degeneration in the CNS without demyelination or oligodendrocyte injury, suggesting that MCT1 is crucial for the normal function of CNS axons through a myelin-independent mechanism.

Oligodendrocyte–specific MCT1 loss causes axonopathy

Although MCT1 is primarily expressed within oligodendroglia in the CNS, it is not exclusive to oligodendroglia and thus we cannot exclude the possibility that the axon degeneration seen in *MCT1*$^{+/-}$ mice is due to downregulating MCT1 in other cell types. To investigate this, we produced two lentiviral constructs that downregulate MCT1 selectively in oligodendroglia through different mechanisms. First, lentiviral constructs were produced that expressed either the same *MCT1* shRNA used in Fig. 3 plus GFP (lenti-MBP-shRNA) or GFP alone (lenti-MBP-GFP) driven by the MBP promoter. Lenti-MBP-shRNA downregulated MCT1 protein in the optic nerve (Fig. 5a, b) despite transfecting only a small segment of nerve (Fig. 5c, d). Transfection was selective for oligodendrocyte-lineage cells, as seen by co-localization of all GFP-labelled cells with OLIG2 (Fig. 5e, f, arrows) and not astroglia (Fig. 5c, d). At the injection site, there were a few pathologically enlarged SMI-32-positive axons in lenti-MBP-GFP-injected optic nerves owing to nerve trauma (Fig. 5g, arrowheads), but markedly more in optic nerves injected with lenti-MBP-shRNA (Fig. 5h, arrowheads). Distal to the injection, there were increased degenerating axons, both myelin ovoids (arrows) and 'dark axons' (asterisks), in optic nerve injected with lenti-MBP-shRNA compared with lenti-MBP-GFP (Fig. 5i–l). Restricted penetration of the lentivirus into the nerve led to some variability in axon degeneration. Nevertheless, there was a significant increase in the number of degenerating fibres in optic nerves injected with lenti-MBP-shRNA compared with lenti-MBP-GFP ($P < 0.05$, $n = 4$ nerves, Fig. 5m, n).

We also developed a tamoxifen-inducible Cre-dependent lentivirus expressing *MCT1* shRNA, and produced oligodendrocyte-specific *MCT1* knockdown by injecting virus into the corpus callosum of transgenic mice expressing a tamoxifen-inducible Cre (CreER) under the transcriptional control of myelin proteolipid protein (PLP1) (Supplementary Fig. 10a)[35,36]. Viral transfection of corpus callosum oligodendroglia was confirmed in control mice by co-localization of GFP with both CC-1—an antibody against adenomatous polyposis coli that labels oligodendrocytes—and MCT1 reporter (Supplementary Fig. 10b–g; arrowheads). In tamoxifen-treated PLP1-CreER mice, the GFP reporter was excised in oligodendroglia, so specific viral localization of GFP to oligodendroglia is generally not visualized. There was clear axonal degeneration near the injection site in the PLP1-CreER mice, as demonstrated by SMI-32-immunoreactive axon swellings (Supplementary Fig. 14k–m, boxed areas) and by axonal beading in GFP-labelled axons (Supplementary Fig. 14n), which was not observed when the identical virus was injected into wild-type mice (Supplementary Fig. 14h–j). Thus, *in vivo* oligodendrocyte-specific downregulation of MCT1 in both the optic nerve and the corpus callosum was capable of producing axon degeneration. Overall, these studies confirm that oligodendrocyte MCT1 is crucial for axon survival as loss of lactate transport from oligodendroglia to axons causes axon degeneration in both viral knockdown experiments and *MCT1*$^{+/-}$ mice.

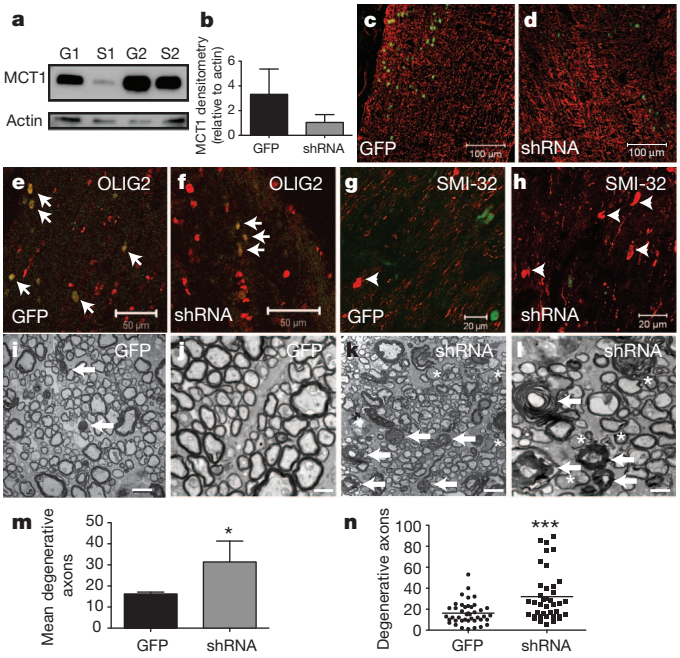

Figure 5 | Selective downregulation of MCT1 in oligodendroglia produces axonal injury. **a**, **b**, Western blot of optic nerves injected with lentivirus expressing MBP-shRNA (S) ($n = 2$) or MBP-GFP (G) ($n = 2$). **c**, **d**, GFAP immunoreactivity in nerve transfected with lenti-MBP-GFP and lenti-MBP-shRNA. **e**, **f**, GFP and shRNA viruses co-localize exclusively with OLIG2 (arrows). **g**, **h**, Axon swellings (arrowheads) labelled with non-phosphorylated neurofilament (SMI-32) after injection of GFP (**g**) and shRNA (**h**) viruses. **i–l**, Low-power (**i**, **k**) and high-power (**j**, **l**) magnification electron microscopy photomicrographs after injection of GFP and shRNA viruses. Arrows indicate myelin ovoids and asterisks indicate dark degenerating axons. **m**, **n**, Mean number (**m**; $n = 4$ nerves per group) and scatterplot (**n**; $n = 40$ fields per group) of degenerative axons per electron microscopy field in lenti-GFP- and lenti-shRNA-injected optic nerves. Scale bars, 100 μm (**c**, **d**), 50 μm (**e**, **f**), 20 μm (**g**, **h**), 1 μm (**i**, **k**) and 0.5 μm (**j**, **l**). Error bars denote s.e.m. $^{*}P < 0.05$; $^{***}P < 0.001$.

MCT1 expression is reduced in ALS

Recent studies suggest oligodendroglia or their precursors may be injured in mutant SOD1 transgenic mice[18]. We proposed that the reduced ability of grey and white matter oligodendroglia to support motoneurons, caused by altered MCT1 expression, may contribute to ALS pathogenesis as seen in our *in vitro* and *in vivo* studies described earlier. We investigated the expression levels of MCT proteins and the MCT-associated protein CD147 (also known as BSG or basigin) in affected (that is, motor cortex) and unaffected (that is, frontal cortex) regions from patients with ALS and control patients. In addition, we investigated MCT1 reporter activity in the spinal cord of SOD1(G93A) transgenic mice—a commonly used model of ALS that had been crossed with MCT1–tdTomato BAC reporter mice. The motor cortex of patients with ALS showed a greater than 50% decline in MCT1 and MCT4 expression ($P < 0.01$ and $P < 0.001$, respectively) compared with gender- and age-matched control patients

(Fig. 6 and Supplementary Table 1). This reduction was not seen in the unaffected frontal cortex, nor was it seen for CD147, an accessory glycoprotein that increases the localization of MCT1 and MCT4 to the plasma membrane[37] (full blots available in Supplementary Figs 12 and 13). Oligodendroglia were still present in the cortical samples as there was no significant alteration in CNP (Fig. 6a, b), although it is possible the oligodendroglia were immature.

In addition to patients with ALS, downregulation of *MCT1* mRNA was also seen in the spinal cords of early symptomatic (Supplementary Fig. 11) and end-stage (Fig. 6) SOD1(G93A) transgenic mice. SOD1(G93A) transgenic mice were mated to MCT1 BAC mice, and *MCT1* mRNA expression was evaluated by tdTomato fluorescence. In SOD1(G93A) transgenic mice, MCT1 reporter continued to exclusively label oligodendroglia throughout the brain, although there was a marked reduction in MCT1 expression in the ventral horn grey matter (outlined by dashes, Fig. 6d, e) as compared with age-matched control mice (Fig. 6f, g). Reduced MCT1 reporter expression was not due to less oligodendroglia, because CC-1-positive oligodendroglia were preserved, although again CC-1 immunoreactivity may not be labelling fully mature oligodendroglia (Fig. 6e). Taken together, these results suggest that alterations in oligodendrocyte MCT1 may contribute to motoneuron degeneration in ALS, and provide a human disease in which downregulation of MCT1 is associated with neurodegeneration.

Discussion

Our results suggest that oligodendroglia support of axons, through MCT1-based transport of lactate (or pyruvate), is crucial for maintaining axon function and neuron survival and seems to be a fundamental property of oligodendroglia. Disruption of MCT1 could hypothetically cause either reduced lactate export out of, or reduced import into, oligodendroglia because the direction of transport is determined by the relative intra- and extracellular concentrations of lactate and hydrogen ions[6]. Our results suggest primarily disruption of lactate export. First, exogenous lactate completely prevents cell loss in organotypic cultures by compensating for reduced lactate export. Second, oligodendroglia do not degenerate in *MCT1*$^{+/-}$ mice or when exposed to MCT1 inhibitor and glucose deprivation in organotypic spinal cord cultures. Third, our study and others[10] demonstrate that MCT1 is predominantly localized to the myelin sheath around CNS axons, as expected for a transporter from oligodendroglia to axons. Taken together, our results suggest that MCT1-regulated lactate export from oligodendroglia is a crucial component of the local energy supply to axons, and the disruption of this transport leads to axon dysfunction and ultimately to neuron degeneration. Oligodendrocyte support of axons was also suggested by a recent paper that found increased brain lactate in transgenic mice with a selective deficit in oligodendroglia mitochondrial function[5]. Of course, lactate may also be imported into oligodendroglia and contribute to the production of myelin, as has been shown in dissociated[38] and cortical slice cultures[39], but attenuation of MCT1 does not seem to cause neuron or axon degeneration through this mechanism.

Our results contribute to the emerging data that oligodendroglia are implicated in ALS pathogenesis. Spinal cord ventral grey matter oligodendrocyte precursor cells markedly replicate in ALS mouse models[18], possibly in response to oligodendroglial injury (J.D.R., unpublished data), and cytoplasmic inclusions are found in human ALS oligodendroglia[40]. We found that MCT1 is reduced in affected brain regions from patients with ALS and the ventral horn of the spinal cord in mutant SOD1 transgenic mice. These changes could reflect downregulation of the transporter within intact oligodendroglia, or perhaps death of oligodendroglia and replacement with immature oligodendroglia. Newly generated oligodendroglia, labelled with CC-1, do not contain MCT1 (Fig. 6), and would therefore be unable to supply energy metabolites to axons, leading to axon injury and neuron loss. We propose that this mechanism contributes to motoneuron degeneration in ALS. Future experiments will investigate this specifically by determining whether MCT1 downregulation is specific for ALS and whether MCT1 upregulation or transplantation of oligodendroglia can prolong survival in ALS mouse models.

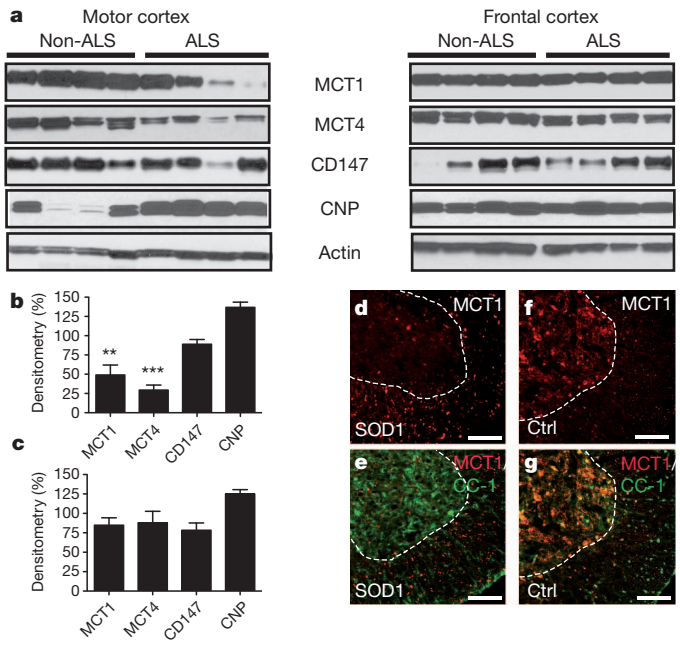

Figure 6 | MCT1 reduced in ALS patients and SOD1(G93A) mice. **a**, Immunoblots of MCT1 and myelin-related proteins from patients with sporadic ALS and non-ALS patients. **b**, **c**, Relative densitometry of proteins from the motor (**b**) and frontal (**c**) cortex ($n = 8$ for each region) of patients with ALS compared with control patients ($n = 9$ for motor and 6 for frontal cortex). Error bars denote s.e.m. **d**–**g**, Immunofluorescence of the MCT1 reporter alone (**d**, **f**; red) and double-labelling with CC-1 (**e**, **g**; green), in end-stage SOD1(G93A) transgenic mice (**d**, **e**) and littermate controls (**f**, **g**). Scale bars, 100 μm. Dashed lines delineate the boundary of ventral horn grey matter.

METHODS SUMMARY

MCT1 BAC mice were developed and MCT1 expression was localized to specific cells by crossing with cell-specific reporter lines, immunostaining for cell-specific markers, or isolating mRNA by FACS and BacTRAP. Critical function of oligodendrocyte MCT1 was evaluated *in vitro* in organotypic spinal cord cultures, and *in vivo* in *MCT1*$^{+/-}$ or wild-type mice injected with lentiviral vectors. Neuronal toxicity, measured by loss of neurofilament-containing neurons and incorporation of propidium iodide, was provoked in organotypic cultures by treating with ASO or MCT1i. *MCT1*$^{+/-}$ mice were evaluated by histology, immunohistochemistry and electron microscopy, and compared with littermate controls. For lentiviral experiments, *MCT1* shRNA was subcloned into lentivirus plasmid along with three different promoters (that is, H1, MBP and Cre-dependent V6). Lenti-shRNA, which expresses *MCT1* shRNA driven by the H1 promoter and GFP by the CMV promoter, was injected into the spinal cord of C57Bl6 wild-type mice and motoneurons in the vicinity of virus were counted and compared with control virus injections. Lenti-MBP-shRNA was injected into the optic nerve of Sprague–Dawley rats, and degenerating axons were quantified by electron microscopy and compared with the contralateral optic nerve injected with control virus. Cre-dependent lenti-V6-shRNA was injected into the corpus callosum of PLP1-CreER mice, and axon pathology was assessed by non-phosphorylated neurofilament immunostaining. Finally, MCT1 expression was evaluated by western blots of cortex from patients with ALS and control patients; and MCT1 expression in SOD1(G93A) transgenic mice, obtained from Jackson laboratories, was evaluating by crossing these mice to MCT1 BAC reporter mice.

Full Methods and any associated references are available in the online version of the paper at www.nature.com/nature.

Received 28 March; accepted 13 June 2012.
Published online 11 July 2012.

1. Trapp, B. D. *et al.* Axonal transection in the lesions of multiple sclerosis. *N. Engl. J. Med.* **338,** 278–285 (1998).

2. Garbern, J. Y. *et al.* Patients lacking the major CNS myelin protein, proteolipid protein 1, develop length-dependent axonal degeneration in the absence of demyelination and inflammation. *Brain* **125,** 551–561 (2002).
3. Griffiths, I. *et al.* Axonal swellings and degeneration in mice lacking the major proteolipid of myelin. *Science* **280,** 1610–1613 (1998).
4. Lappe-Siefke, C. *et al.* Disruption of *Cnp1* uncouples oligodendroglial functions in axonal support and myelination. *Nature Genet.* **33,** 366–374 (2003).
5. Fünfschilling, U. *et al.* Glycolytic oligodendrocytes maintain myelin and long-term axonal integrity. *Nature* **485,** 517–521 (2012).
6. Pierre, K. & Pellerin, L. Monocarboxylate transporters in the central nervous system: distribution, regulation and function. *J. Neurochem.* **94,** 1–14 (2005).
7. Koehler-Stec, E. M., Simpson, I. A., Vannucci, S. J., Landschulz, K. T. & Landschulz, W. H. Monocarboxylate transporter expression in mouse brain. *Am. J. Physiol.* **275,** E516–E524 (1998).
8. Pierre, K., Pellerin, L., Debernardi, R., Riederer, B. M. & Magistretti, P. J. Cell-specific localization of monocarboxylate transporters, MCT1 and MCT2, in the adult mouse brain revealed by double immunohistochemical labeling and confocal microscopy. *Neuroscience* **100,** 617–627 (2000).
9. Halestrap, A. P. & Price, N. T. The proton-linked monocarboxylate transporter (MCT) family: structure, function and regulation. *Biochem. J.* **343,** 281–299 (1999).
10. Rinholm, J. E. *et al.* Regulation of oligodendrocyte development and myelination by glucose and lactate. *J. Neurosci.* **31,** 538–548 (2011).
11. Pellerin, L. & Magistretti, P. J. Glutamate uptake into astrocytes stimulates aerobic glycolysis: a mechanism coupling neuronal activity to glucose utilization. *Proc. Natl Acad. Sci. USA* **91,** 10625–10629 (1994).
12. Walz, W. & Mukerji, S. Lactate production and release in cultured astrocytes. *Neurosci. Lett.* **86,** 296–300 (1988).
13. Pellerin, L. *et al.* Evidence supporting the existence of an activity-dependent astrocyte-neuron lactate shuttle. *Dev. Neurosci.* **20,** 291–299 (1998).
14. Berthet, C. *et al.* Neuroprotective role of lactate after cerebral ischemia. *J. Cereb. Blood Flow Metab.* **29,** 1780–1789 (2009).
15. Suzuki, A. *et al.* Astrocyte-neuron lactate transport is required for long-term memory formation. *Cell* **144,** 810–823 (2011).
16. Benarroch, E. E. Oligodendrocytes: susceptibility to injury and involvement in neurologic disease. *Neurology* **72,** 1779–1785 (2009).
17. Yamanaka, K. *et al.* Astrocytes as determinants of disease progression in inherited amyotrophic lateral sclerosis. *Nature Neurosci.* **11,** 251–253 (2008).
18. Kang, S. H., Fukaya, M., Yang, J. K., Rothstein, J. D. & Bergles, D. E. $NG2^+$ CNS glial progenitors remain committed to the oligodendrocyte lineage in postnatal life and following neurodegeneration. *Neuron* **68,** 668–681 (2010).
19. Pellerin, L., Pellegri, G., Martin, J. L. & Magistretti, P. J. Expression of monocarboxylate transporter mRNAs in mouse brain: support for a distinct role of lactate as an energy substrate for the neonatal vs. adult brain. *Proc. Natl Acad. Sci. USA* **95,** 3990–3995 (1998).
20. Chiry, O. *et al.* Expression of the monocarboxylate transporter MCT1 in the adult human brain cortex. *Brain Res.* **1070,** 65–70 (2006).
21. Gerhart, D. Z., Enerson, B. E., Zhdankina, O. Y., Leino, R. L. & Drewes, L. R. Expression of monocarboxylate transporter MCT1 by brain endothelium and glia in adult and suckling rats. *Am. J. Physiol.* **273,** E207–E213 (1997).
22. Regan, M. R. *et al.* Variations in promoter activity reveal a differential expression and physiology of glutamate transporters by glia in the developing and mature CNS. *J. Neurosci.* **27,** 6607–6619 (2007).
23. Zhou, Q., Wang, S. & Anderson, D. J. Identification of a novel family of oligodendrocyte lineage-specific basic helix-loop-helix transcription factors. *Neuron* **25,** 331–343 (2000).
24. Hanu, R., McKenna, M., O'Neill, A., Resneck, W. G. & Bloch, R. J. Monocarboxylic acid transporters, MCT1 and MCT2, in cortical astrocytes *in vitro* and *in vivo*. *Am. J. Physiol. Cell Physiol.* **278,** C921–C930 (2000).
25. Pellerin, L., Bergersen, L. H., Halestrap, A. P. & Pierre, K. Cellular and subcellular distribution of monocarboxylate transporters in cultured brain cells and in the adult brain. *J. Neurosci. Res.* **79,** 55–64 (2005).
26. Bergersen, L., Rafiki, A. & Ottersen, O. P. Immunogold cytochemistry identifies specialized membrane domains for monocarboxylate transport in the central nervous system. *Neurochem. Res.* **27,** 89–96 (2002).
27. Murray, C. M. *et al.* Monocarboxylate transporter MCT1 is a target for immunosuppression. *Nature Chem. Biol.* **1,** 371–376 (2005).
28. Suh, S. W. *et al.* Astrocyte glycogen sustains neuronal activity during hypoglycemia: studies with the glycogen phosphorylase inhibitor CP-316,819 ([R-R*,S*]-5-chloro-N-[2-hydroxy-3-(methoxymethylamino)-3-oxo-1-(phenylmet hyl)propyl]-1H-indole-2-carboxamide). *J. Pharmacol. Exp. Ther.* **321,** 45–50 (2007).
29. Heyer, E. J., Nowak, L. M. & Macdonald, R. L. Membrane depolarization and prolongation of calcium-dependent action potentials of mouse neurons in cell culture by two convulsants: bicuculline and penicillin. *Brain Res.* **232,** 41–56 (1982).
30. Mayer, M. L. & Westbrook, G. L. Mixed-agonist action of excitatory amino acids on mouse spinal cord neurones under voltage clamp. *J. Physiol. (Lond.)* **354,** 29–53 (1984).
31. Edgar, J. M. *et al.* Early ultrastructural defects of axons and axon-glia junctions in mice lacking expression of Cnp1. *Glia* **57,** 1815–1824 (2009).
32. Morrison, B. M., Shu, I. W., Wilcox, A. L., Gordon, J. W. & Morrison, J. H. Early and selective pathology of light chain neurofilament in the spinal cord and sciatic nerve of G86R mutant superoxide dismutase transgenic mice. *Exp. Neurol.* **165,** 207–220 (2000).
33. Sasaki, S. & Maruyama, S. Increase in diameter of the axonal initial segment is an early change in amyotrophic lateral sclerosis. *J. Neurol. Sci.* **110,** 114–120 (1992).
34. Tekkök, S. B., Brown, A. M., Westenbroek, R., Pellerin, L. & Ransom, B. R. Transfer of glycogen-derived lactate from astrocytes to axons via specific monocarboxylate transporters supports mouse optic nerve activity. *J. Neurosci. Res.* **81,** 644–652 (2005).
35. Ventura, A. *et al.* Cre-lox-regulated conditional RNA interference from transgenes. *Proc. Natl Acad. Sci. USA* **101,** 10380–10385 (2004).
36. Doerflinger, N. H., Macklin, W. B. & Popko, B. Inducible site-specific recombination in myelinating cells. *Genesis* **35,** 63–72 (2003).
37. Kirk, P. *et al.* CD147 is tightly associated with lactate transporters MCT1 and MCT4 and facilitates their cell surface expression. *EMBO J.* **19,** 3896–3904 (2000).
38. Sánchez-Abarca, L. I., Tabernero, A. & Medina, J. M. Oligodendrocytes use lactate as a source of energy and as a precursor of lipids. *Glia* **36,** 321–329 (2001).
39. Rinholm, J. E. *et al.* Regulation of oligodendrocyte development and myelination by glucose and lactate. *J. Neurosci.* **31,** 538–548 (2011).
40. Seilhean, D. *et al.* Accumulation of TDP-43 and α-actin in an amyotrophic lateral sclerosis patient with the K17I *ANG* mutation. *Acta Neuropathol.* **118,** 561–573 (2009).

Supplementary Information is linked to the online version of the paper at www.nature.com/nature.

Acknowledgements We thank C. Coccia, S. Vidensky, I. Shats, L. Chakravarti, Y. Ayukawa and L. Mamedova for technical support, E. Potter for oligodendrocyte cultures, C. Cooke for electron microscopy, and S. Kang and D. Bergles for providing MOBP–eGFP BAC and CNP BacTrap mice, CASPR and Nav1.6 antibodies. Autopsy specimens were provided by the Johns Hopkins ALS Tissue Bank and the Johns Hopkins University Brain Resource Center supported by National Institutes of Health grants P50AG05146 and PO1NS16375. Support was provided by the Muscular Dystrophy Association (B.M.M. and Yo.L.), NIH-NS33958 (J.D.R.), P2ALS (J.D.R.), Packard Center for ALS (J.D.R.), Human Frontier Science Program-RG118/1998-B (L.P.), Swiss Fonds National de Recherche Scientifique-31003A-125063 (L.P.), Swiss National Science Foundation (FNRS)-3100AO-108336/1 (P.J.M.), Biaggi and Puccini Foundations (P.J.M). We dedicate this manuscript to J. W. Griffin, who passed away while this manuscript was under revision, and are grateful for his contributions to this manuscript and mentorship to many of the authors on this paper.

Author Contributions All of the authors contributed to the design of the experiments. MCT1 BAC reporter experiments were designed and performed by Yo.L., L.J. and P.-W.Z. MCT1 ASO, MCT1i and human western blot experiments were designed and performed by B.M.M., Yu.L., A.T., Yi.L. and J.D.R. Lentiviral experiments were designed and performed by Yo.L., B.M.M., Yu.L. and J.D.R. The heterozygous *MCT1*-null mice were produced by S.L., L.P. and P.J.M., and analysed by Yo.L. Electron miscroscopy work was completed by M.H.F., Yo.L., B.M.M. and J.D.R. Optic nerve lentiviral injections were performed by P.N.H. The manuscript and figures were prepared by B.M.M. and J.D.R. with input from co-authors.

Author Information Reprints and permissions information is available at www.nature.com/reprints. The authors declare no competing financial interests. Readers are welcome to comment on the online version of this article at www.nature.com/nature. Correspondence and requests for materials should be addressed to J.D.R. (jrothstein@jhmi.edu).

METHODS

Development of MCT1 BAC reporter and MCT1 overexpressor mice. MCT1–tdTomato BAC reporter mice were produced as described previously[22]. The BAC construct was modified to include the entire 19.8 kilobase (kb) *MCT1* gene plus 50 kb upstream of the first exon and 132.2 kb downstream of the last exon (Supplementary Fig. 2a). Founder lines were identified by PCR (primer pair was 5′-CGAGGAGGTCATCAAAGAGT-3′ and 5′-AGAACTTGAGGTGGTC CATC-3′) and also by tdTomato fluorescence within red blood cells. Two expression lines were produced and backcrossed with B6 or C57BL/6 wild-type mice. To produce MCT1 overexpressor mice, the promoter for the astrocyte-specific gene, *Gfap*, was used to drive MCT1 overexpression specifically in astrocytes[41]. *MCT1* was inserted between the *Gfap* promoter sequence and an internal ribosomal entry site (IRES)-eGFP sequence, resulting in expression of MCT1 and eGFP together in astrocytes. Six founder lines were generated, of which five expressed MCT1 and eGFP within CNS astrocytes.

Generation of lines coexpressing the MCT1 BAC reporter and other transgenes. GLT1–eGFP BAC[22], MOBP–eGFP BAC (GENSAT), PLP1–eGFP (Jackson laboratory), PLP1-CreER (Jackson laboratory), CNP–eGFP/RPL10A (Jackson Laboratory), ALDH1L1 (GENSAT), Thy-I–yellow fluorescent protein (YFP) (Jackson laboratory), and SOD1 G93A transgenic mice (Jackson laboratory) were crossed with MCT1 BAC reporter mice to establish double transgenic mice.

FACS, rtPCR and BacTRAP. Brains from 1-month-old MCT1–tdTomato BAC reporter mice were prepared as described previously[42]. Cells were sorted into three groups with a MoFlo MLS high-speed cell sorter (Beckman coulter) running Summit version 4.3 software in the FACS core at The Johns Hopkins University. Total RNA prepared from sorted cells and tissue using Absolutely RNA miniprep kit (Stratagene) was converted to complementary DNA using a cDNA synthesis kit (Applied Biosystems). PCR for *MCT1* or *Actin* (control) was completed using the following primer pairs: *MCT1*, 5′- AAAATGCCACCTGCGATTG GA-3′ and 5′-GCCTGATTAAGTGGAGCCAGG-3′; *Actin,* 5′-AGGCCAACCGTGA AAAGATG-3′ and 5′-CACAGCCTGGATGGCTACGT-3′. TaqMan premade gene-specific probes and 18S ribosomal RNA (as a control) were used for rtPCR. For the FACS isolation of oligodendroglia and astrocytes in the brains, young adult MOBP–eGFP and GLT1–eGFP BAC mice (1–2 months) were used as described previously[42]. For affinity purification of polysomal mRNAs from oligodendroglia and astrocytes in the brain, adult CNP BacTRAP (translating ribosome affinity purification) and ALDH1L1 BacTRAP mice were used, respectively, as described previously[43].

Primary antibodies for western blots and immunohistochemistry. Detailed protocols for western blots and immunohistochemistry are described below. The following primary antibodies were used for western blots: human MCT1 (AbGent; 1:75), mouse MCT1 (Santa Cruz; 1:50), MCT4 (Millipore; 1:400), CD147 (Novus Biologicals; 1:500), CNP (Millipore; 1:1,000), Connexin 43 (Millipore; 1: 500), and β-actin (Millipore; 1:1,000). The following primary antibodies were used for immunofluorescence: mouse MCT1 (Santa Cruz; 1:50), human MCT1 (Santa Cruz; 1:50), OLIG2 (Millipore; 1:500), CC-1 (Calbiochem; 1:50), CNP (Millipore; 1:250), MBP (Covance; 1:250), PDGFRα (BD Pharmingen; 1:100), NG2 (Millipore; 1:100), GFAP (Dako; 1:2,000), IBA1 (Wako; 1:500), NeuN (Millipore; 1:250), SMI-32 (Covance; 1:1,000) ubiquitin (Millipore; 1:250), CASPR (from D. Bergles; 1:1,500), Nav1.6 (from D. Bergles; 1:100), DsRed (Clontech; 1:250), TUJ1 (Millipore; 1:1,000), NeuN (Millipore; 1:1,000) and ALDH1L1 (Neuromab/UC Davis; 1:10).

Lactate uptake assay in oligodendroglioma and astrocytoma cell lines. MO3.13 oligodendroglioma and U87 astrocytoma cell lines are cultured as described in previous reports[44,45]. The lactate uptake assay was completed as described previously[46] with only small modifications. In brief, cells were incubated with 0.5 μCi ml^{-1} L-[1-^{14}C] lactic acid (Perkin-Elmer) in HEPES-buffered, Earl's balanced salt solution (HEBSS) buffer, pH 6.0, containing 150 mM NaCl, 5 mM KCl, 1 mM KH_2PO_4, 0.2 mM $CaCl_2 \cdot 2H_2O$, 3.3 mM MOPS, 10 mM HEPES, 1 mM $MgSO_4 \cdot 7H_2O$. After incubation, uptake was stopped by quickly chilling the cultures to 4 °C. Cells were washed with ice-cold HEPES buffer, homogenized in 0.1 M NaOH and 0.1% Triton X100, and centrifuged at 13,780*g* for 10 min. Radioactivity was measured by scintillation counting and corrected by protein amount.

Immunohistochemistry, histology, light and electron microscopy. Mice were anaesthetized with isoflurane/oxygen and perfused transcardially with 1× PBS followed by 4% paraformaldehyde in PBS (for light microscopy) or 4% paraformaldehyde/2.5% glutaraldehyde in PBS (for electron microscopy), tissue collected, and either cryoprotected in graded concentrations of sucrose and sectioned at 20 μm on a Leica CM1900 cryostat (for light microscopy) or embedded in Epon resin after postfixing in osmium tetroxide (for electron microscopy).

To assess neuropathology by light microscopy, tissue sections were stained with haematoxylin and eosin, eriochrome staining, Bielschowsky silver-staining, or immunohistochemistry. For lectin staining of endothelial cells, biotinylated *Lycopersicon esculentum* lectin (Vector Laboratories; 1:200) was incubated with sections for 1 h. As a secondary antibody, sections were incubated in streptavidin-488 (Vector Laboratories; 1:100). For immunohistochemistry of MCT1, tissue slices were pre-treated with sodium citrate buffer (10 mM sodium citrate, 0.05% Tween 20, pH 6.0) for antigen retrieval (other primary antibodies did not require antigen retrieval) before 1 h incubation at room temperature in blocking buffer (0.3% BSA, 5% skimmed milk and 0.3% Triton-X 100 in PBS). Primary antibodies were incubated overnight at 4 °C, washed and then incubated for 2 h at room temperature in anti-mouse or anti-rabbit IgG Alexa-fluor secondary antibodies (Invitrogen; 1:200). Photomicrographs were taken on Zeiss LSM510 meta confocal microscopy or Zeiss image Z1 fluorescent microscopy. Co-labelled cells with either immunostaining or transgenic reporters were manually counted in Axiovision from digital images taken by fluorescent microscopy. For electron microscopy, 1-mm thick sections were stained for toluidine blue and examined under light microscopy with ×100 oil-immersion objective. Thin sections (70 nm) were obtained and stained for citrate/uranyl acetate. For quantification of axon degeneration in the optic nerves of *MCT1* heterozygous mice and mice treated with lenti-MBP-shRNA, three and ten ×7,000 electron micrographs, respectively, were acquired for each optic nerve using a Zeiss Libra transmission electron microscope. The total number of axons and degenerating axons, as defined by degenerating myelin or dark axons, on each electron micrograph was counted and the percentage of axonal degeneration calculated. All quantification was completed by an investigator blinded to the genotype or treatment group.

Production of cell cultures. Oligodendrocyte cultures were produced from postnatal day (PND) 2–3 mouse cortical tissues of PLP1–eGFP × NG2-tdTomato double transgenic mice. In brief, oligodendrocyte progenitor cells (OPCs) were isolated by FACS and maintained in OPC culture medium (SATO medium containing PDGFRα) for 4 days. OPCs were further differentiated into mature oligodendroglia in the differentiation media (SATO media containing T3 without PDGFRα).

Primary astrocyte cultures were produced from PND 2–3 mouse pups. Cortices were dissected out and dissociated with papain and subsequently cultured on collagen-coated T75 flask in DMEM containing 10% FBS. At 14 days *in vitro* (DIV) astroglial cells were seeded into collagen-coated 6-well plates at a concentration of 7×10^5 cells per well.

Organotypic or cortical spinal cord cultures were produced from PND 7 Sprague–Dawley rat pups or MCT1–tdTomato reporter mice, as described previously[47].

ASOs or MCT1i treatment in organotypic spinal cord cultures. One week after plating organotypic spinal cord cultures, 5 μM MCT1 ASO (IDT) or various doses of MCT1i were added to media for 3 weeks. Sections were either visualized with propidium iodide (7.5 μM, 2 h, Sigma) or fixed with 4% paraformaldehyde, and immunostained with the neuronal marker SMI-32 (Covance; 1:1,000). Large, ventral horn SMI-32-positive neurons were counted by an investigator blinded to the treatment condition.

MCT1i and glucose deprivation in organotypic spinal cord cultures. Two weeks after collection, cultures were pre-treated with MCT1i (ref. 27) or DMSO for 24 h, incubated in propidium iodide for 2 h, and then photographed on a Nikon epifluorescence scope (pre-treatment). Sections were then washed, incubated with glucose-free or normal buffer with or without MCT1i for 2 h, allowed to recover for 2 h, re-incubated with propidium iodide for 2 h, and photographed images were quantified by fluorescent intensity (post-treatment). To examine motoneuron loss, sections were returned to normal media for 2 weeks, fixed in 4% paraformaldehyde, and immunostained with SMI-32 (Covance, 1:1,000). To study cellular localization of propidium iodide, sections were immediately fixed in 4% paraformaldehyde and then processed for immunocytochemistry with primary antibodies. Secondary antibodies used for detection were AlexaFluor 488-conjugated goat anti-rabbit, anti-mouse or anti-chicken antibodies (Invitrogen; 1:1,000).

Organotypic spinal cord cultures treated with bicuculline or glutamate. For bicuculline (BIC) experiment, spinal cord slice cultures (2 weeks post-culture) were treated with 100 μM BIC (or vehicle) in the presence or absence of 1 mM MCT1i for 3 days. To measure cell death, cultures were incubated with propidium iodide and then photographed on a Nikon epifluorescence scope. For glutamate experiment, spinal cord cultures were incubated with MCT1i (or DMSO vehicle for controls) for 24 h, followed by media with or without 250 μM glutamate buffer for 60 min. Propidium iodide staining was performed before and after the glutamate treatment to visualize dead cells. For quantification, fluorescent intensities of pre-treatment sections measured by Image J software for the dorsal

horn in BIC-treated sections, and total spinal cord in glutamate treated sections, were subtracted from post-treatment sections. All values were normalized to untreated control sections.

Production of lentiviral constructs. On the basis of pre-designed ON-TARGETplus SMARTPool siRNA sequences (Dharmacon), DNA oligonucleotides that contain *MCT1* shRNA sequences were synthesized and directly subcloned into pSuper vector (Oligoengine). The sense and antisense oligonucleotide sequences for the most efficient *MCT1* shRNA were as follows: 5′-GATCCC CGTATCATGCTTTACGATTATTCAAGAGATAATCGTAAAGCATGATAC TTTTTTC-3′, 5′-TCGAGAAAAAAGTATCATGCTTTACGATTATCTCTTG AATAATCGTAAAGCATGATACGGG-3′.

DNA fragments spanning the H1 promoter and the shRNA sequences in pSuper construct were amplified by PCR and subcloned into FUGW-CMV to produce lenti-shRNA (in which *MCT1* shRNA is driven by the H1 promoter and GFP by the CMV promoter). Fragments spanning MBP promoter, shRNA and IRES-eGFP sequences were subcloned into FUGW-CMV to produce lenti-MBP-shRNA. V6::*MCT1* shRNA was subcloned into the HpaI and XhoI restriction sites of pSico (Addgene) to produce Cre-inducible lentivirus. Lentiviral constucts, including control GFP constructs, were produced in HEK293 T cells using the FUGW-CMV/Δ8.9/VSVG system.

***MCT1* shRNA lentivirus injected into spinal cord.** Unilateral injections of lenti-shRNA ($n = 10$) or lenti-GFP ($n = 8$) were performed in C57BL6 wild-type mice at 100 days of age at cervical spinal cord levels 4–6 (C4–6), delivering 1.7×10^5 plaque-forming units (p.f.u.) for lenti-GFP or 1.8×10^5 p.f.u. for lenti-shRNA per mouse. In brief, the transverse processes of C4–6 were removed, the dura removed, and three 1-μl injections of lentivirus or media were injected with a 34-gauge Hamilton syringe needle. Animals were euthanized after 4 weeks by transcardial perfusion with 4% paraformaldehyde. Spinal cord sections were cryoprotected, sectioned on a cryostat, and immunostained for neurofilaments (SMI-32), oligodendrocyte-lineage cells (OLIG2), microglia (IBA1) or astrocytes (GFAP), as described earlier. Large (diameter greater than 20 μm) neurofilament-containing neurons in the ventral spinal cord were counted from every third section that localized GFP to the ventral horns on both the virus- and media-injected halves of the spinal cord (mean number of sections counted 11.9 for shRNA group and 12 for GFP group). For each animal, the mean number of motoneurons per section from the virus-injected spinal cord hemisection was divided by the mean number of motoneurons per section from the contralateral media-injected motor neurons per section.

Generation of heterozygous *MCT1*-null mice. Heterozygous *MCT1*-null mice were generated by targeted homologous recombination to replace a 640-base-pair sequence of the *MCT1* gene starting at the translation initiation codon and containing exon 1 as well as part of the first intron with the *LacZ* gene sequence fused with a neomycin (*Neo*) resistance gene sequence and put in frame with the *MCT1* promoter (S. Lengacher *et al.*, manuscript in preparation). Successful recombination event and proper insertion of the *LacZ/Neo* sequence in the targeted locus was controlled by Southern blot on DNA from embryonic stem cells previously electroporated with the targeted vector and selected with gancyclovir and G418. Genotyping of animals was performed by PCR with appropriate set of primers.

***MCT1* shRNA driven by MBP promoter injected into rat optic nerves.** Sixty-day-old Sprague–Dawley rats were anaesthetized with 2% isofluorane, an incision placed in the scalp overlying the orbital ridge, the skin overlying the orbital ridge retracted, and a conjunctival suture placed to provide traction to the globe. The optic nerve was localized, a window cut in the overlying dura, the nerve pierced with a pulled micropipette, and each nerve infused with 3 μl of either lenti-MBP-shRNA or lenti-MBP-GFP (2.4×10^{11} virus particles per ml). After 4 weeks, the rats were transcardially perfused with 4% paraformaldehyde and the optic nerves from the globe to the optic chiasm carefully dissected. The optic nerve near the injection site was post-fixed in 4% paraformaldeyde, cryoprotected in 25% sucrose and cut on a cryostat. These nerve segments were later immunostained with OLIG2, GFAP and SMI-32. Optic nerve distal to the injection was post-fixed in 4% paraformaldehyde, 2.5% glutaraldehyde for 3 days and then processed for electron microscopy as described earlier.

Cre-dependent *MCT1* shRNA lentivirus injected into corpus callosum. Cre-inducible *MCT1* shRNA lentivirus was injected bilaterally into the corpus callosum of PLP-CreER[36], MCT1–tdTomato reporter, and wild-type mice at approximately 60 days of age. Mice were anaesthetized with ketamine and xylazine, placed in a stereotaxic device, and the corpus callosum injected bilaterally with 2 μl lentivirus (2.6×10^{11} virus particles per ml), as previously described[48]. After 1 week, mice were injected intraperitoneally with 1 mg tamoxifen for 5 consecutive days to induce Cre recombination of nucleus-integrated virus. Mice were euthanized 4 weeks later by transcardial perfusion with 4% paraformaldehyde. Sections were cryoprotected, sectioned on a cryostat, and immunostained for neurofilaments (SMI-32) and GFP, as described above.

Western blotting of human autopsy samples, primary cells and mouse tissues. Autopsy samples were obtained from the Johns Hopkins University Brain Resource Center and the Johns Hopkins ALS Tissue Bank. Human or mouse samples were homogenized in TBS with 0.1% SDS, 1% Triton and 10% glycerol, primary cultures were lysed as described previously[49]. Western blotting and densitometry was performed using the enhanced chemilluminescence (ECL) system (GE Healthcare) and NIH Image J.

Statistics. *In-vitro* ASO and MCT1i experiments were analysed using one-way ANOVA followed by Tukey–Kramer post-hoc test. Western blots, rtPCR, and *in-vivo* lenti-shRNA quantifications were analysed using unpaired Student's *t*-tests. Quantification of axon degeneration in lentivirus injections of optic nerve was evaluated with a Mann–Whitney test.

41. Brenner, M., Kisseberth, W. C., Su, Y., Besnard, F. & Messing, A. GFAP promoter directs astrocyte-specific expression in transgenic mice. *J. Neurosci.* **14,** 1030–1037 (1994).
42. Yang, Y. *et al.* Molecular comparison of GLT1$^+$ and ALDH1L1$^+$ astrocytes *in vivo* in astroglial reporter mice. *Glia* **59,** 200–207 (2011).
43. Doyle, J. P. *et al.* Application of a translational profiling approach for the comparative analysis of CNS cell types. *Cell* **135,** 749–762 (2008).
44. Buntinx, M. *et al.* Characterization of three human oligodendroglial cell lines as a model to study oligodendrocyte injury: morphology and oligodendrocyte-specific gene expression. *J. Neurocytol.* **32,** 25–38 (2003).
45. You, F., Osawa, Y., Hayashi, S. & Nakashima, S. Immediate early gene IEX-1 induces astrocytic differentiation of U87-MG human glioma cells. *J. Cell. Biochem.* **100,** 256–265 (2007).
46. Maekawa, F., Minehira, K., Kadomatsu, K. & Pellerin, L. Basal and stimulated lactate fluxes in primary cultures of astrocytes are differentially controlled by distinct proteins. *J. Neurochem.* **107,** 789–798 (2008).
47. Rothstein, J. D., Jin, L., Dykes-Hoberg, M. & Kuncl, R. W. Chronic inhibition of glutamate uptake produces a model of slow neurotoxicity. *Proc. Natl Acad. Sci. USA* **90,** 6591–6595 (1993).
48. McIver, S. R. *et al.* Lentiviral transduction of murine oligodendrocytes *in vivo*. *J. Neurosci. Res.* **82,** 397–403 (2005).
49. Yang, Y., Gozen, O., Vidensky, S., Robinson, M. B. & Rothstein, J. D. Epigenetic regulation of neuron-dependent induction of astroglial synaptic protein GLT1. *Glia* **58,** 277–286 (2010).

nature neuroscience

Degeneration and impaired regeneration of gray matter oligodendrocytes in amyotrophic lateral sclerosis

Shin H Kang[1,6,7], Ying Li[2,7], Masahiro Fukaya[3], Ileana Lorenzini[1,4], Don W Cleveland[5], Lyle W Ostrow[2,4], Jeffrey D Rothstein[1,2,4] & Dwight E Bergles[1]

Oligodendrocytes associate with axons to establish myelin and provide metabolic support to neurons. In the spinal cord of amyotrophic lateral sclerosis (ALS) mice, oligodendrocytes downregulate transporters that transfer glycolytic substrates to neurons and oligodendrocyte progenitors (NG2$^+$ cells) exhibit enhanced proliferation and differentiation, although the cause of these changes in oligodendroglia is unknown. We found extensive degeneration of gray matter oligodendrocytes in the spinal cord of SOD1 (G93A) ALS mice prior to disease onset. Although new oligodendrocytes were formed, they failed to mature, resulting in progressive demyelination. Oligodendrocyte dysfunction was also prevalent in human ALS, as gray matter demyelination and reactive changes in NG2$^+$ cells were observed in motor cortex and spinal cord of ALS patients. Selective removal of mutant SOD1 from oligodendroglia substantially delayed disease onset and prolonged survival in ALS mice, suggesting that ALS-linked genes enhance the vulnerability of motor neurons and accelerate disease by directly impairing the function of oligodendrocytes.

ALS is an adult-onset neurodegenerative disease characterized by progressive muscle weakness and eventual paralysis. Although disease culminates in the degeneration of motor neurons, non-neuronal cells such as astrocytes and microglia are critical for the pathogenic process of ALS[1–4]. ALS-linked genes such as *Sod1* are expressed in glia and motor neurons, and glial cell dysfunction appears to exacerbate injury to motor neurons, as selective removal of mutant SOD1 from subsets of glia slows disease progression[2,3]. However, the vulnerability of distinct populations of glial cells to disease-induced stress and the contributions of these alterations to the pathogenesis of ALS are not well understood.

Degeneration of motor neurons in the spinal cord is associated with reactive changes in surrounding glia that include cellular hypertrophy and enhanced proliferation. In particular, recent studies have found that the behavior of NG2$^+$ glial cells, a distinct, widely distributed class of progenitor cells that have the capacity to differentiate into oligodendrocytes, is markedly altered in the spinal cord of a mouse model of ALS (*SOD1 (G93A)*)[5,6]. By end stage of disease, NG2$^+$ cells exhibit the highest rate of proliferation of any cell type in the spinal cord of these mice, and their differentiation into oligodendrocytes is markedly enhanced[5], suggesting that there may be a progressive dysfunction of oligodendrocytes in ALS.

In addition to their role in forming myelin, there is emerging evidence that oligodendrocytes provide crucial metabolic support to neurons[7,8]. The monocarboxylic acid transporter 1 (MCT1), a transporter that motor neurons depend on for transfer of glycolytic substrates[9,10], is expressed predominantly by oligodendrocytes[9,11] and is downregulated in the motor cortex of ALS patients and the spinal cord of *SOD1 (G93A)* mice[9]. Together, these abnormalities in the oligodendrocyte lineage in ALS may affect motor neuron survival; however, the cause of the enhanced proliferation and differentiation of oligodendrocyte progenitors in *SOD1 (G93A)* mice, and the extent of oligodendrocyte abnormalities in human ALS[12,13] are uncertain.

Using *in vivo* genetic fate tracing of oligodendrocytes and their progenitors, we found an extensive, progressive degeneration of oligodendrocytes in the spinal cord of *SOD1 (G93A)* mice, with less than half of the oligodendrocytes produced in first postnatal month surviving by end stage of disease. Mobilization of oligodendrocyte progenitors occurred first in the ventral gray matter, where motor neurons are located, before behavioral manifestation of disease; however, newly formed oligodendrocytes in this region exhibited abnormal morphologies and failed to fully differentiate. Dysfunction of gray matter oligodendrocytes was also prevalent in human ALS, as reactive changes in NG2$^+$ cells and demyelination were observed in the gray matter of the ventral spinal cord and motor cortex of ALS patients. Genetic deletion of mutant human *SOD1* (G37R) from NG2$^+$ cells and their oligodendrocyte progeny in mice substantially delayed disease onset and prolonged survival, indicating that expression of this ALS-linked gene in the oligodendrocyte lineage accelerates motor neuron degeneration. The progressive loss of gray matter oligodendrocytes, and failure to restore these crucial cells, may accelerate disease progression in ALS by depriving motor neurons of essential metabolic support.

RESULTS

Enhanced proliferation of NG2$^+$ cells in young ALS mice

The progressive loss of motor neurons in *SOD1 (G93A)* mice is accompanied by prominent changes in the behavior of NG2$^+$ cells[5].

[1]The Solomon H. Snyder Department of Neuroscience, Johns Hopkins University School of Medicine, Baltimore, Maryland, USA. [2]Department of Neurology, Johns Hopkins University School of Medicine, Baltimore, Maryland, USA. [3]Department of Anatomy, Kitasato University School of Medicine, Sagamihara, Japan. [4]Brain Science Institute, Johns Hopkins University School of Medicine, Baltimore, Maryland, USA. [5]Ludwig Institute, University of California, San Diego, California, USA. [6]Present address: Shriners Hospital Pediatric Research Center, Department of Anatomy and Cell Biology, Temple University School of Medicine, Philadelphia, Pennsylvania, USA. [7]These authors contributed equally to this work. Correspondence should be addressed to J.D.R. (jrothstein@jhmi.edu) or D.E.B. (dbergles@jhmi.edu).

Received 23 December 2012; accepted 13 February 2013; published online 31 March 2013; doi:10.1038/nn.3357

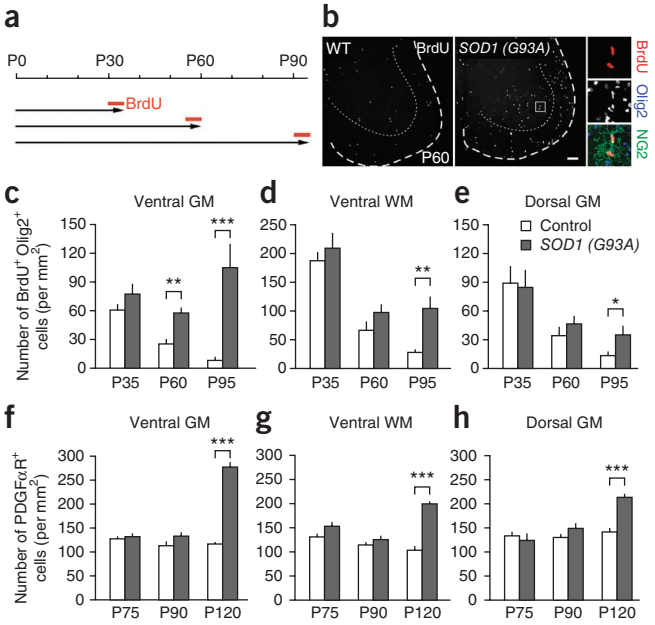

Figure 1 Enhanced proliferation of NG2$^+$ cells in the spinal cord of presymptomatic ALS mice. (**a**) BrdU protocol used to assess proliferation of NG2$^+$ cells in control and *SOD1 (G93A)* mice. (**b**) Fluorescence images showing BrdU$^+$ cells in the ventral horn of the spinal cord in control and *SOD1 (G93A)* mice at P60. Scale bar represents 100 µm. Right, two BrdU$^+$ NG2$^+$ cells (from the region highlighted by the white box) in the ventral gray matter. (**c**–**e**) Graphs showing the density of proliferating oligodendrocyte lineage cells (BrdU$^+$ Olig2$^+$) in different regions of spinal cord at different ages in control and *SOD1 (G93A)* mice. (**f**–**h**) Graphs showing the density of NG2$^+$ cells (PDGFαR$^+$) in different regions of the spinal cord at different stages of disease (P75 (presymptomatic), P90 (symptomatic) and P120 (end stage)), as compared with wild-type mice. GM, gray matter; WM, white matter. Data are presented as mean + s.e.m. ($n = 9$ sections obtained from 3 mice per group). $^*P < 0.05$, $^{**}P < 0.001$, $^{***}P < 0.0005$, unpaired Student's *t* test.

By end stage of disease, their proliferation rate is 20-fold higher than in wild-type mice[5], and they comprise the majority of actively dividing cells in the spinal cord[5,6]. However, the cause of this enhanced proliferation in ALS is unknown. To determine when and where NG2$^+$ cells first exhibit this altered behavior, we examined the spatiotemporal profile of NG2$^+$ cell proliferation over the course of disease. Mice were administered BrdU for 5 d and cumulative BrdU incorporation was measured in lumbar spinal cord (**Fig. 1a**,**b** and **Supplementary Fig. 1a**). In wild-type mice, the number of BrdU$^+$ NG2$^+$ cells declined with age in all of the regions that were examined ($P < 0.001$, one-way ANOVA; **Fig. 1c**–**e**), following the developmental decline in the generation of oligodendrocytes from these progenitors[5,14,15]. However, in *SOD1 (G93A)* mice, NG2$^+$ cells sustained high rates of proliferation into adulthood (**Fig. 1c**–**e**). Moreover, unlike the uniform decline in proliferation in wild-type mice, NG2$^+$ cells in *SOD1 (G93A)* mice exhibited regional differences in their response. Enhanced proliferation was most prominent in ventral gray matter, where their rate of division was elevated 2.3-fold compared with wild-type mice by postnatal day 60 (P60, $P < 0.001$, Student's *t* test), before *SOD1 (G93A)* mice show disease symptoms[16], and 12.9-fold by P95 ($P < 0.0005$), after they exhibit muscle weakness and tremor[17]. NG2$^+$ cells in ventral white and dorsal gray matter of ALS mice eventually exhibited enhanced proliferation, although it occurred later and the magnitude of increased cell division was lower than in ventral gray matter (**Fig. 1c**–**e**). Thus, NG2$^+$ cells in *SOD1 (G93A)* mice display abnormal behavior in ventral gray matter before behavioral manifestation of disease.

Despite the enhanced generation of NG2$^+$ cells in early stages of disease, their density was not significantly altered before end stage ($P > 0.05$; **Fig. 1f**–**h**), suggesting that they are continually removed through death or differentiation. To determine the fate of NG2$^+$ cells at early stages of disease, we carried out genetic lineage tracing with *Pdgfra-creER; Z/EG* mice[5]. After breeding to *SOD1 (G93A)* mice, we administered 4-hydroxytamoxifen (4HT) at P30 or P60 to induce EGFP expression in cohorts of NG2$^+$ cells, and identified EGFP$^+$ cells in lumbar spinal cord 15–60 d later (**Fig. 2a** and **Supplementary Fig. 1b**,**c**). Consistent with the regional differences in NG2$^+$ cell proliferation, more EGFP$^+$ cells were observed in ventral gray matter by P90 in *SOD1 (G93A)* mice (**Fig. 2b** and **Supplementary Fig. 1d**–**f**), whereas the number of EGFP$^+$ cells in other areas was not significantly increased relative to controls ($P > 0.05$). However, by end stage, EGFP$^+$ cell density in *SOD1 (G93A)* mice was higher than controls in all of the regions examined, with ventral gray matter exhibiting the greatest accumulation of NG2$^+$ cell progeny (**Supplementary Fig. 1d**–**f**). As the number of EGFP$^+$ cells should remain constant if they have an equal probability of dividing or dying, these results suggest that the enhanced proliferation of NG2$^+$ cells is not induced solely by accelerated death of these progenitors.

Oligodendrogenesis without oligodendrocyte accumulation

NG2$^+$ cells in the spinal cord of end stage *SOD1 (G93A)* mice not only proliferate more rapidly, but also differentiate more frequently into oligodendrocytes[5]. To determine where and when this increase in oligodendrogenesis occurs, we followed the appearance of EGFP$^+$ cells in *Pdgfra-creER; Z/EG; SOD1 (G93A)* and *Pdgfra-creER; Z/EG* mice that were immunoreactive to antibody to APC (CC1), a feature of mature oligodendrocytes. Consistent with the early maturation of myelinated tracts in the spinal cord[18], few oligodendrocytes (EGFP$^+$ CC1$^+$ cells) were generated from P60–120 in controls (**Fig. 2c**–**h**). In contrast, there was a marked increase in newly generated oligodendrocytes in ventral gray matter of *SOD1 (G93A)* mice ($P < 0.001$, one-way ANOVA; **Fig. 2c**–**f**); there were 10.9-fold more EGFP$^+$ CC1$^+$ cells in this region relative to wild-type mice 60 d after labeling ($P < 0.0005$, Student's *t* test; **Fig. 2f**).

An increase in EGFP$^+$ oligodendrocytes also was observed in ventral white matter at P90 and end stage in ALS mice, although this increase was smaller than in ventral gray matter (**Fig. 2g**), and there was no significant change ($P > 0.05$) in EGFP$^+$ oligodendrocytes relative to control in dorsal gray matter (**Fig. 2g**,**h**). As the fate of only a small fraction (~15%) of NG2$^+$ cells was followed in these experiments, the total number of oligodendrocytes generated during this period is expected to be much greater (by ~6–7-fold). Despite this marked increase in oligodendrogenesis, the overall density of oligodendrocytes in the spinal cord of *SOD1 (G93A)* mice at end stage was unchanged relative to wild type (**Fig. 2i**). These results suggest that there must be a concomitant loss of oligodendrocytes with advancing disease.

Degeneration of early-born oligodendrocytes in ALS mice

To determine the extent of oligodendrocyte survival during the course of disease, we performed genetic fate tracing of oligodendrocytes using *Plp1-creER; ROSA26-EYFP; SOD1 (G93A)* and *Plp1-creER; ROSA26-EYFP* mice (**Fig. 3a**,**b**). Administration of 4HT at P35 resulted in labeling of 15–25% of oligodendrocytes in ventral gray and white matter regions of the spinal cord. Although Cre-mediated recombination

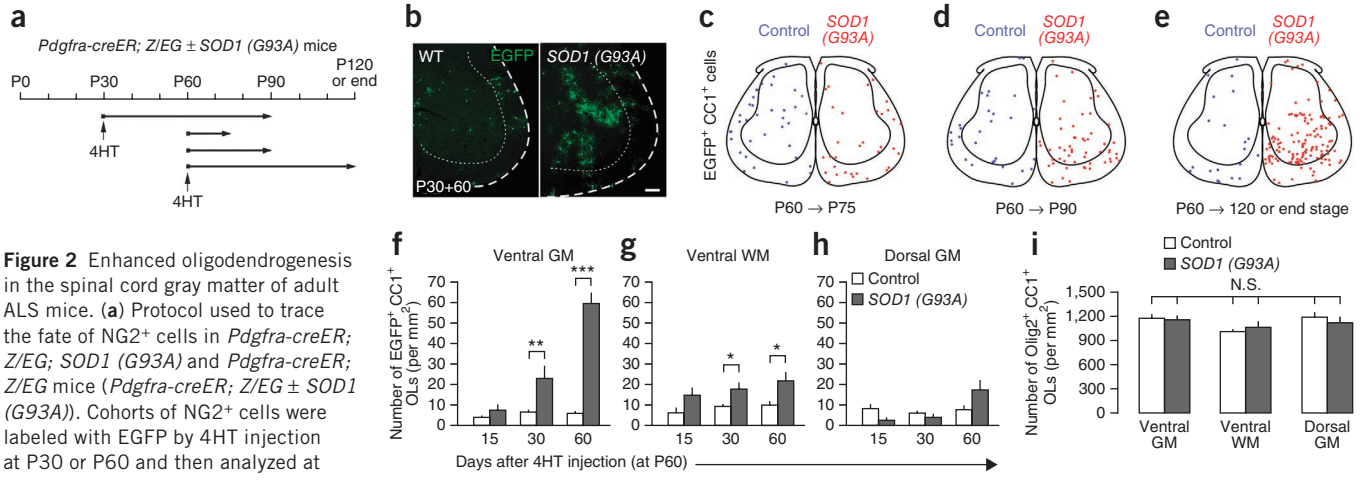

Figure 2 Enhanced oligodendrogenesis in the spinal cord gray matter of adult ALS mice. (**a**) Protocol used to trace the fate of NG2+ cells in *Pdgfra-creER; Z/EG; SOD1 (G93A)* and *Pdgfra-creER; Z/EG* mice (*Pdgfra-creER; Z/EG ± SOD1 (G93A)*). Cohorts of NG2+ cells were labeled with EGFP by 4HT injection at P30 or P60 and then analyzed at different ages. (**b**) Fluorescence images showing EGFP+ NG2+ cell progeny in the ventral horn of the spinal cord in control or *SOD1 (G93A)* mice 60 d after 4HT administration at P30 (P30+60). Scale bar represents 100 μm. (**c**–**e**) Maps of the location of adult born oligodendrocytes generated from NG2+ cells in the spinal cord of control and *SOD1 (G93A)* mice from P60–75 (**c**), P60–90 (**d**) or P60–120 (or end stage for ALS mice, **e**). Oligodendrocytes (EGFP+ CC1+) in four randomly sampled lumbar spinal cord sections from each group (from 3–4 mice) are shown. (**f**–**h**) Graphs showing the density of newly generated EGFP+ CC1+ oligodendrocytes (OLs) in different regions of the adult spinal cord from control and *SOD1 (G93A)* mice. Data are presented as mean + s.e.m. ($n = 9$ sections from 3 mice per group). $^*P < 0.05$, $^{**}P < 0.001$, $^{***}P < 0.0005$, unpaired Student's t test. (**i**) Graph showing the overall density of oligodendrocytes (Olig2+ CC1+) in different regions of the spinal cord of P120 and end-stage *SOD1 (G93A)* mice. Data are presented as mean + s.e.m. ($n = 12$ sections per group from 4 mice per group) N.S., non-significant, $P > 0.05$, one-way ANOVA with Tukey test.

occurs in some NG2+ cells in the brains of *Plp1-creER; ROSA26-EYFP* mice[19], EYFP was not expressed by these progenitors in the spinal cord of either control or *SOD1 (G93A)* mice (**Supplementary Fig. 2**), indicating that this approach can be used to track the survival of spinal cord oligodendrocytes *in vivo*. Quantitative analysis of spinal cords sampled at early time points revealed that the number of EYFP+ oligodendrocytes increased gradually for the first 2 weeks after 4HT administration in both control and *SOD1 (G93A)* mice[19], and initial labeling of these cells was substantially higher in *SOD1 (G93A)* mice than in control mice in ventral gray matter (at P35+15), possibly reflecting enhanced activity of the *Plp1* transgene promoter. To allow direct comparison of oligodendrocyte survival between control and *SOD1 (G93A)* mice, we normalized the number of EYFP-labeled oligodendrocytes in each cohort to that observed at P35+15, when oligodendrocyte labeling in *SOD1 (G93A)* mice was near maximum (**Fig. 3c**,**d**). In control mice, there was a small increase in EYFP+ oligodendrocytes in lumbar spinal cord (EYFP+ CC1+ Olig2+) 40 and 70 d after initial labeling (at P50) (**Fig. 3c**), indicating a modest, but continuous, labeling of oligodendrocytes during this period. In contrast, the number of EYFP+ oligodendrocytes in *SOD1 (G93A)* mice was reduced by 22% at 40 d after labeling ($P < 0.05$, one-way ANOVA with Tukey; **Fig. 3c**). This loss was progressive, as the number of labeled oligodendrocytes was reduced by 65% at end stage ($P < 0.0005$, one-way ANOVA; **Fig. 3c**,**e**). Moreover, as expected from the regional

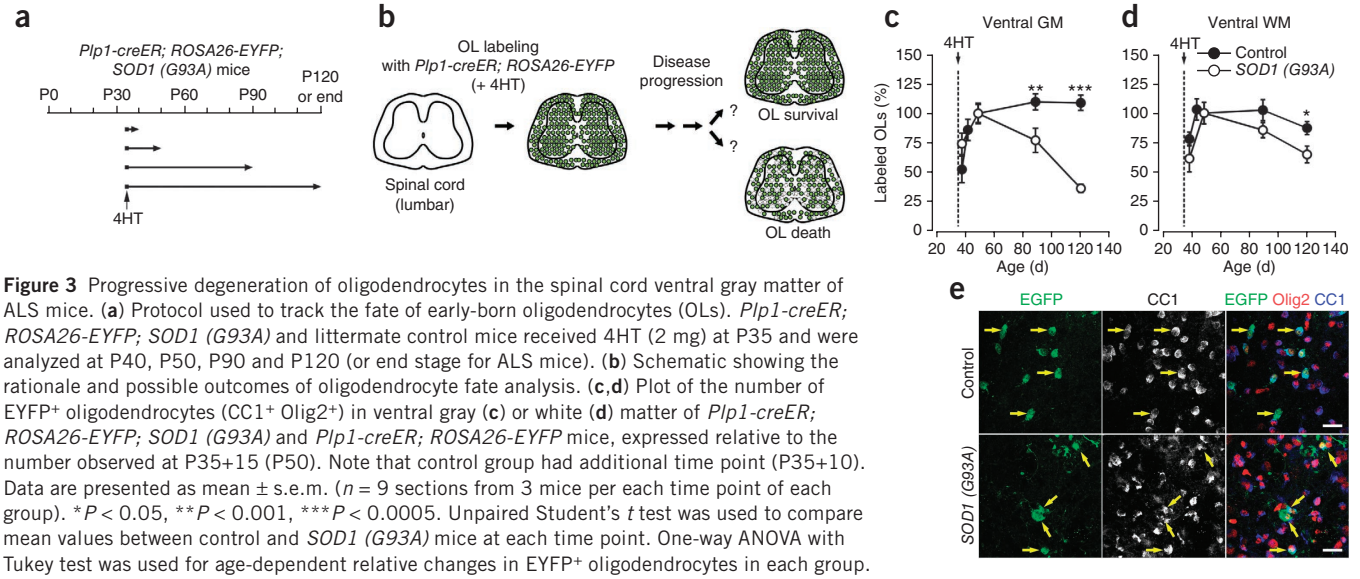

Figure 3 Progressive degeneration of oligodendrocytes in the spinal cord ventral gray matter of ALS mice. (**a**) Protocol used to track the fate of early-born oligodendrocytes (OLs). *Plp1-creER; ROSA26-EYFP; SOD1 (G93A)* and littermate control mice received 4HT (2 mg) at P35 and were analyzed at P40, P50, P90 and P120 (or end stage for ALS mice). (**b**) Schematic showing the rationale and possible outcomes of oligodendrocyte fate analysis. (**c**,**d**) Plot of the number of EYFP+ oligodendrocytes (CC1+ Olig2+) in ventral gray (**c**) or white (**d**) matter of *Plp1-creER; ROSA26-EYFP; SOD1 (G93A)* and *Plp1-creER; ROSA26-EYFP* mice, expressed relative to the number observed at P35+15 (P50). Note that control group had additional time point (P35+10). Data are presented as mean ± s.e.m. ($n = 9$ sections from 3 mice per each time point of each group). $^*P < 0.05$, $^{**}P < 0.001$, $^{***}P < 0.0005$. Unpaired Student's t test was used to compare mean values between control and *SOD1 (G93A)* mice at each time point. One-way ANOVA with Tukey test was used for age-dependent relative changes in EYFP+ oligodendrocytes in each group. (**e**) Confocal images showing the density and morphology of EYFP+ (stained with antibody to EGFP) CC1+ Olig2+ spinal cord oligodendrocytes (yellow arrows) in ventral gray matter at P120 (control) or at end stage *SOD1 (G93A)* mice. Scale bars represent 20 μm.

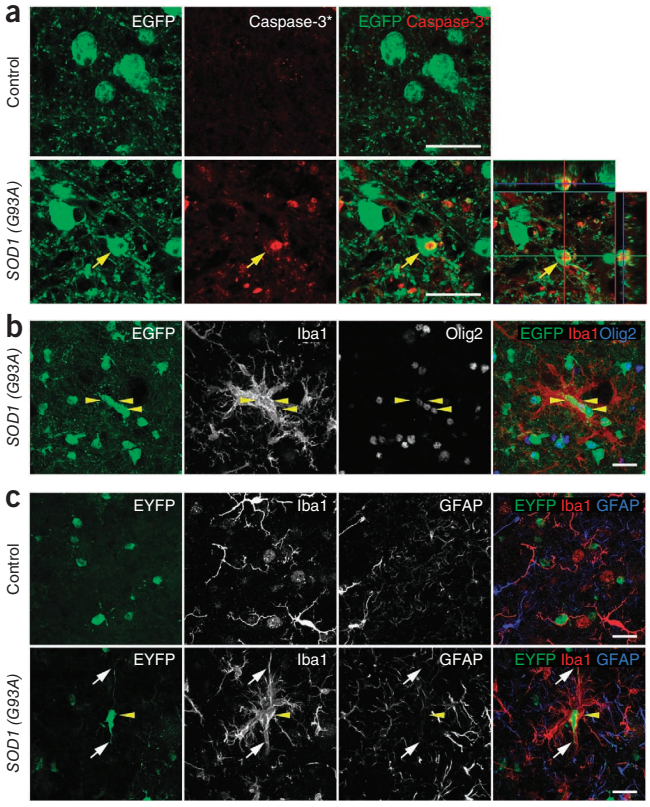

Figure 4 Apoptosis of oligodendrocytes in the spinal cord of ALS mice. (**a**) Confocal images from the spinal cord ventral gray matter of a *Mobp-EGFP; SOD1 (G93A)* mouse at end stage showing an EGFP$^+$ oligodendrocyte (yellow arrows) that was immunopositive for activated caspase-3. Lower right panel is an orthogonal view showing colocalization of activated caspase-3 and EGFP. (**b**,**c**) Confocal images of the spinal cord ventral gray matter showing Iba1$^+$ activated microglia surrounding oligodendrocytes labeled with EGFP (**b**) or EYFP (**c**) in *Mobp-EGFP; SOD1 (G93A)* (P90) or *Plp1-creER; ROSA26-EYFP; SOD1 (G93A)* (P30+60) mice, respectively. Yellow arrowheads highlight several labeled oligodendrocytes, and white arrows in **c** highlight the processes of one EYFP$^+$ oligodendrocyte. Scale bars represent 20 μm.

difference in NG2$^+$ cell proliferation and oligodendrogenesis, loss of early-born oligodendrocytes in ALS mice was most prominent in ventral gray matter (**Fig. 3c**,**d**). These results indicate that there is already pronounced degeneration of oligodendrocytes in ventral gray matter near motor neurons when mice first exhibit overt signs of disease.

If oligodendrocytes degenerate in the spinal cord of ALS mice, other indications of cell death should be visible. Indeed, some EGFP-expressing oligodendrocytes were immunopositive for activated caspase-3 in the spinal cord of end stage *Mobp-EGFP; SOD1 (G93A)* mice (**Fig. 4a**), in which only mature oligodendrocytes express EGFP (**Supplementary Fig. 3**). Moreover, we observed dense cell clusters consisting of EGFP$^+$ oligodendrocytes surrounded by activated microglial cells at P90 in ventral gray matter (**Fig. 4b**). Consistent with the death of early born oligodendrocytes observed through genetic fate tracing, we found similar microglia-oligodendrocyte (EYFP$^+$) aggregates in P90 *Plp1-creER; ROSA26-EYFP; SOD1 (G93A)* mice, in which oligodendrocytes were labeled at P35 (P35+55) (**Fig. 4c**); however, we did not find microglial clustering near GFAP$^+$ astrocytes (**Fig. 4c**). Given that microglia are attracted to apoptotic cells[20], the presence of these cell aggregates may indicate that mature oligodendrocytes in this region are dying via apoptotic death.

Widespread axonal degeneration can lead to loss of oligodendrocytes and reactive changes in their progenitors[21,22], raising the possibility that degeneration of gray matter oligodendrocytes in ALS mice is secondary to motor neuron degeneration. To address whether loss of motor neurons is sufficient to induce mobilization of NG2$^+$ cells, we partially ablated motor neurons by injecting ricin into the sciatic nerve[23]. Approximately half of the motor neurons in the ventral horn degenerated on the side ipsilateral to the injection by 1 week after this manipulation ($P < 0.0005$, paired Student's t test; **Supplementary Fig. 4a–c**). However, neither the morphology nor the proliferation rate of NG2$^+$ cells, as assessed by NG2 and Ki67 immunoreactivity, respectively, was altered by this loss of motor neurons (**Supplementary Fig. 4b**,**d**), suggesting that acute motor neuron death is not sufficient to induce activation and recruitment of these progenitors.

To determine when oligodendrocytes begin to exhibit abnormalities in ALS mice, we examined their morphology in *Mobp-EGFP; SOD1 (G93A)* and *Mobp-EGFP* mice at different stages of disease. Oligodendrocyte somata (EGFP$^+$ Olig2$^+$) in the spinal cord of *Mobp-EGFP* mice had a consistent oval shape (**Fig. 5a**,**b** and **Supplementary Fig. 3**). In the spinal cord of end stage *Mobp-EGFP; SOD1 (G93A)* mice, there was a marked increase in irregularly shaped EGFP$^+$ structures, many of which were Olig2$^-$ and lacked nuclei (**Fig. 5a**,**b** and **Supplementary Fig. 5a**), reminiscent of the fragmentation that occurs during apoptotic cell death[24]. Despite this increase in EGFP$^+$ structures, the density of EGFP$^+$ Olig2$^+$ oligodendrocytes in end stage *SOD1 (G93A)* mice was not different from that in control mice (control, 1,137 ± 61 cells; *SOD1 (G93A)*, 1,233 ± 73 cells per mm^2; $n = 9$ sections, 3 mice per group, $P = 0.33$, Student's t test), consistent with results obtained using CC1 immunoreactivity (**Fig. 2i**). We also observed irregularly shaped EGFP$^+$ oligodendrocyte somata with reduced or absent Olig2 immunoreactivity at earlier stages of disease (**Supplementary Fig. 5b**,**c**). To evaluate the progressive nature of these changes, we measured the area of EGFP$^+$ cell fragments following digital subtraction of EGFP$^+$ Olig2$^+$ somata (**Supplementary Fig. 5d**). EGFP$^+$ cellular fragments were evident at P90 in *SOD1 (G93A)* mice, but were rarely observed in aged matched controls (volume of fragments: control, 10 ± 5.1 μm^3; *SOD1 (G93A)*, 131 ± 13 μm^3; $P < 7.9 \times 10^{-6}$, Student's t test; **Fig. 5c**), indicating that pathological alterations in oligodendrocytes are widespread by the time mice begin to show behavioral manifestation of disease.

Myelin deficits in spinal cord gray matter of ALS mice

The accelerated turnover (that is, death and subsequent regeneration) and abnormal structure of oligodendrocytes in ALS mice suggests that the state of myelination in gray matter may be altered in disease. Indeed, electron microscopic analysis of ventral gray matter revealed that the proportion of ultrastructurally normal axons with immature myelin, as evidenced by the presence of a thick layer of oligodendrocyte cytoplasm between the axon and initial myelin wraps, was 49% higher in end stage *SOD1 (G93A)* mice than in age-matched controls (percentage of axons with immature myelin: control, 9.3 ± 1.2%; *SOD1 (G93A)*, 13.9 ± 1.0%; $n = 3$ mice per group, $P < 0.01$, unpaired Student's t test; **Fig. 6a**), suggesting that viable, uninjured axons were being remyelinated in ALS mice. Axons with disorganized microtubules, electron dense bodies and spheroids surrounded by swollen, electron dense myelin, typical of Wallerian degeneration[17], were also common in the ventral gray matter of *SOD1 (G93A)* mice (**Supplementary Fig. 6a**). Moreover, myelin basic protein (MBP) immunoreactivity was more diffuse in ventral gray matter of *SOD1 (G93A)* mice at end stage and was often not colocalized with EGFP, in contrast with the filamentous EGFP$^+$ processes present in

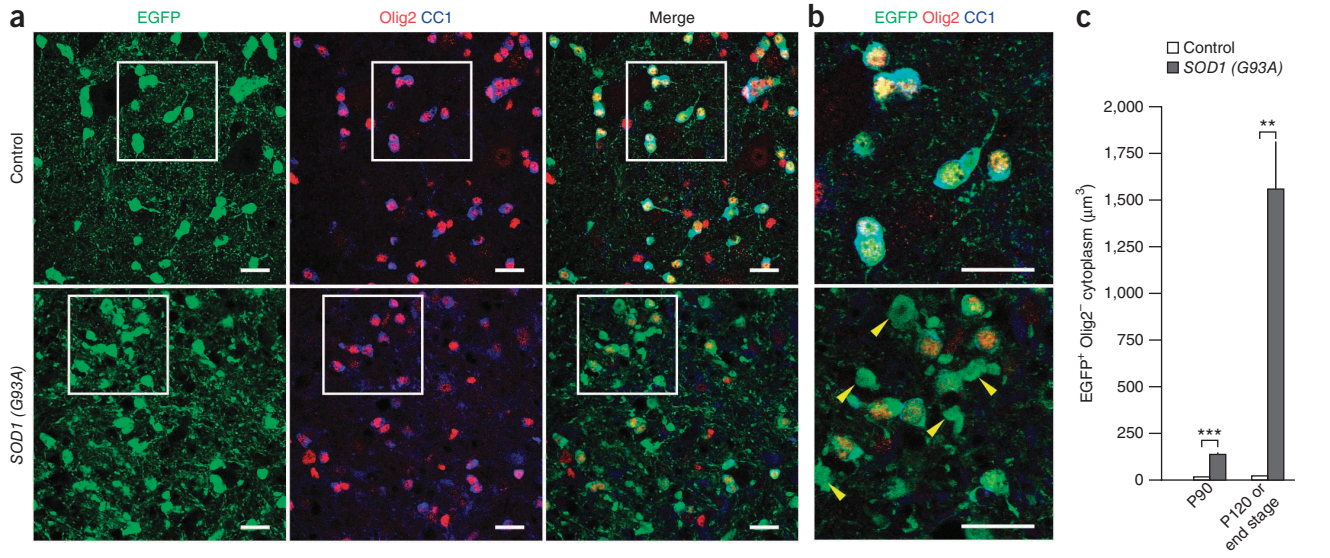

Figure 5 Early disruption of oligodendrocyte structure in the spinal cord of ALS mice. (**a**) Confocal images of EGFP$^+$ structures in the ventral spinal cord gray matter from control *Mobp-EGFP* (P120) and *Mobp-EGFP; SOD1 (G93A)* mice (end stage). (**b**) Higher magnification of regions highlighted by white squares in **a**. Arrowheads indicate large EGFP$^+$ structures that were Olig2$^-$ and CC1$^-$. Scale bars represent 20 μm. (**c**) Measured volume of Olig2$^-$ EGFP$^+$ fragments in each 250,000 μm^3 imaged volume. Data are presented as mean + s.e.m. (n = 6–9 sections from 3 mice per group). $^{**}P = 1.5 \times 10^{-5}$, $^{***}P = 8 \times 10^{-6}$, unpaired Student's t test.

Mobp-EGFP mice (**Fig. 6b**). Axons with mature myelin had thicker myelin sheaths and lower g ratios (ratio of axon diameter to myelin diameter) in *SOD1 (G93A)* mice than those in control mice (**Supplementary Fig. 6b–d**), possibly reflecting shrinkage of axons from metabolic stress or abnormal patterns of gene expression in oligodendrocytes.

To determine the structure of oligodendrocytes generated after P60, we used membrane-anchored EGFP Cre reporter mice (*ROSA26-mEGFP*, *mT/mG*) to visualize their fine cellular processes[5]. *Pdgfra-creER; ROSA26-mEGFP; SOD1 (G93A)* and *Pdgfra-creER; ROSA26-mEGFP* mice were injected with 4HT at P60 and analyzed 2 months later (**Fig. 6c**). In control mice (P60+60), numerous thin, unbranched EGFP$^+$ processes were visible throughout the ventral gray matter, consistent with the morphology of normal internodal segments (**Fig. 6d**). Although oligodendrocytes generated after P60 in

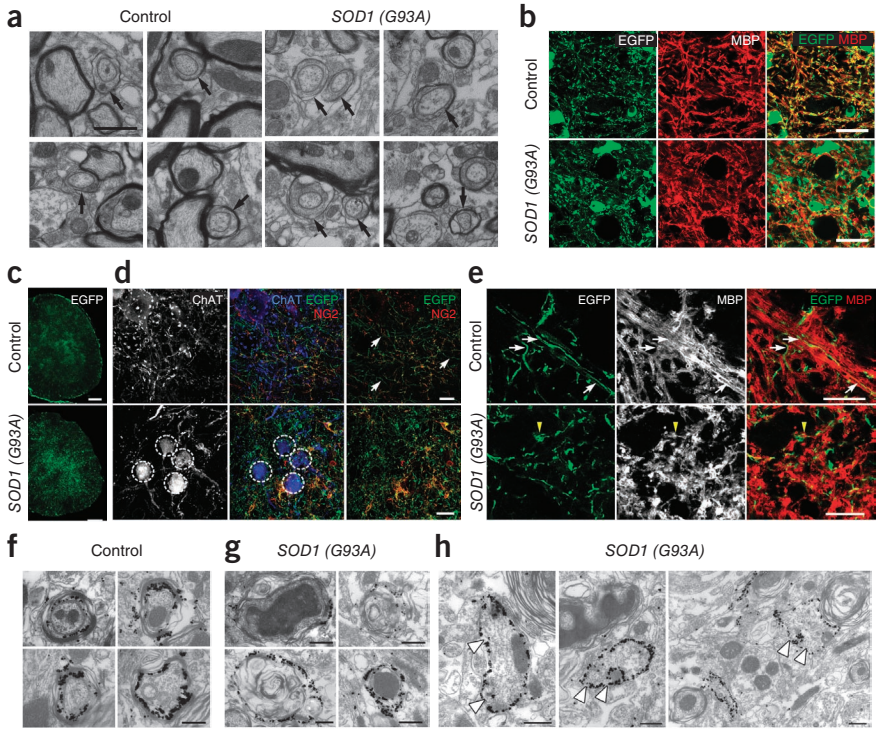

Figure 6 Myelin abnormalities and impaired maturation of adult-born oligodendrocytes in the spinal cord of ALS mice. (**a**) Electron micrographs of ventral gray matter spinal cord of control (P120) and *SOD1 (G93A)* mice at end stage. Arrows highlight partially myelinated axons. Note the presence of thick oligodendrocyte cytoplasm surrounding these axons. (**b**) Confocal images of MBP immunoreactivity in ventral gray matter of P120 *Mobp-EGFP* mice or end stage *Mobp-EGFP; SOD1 (G93A)* mice. Optical sections: 1.5 μm. (**c**) Fluorescent images of membrane-anchored EGFP in the spinal cord of *Pdgfra-creER; ROSA26-mEGFP* mice (P60+60). (**d**) Confocal images showing fine EGFP$^+$ processes of adult-born oligodendrocytes in ventral gray matter of *Pdgfra-creER; ROSA26-mEGFP; SOD1 (G93A)* and *Pdgfra-creER; ROSA26-mEGFP* mice (P60+60). Circles indicate ChAT$^+$ motor neuron cell bodies and white arrows indicate NG2$^-$ oligodendrocyte processes. (**e**) Confocal images showing colocalization of EGFP$^+$ thin processes and MBP immunoreactivity (white arrows) in control *Pdgfra-creER; ROSA26-mEGFP* mice (P60+60, top). MBP immunoreactivity was more disorganized in *Pdgfra-creER; ROSA26-mEGFP; SOD1 (G93A)* mice (bottom) and rarely colocalized with EGFP$^+$ processes (P60+60) (yellow arrowheads). Optical sections: 0.5 μm. (**f–h**) Thin section electron micrographs from *Pdgfra-creER; ROSA26-mEGFP; SOD1 (G93A)* and *Pdgfra-creER; ROSA26-mEGFP* mice at P60+60 showing silver-intensified gold labeling of EGFP$^+$ oligodendrocyte processes. Large, non-myelinating EGFP$^+$ structures (arrowheads) reminiscent of apoptotic bodies were observed frequently in *SOD1 (G93A)* mice (**h**). Scale bars represent 1 μm (**a**), 20 μm (**b**,**d**,**e**), 200 μm (**c**) and 500 nm (**f–h**).

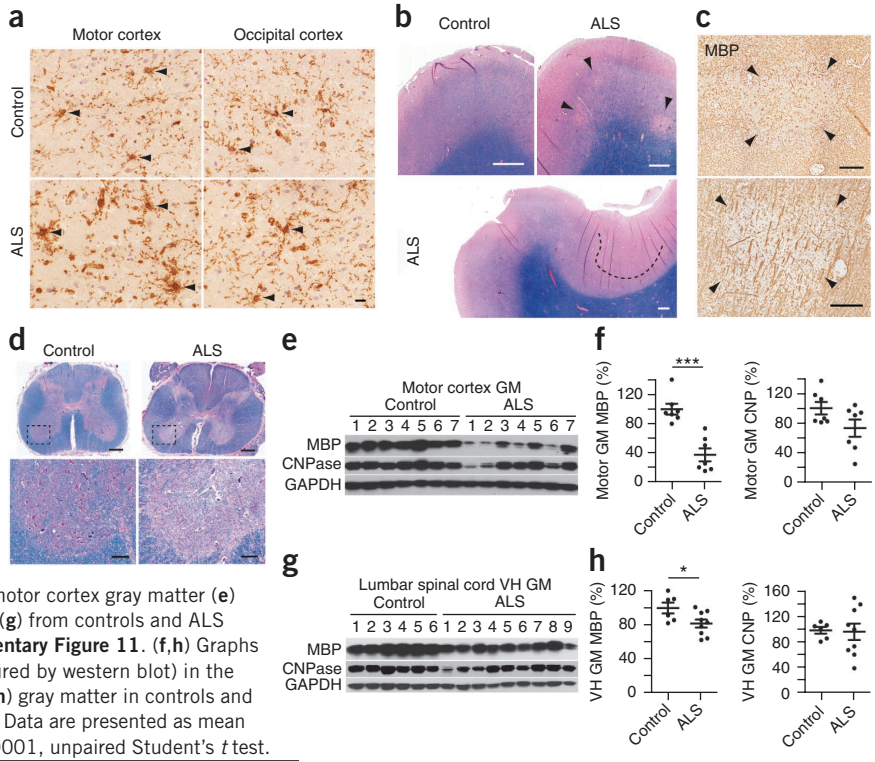

Figure 7 Demyelination in gray matter regions of the motor cortex and spinal cord in human ALS. (**a**) Sections of motor cortex gray matter from control and ALS patients showing immunoreactivity to NG2. NG2$^+$ cells are highlighted by arrowheads (see **Supplementary Fig. 8a**). Images were acquired from cortical layers IV and V. Scale bar represents 20 µm. (**b**) Luxol fast blue staining of motor cortices from control subjects and ALS patients. Demyelinated lesions are highlighted by arrowheads (upper right) or a dashed line (bottom). (**c**) MBP immunoreactivity in ALS motor cortex. Adjacent sections to those shown in the upper right and lower panels in **b** were used. Images show demyelinated plaques in layer III (top) and layer V (bottom). (**d**) Sections of lumbar spinal cord from an ALS patient stained with Luxol fast blue showing demyelination in the ventral horn gray matter and lateral corticospinal tract (arrowhead). Lower panels are higher magnification images of the boxed regions in the upper panels. Scale bars represent 1 mm (**b** and upper panels of **d**) and 200 µm (**c** and lower panels of **d**). (**e**,**g**) Western blots of oligodendrocyte lineage–specific myelin proteins in motor cortex gray matter (**e**) and lumbar spinal cord ventral horn (VH) gray matter (**g**) from controls and ALS patients. Full-length blots are presented in **Supplementary Figure 11**. (**f**,**h**) Graphs of MBP and CNPase protein expression levels (measured by western blot) in the motor cortex (**f**) and lumbar spinal cord ventral horn (**h**) gray matter in controls and ALS patients, normalized to average value in controls. Data are presented as mean ± s.e.m. with individual values. $^*P < 0.05$, $^{***}P < 0.0001$, unpaired Student's *t* test.

SOD1 (G93A) mice also expressed CC1 (**Fig. 2c–e**), their processes were highly branched with numerous varicosities (**Fig. 6d**); the processes of these newly generated oligodendrocytes often did not colocalize with MBP, in contrast with oligodendrocyte processes in control mice (**Fig. 6e**). Immunogold electron microscopic labeling of EGFP revealed that adult-born oligodendrocytes in *SOD1 (G93A)* mice were frequently associated with degenerating axons (**Fig. 6f**,**g**), suggesting that these axons had experienced at least one round of demyelination and remyelination. In addition, there were many irregularly shaped, immunogold-positive structures in *SOD1 (G93A)* mice that were not associated with axons (**Fig. 6h**), reminiscent of the oligodendrocyte fragmentation observed through confocal microscopy (**Fig. 5b**). Thus, oligodendrocytes generated in this disease context do not achieve the normal structure of myelinating oligodendrocytes.

Western blot analysis revealed that the protein levels of myelin-associated proteins MBP, CNPase (2′,3′-cyclic nueotide-3′-phosphodiesterase) and MOG (myelin-oligodendrocyte glycoprotein) progressively decreased with age (**Supplementary Fig. 7a**,**b**), with the mature myelin protein MOG exhibiting the earliest decline by P60; this reduction in myelin was most prominent in ventral gray matter (**Supplementary Fig. 7c**). The decrease in myelin protein expression was accompanied by a concomitant increase in PDGFαR expression in both symptomatic (P90) and end stage mice (**Supplementary Fig. 7a**,**b**). Although NG2$^+$ cell density in the spinal cord of *SOD1 (G93A)* mice was not significantly changed ($P > 0.05$) at earlier stages of disease (**Fig. 2f–h**), the increased expression of PDGFαR from P90 is consistent with progressive mobilization of these progenitors in response to the loss of oligodendrocytes[25–27]. Together, these findings indicate that myelination is disrupted in the spinal cord ventral gray matter of ALS mice.

Reactive NG2$^+$ cells and focal gray matter demyelination in ALS

NG2$^+$ cells are abundant in the human CNS and are likely to be major contributors to the regeneration of oligodendrocytes in demyelinating diseases such as multiple sclerosis[28]. To determine whether NG2$^+$ cells also undergo reactive changes in ALS patients, we carried out immunohistochemistry on human motor cortices. We analyzed motor cortex rather than spinal cord, as this tissue is better preserved in human autopsies, which is required to preserve the NG2 proteoglycan. Sections were immunostained for the microglial antigen Iba1 to distinguish NG2$^+$ glial cells from NG2-expressing macrophages and microglia that often appear in chronic disease and CNS injury[29,30]. NG2 immunoreactivity was markedly higher in the motor cortex of ALS patients than in either motor cortex from non-ALS subjects (control, 106.2 ± 5.3%; ALS, 200.2 ± 9.4%; $P < 0.0001$, unpaired Student's *t* test) or occipital cortex from the same patients, as determined by the intensity of NG2 immunoreactivity (**Fig. 7a** and **Supplementary Fig. 8a**,**b**). Although NG2$^+$ Iba1$^+$cells were observed in both control and ALS motor cortex, thicker NG2$^+$ processes that exhibited signs of hypertrophy in ALS tissue did not express Iba1 (**Supplementary Fig. 8a**), indicating that NG2$^+$ glial cells exhibit reactive changes in regions of brain in which motor neurons degenerate in ALS.

To assess whether these changes in NG2$^+$ cells also were associated with degeneration of oligodendrocytes in gray matter, we examined the integrity of myelin in motor cortex and spinal cord of sporadic and familial ALS patients. Myelin staining (Luxol fast blue) and MBP immunolabeling revealed areas of focal loss of myelin in motor cortex gray matter of ALS patients that were not observed in control patients (**Fig. 7b**,**c** and **Supplementary Table 1**). Moreover, in addition to the well-described reduction in myelination of corticospinal tracts, myelin was also reduced in ventral horn gray matter of the spinal cord from ALS patients (**Fig. 7d**). To quantify the extent of myelin loss, we determined MBP and CNPase abundance in randomly sampled regions of primary motor cortex gray matter (**Fig. 7e**,**f** and **Supplementary Fig. 8c**,**d**), as well as in spinal cord ventral gray matter (**Fig. 7g**,**h**). MBP expression was significantly lower ($P < 0.001$ and $P < 0.05$ for motor cortex and spinal cord ventral horn, respectively) in most ALS patients relative to controls, whereas CNPase levels were substantially reduced in one patient and trended lower in a second patient. Furthermore, the

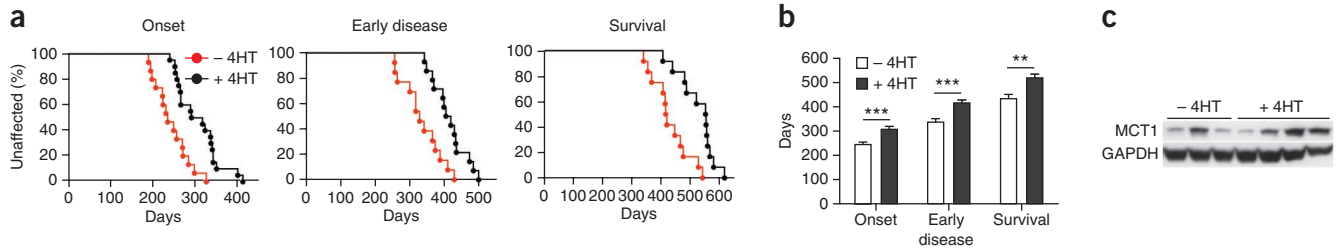

Figure 8 Excision of mutant SOD1 (G37R) from NG2$^+$ cells delays disease onset and prolongs survival in ALS mice. (**a**) Plots of disease onset (median: –4HT, 235 d (n = 15); +4HT, 304 d (n = 20); P = 0.0003, log-rank test), early disease (median: –4HT, 330 d (n = 13); +4HT, 413 d (n = 14); P = 0.001) and survival (median: –4HT, 419 d (n = 12); +4HT, 554 d (n = 14); P = 0.0005) of *Pdgfra-creER; loxSOD1(G37R)* mice. (**b**) Comparison of mean age at disease onset (–4HT, 244 ± 10 d; +4HT, 307 ± 11 d; P = 0.0005), early disease (–4HT, 336 ± 16 d; +4HT, 415 ± 13 d; P = 0.001) and survival (–4HT, 433 ± 18 d; +4HT, 518 ± 16 d; P = 0.0025,). Data are presented as mean + s.e.m. $^{**}P < 0.01$, $^{***}P < 0.005$, Mann-Whitney test. (**c**) Western blots of MCT1 expression from several –4HT and +4HT mice examined at disease onset. Full-length blots are presented in **Supplementary Figure 11**.

reduction in expression of myelin proteins was greater in motor cortices than in occipital cortices from the same ALS patients, consistent with motor cortex specific lesions (**Supplementary Fig. 8c**,**d**). Although it is not yet possible in these tissues to determine the relative contributions of primary oligodendrocyte death and secondary oligodendrocyte death because of Wallerian degeneration, these results indicate that demyelination of gray matter regions in which motor neurons are located is a common feature of human ALS.

Mutant SOD1 deletion from oligodendroglia reduces disease

Oligodendrocytes are vulnerable to damage through cell-autonomous expression of genes linked to neurodegeneration[31,32], particularly aggregation-prone proteins, raising the possibility that expression of mutant SOD1 in oligodendrocytes may impair their function and promote motor neuron degeneration. To determine whether there is an oligodendroglial contribution to disease in ALS, we selectively removed mutant human SOD1 (G37R) from NG2$^+$ cells in *Pdgfra-creER; loxSOD1(G37R)* mice[2]. Administration of 4HT to these mice at P18 and P30 markedly delayed disease onset by 69 d (median, P = 0.0003), delayed early disease by 83 d (median, P = 0.001) and prolonged survival by more than 130 d (median, $P < 0.001$) (**Fig. 8a**,**b**). Consistent with this delay in disease, these mice exhibited less astrogliosis and microglial activation in the spinal cord (**Supplementary Fig. 9a**). The time from symptom onset to death (that is, disease duration) was not altered by removal of SOD1 (G37R) from oligodendroglia (–4HT, 180 ± 17 d; +4HT, 209 ± 15 d; mean ± s.e.m., n = 12 mice per group, P = 0.246, Mann Whitney test), indicating that the prolonged survival of these mice resulted primarily from a delay in disease onset. This manipulation decreased *SOD1 (G37R)* gene expression in the NG2$^+$ cell population by ~43%, as determined by quantitative PCR from isolated NG2$^+$ cells (data not shown), but preserved its expression in motor neurons (**Supplementary Fig. 9b**). Although this approach had little effect on overall tissue levels of SOD1 (G37R) (**Supplementary Fig. 9c**,**d**), consistent with the relatively small number of NG2$^+$ cells present (2–5% of all neural cells in the spinal cord)[33], it presumably affected all oligodendrocytes generated from *SOD1 (G37R)*–deleted NG2$^+$ cells.

Previous studies have found that oligodendrocytes present at end stage of disease in *SOD1 (G93A)* mice express much less MCT1 (ref. 9). Given that oligodendrocytes provide metabolic support to axons via this transporter and that its expression is downregulated in *SOD1 (G93A)* mice[9], we evaluated MCT1 expression in *SOD1 (G37R)*–deleted mice. Removal of SOD1 (G37R) from oligodendroglia helped preserve MCT1 expression in some mice at early stages of disease (**Fig. 8c**). Together, these data indicate that expression of mutant SOD1 in NG2$^+$ cells and their oligodendrocyte progeny has a deleterious effect on motor neuron survival, and suggest that one negative consequence of mutant SOD1 expression in oligodendrocytes is to diminish their capacity to provide metabolic support to neurons.

DISCUSSION

Oligodendrocytes form myelin sheaths around axons in the CNS that enable rapid conduction of action potentials at minimal energetic cost. However, the perception that oligodendrocytes are primarily structural elements has been challenged by recent evidence that they also provide metabolic support to neurons by transferring glycolytic intermediates[34] through the monocarboxylic transporter MCT1 (ref. 9). Motor neurons in the spinal cord depend on this transporter for survival, suggesting that oligodendrocyte integrity affects motor neuron fate. We found extensive degeneration of gray matter oligodendrocytes in ALS mice that began before the onset of behavioral symptoms of disease. Although NG2$^+$ progenitor cells are mobilized to regenerate oligodendrocytes, oligodendrocytes generated in later stages of disease exhibited aberrant morphologies and failed to restore myelin (**Supplementary Fig. 10**). A reduction in gray matter myelin and reactive changes in NG2$^+$ cells were frequently observed in the motor cortex and spinal cord of ALS patients, indicating that degeneration of gray matter oligodendrocytes is prevalent in human ALS. Selective deletion of mutant SOD1 protein from oligodendroglia delayed disease onset and prolonged survival in mice, pointing to a key role for these cells in the precipitation of disease in ALS. Together, these results suggest that the marked loss of gray matter oligodendrocytes in ALS, and the inability to restore oligodendrocyte function, accelerates injury to vulnerable motor neurons.

There is accumulating evidence that ALS is not strictly a disease of motor neurons[1–3,35,36]. Selective removal of mutant *SOD1 (G37R)* from motor neurons slowed disease onset, but did not alter disease progression, indicating that expression of this mutant gene in other cell types is sufficient to cause motor neuron death[2]. In particular, astrocytes appear to be important contributors to disease, as there is a marked reduction in astrocyte glutamate transporter expression in mouse models of ALS[35] and ALS patients[37], astrocytes from *SOD1 (G93A)* mice secrete factors that are toxic to motor neurons[38], and removal of mutant SOD1 from astrocytes delays microglial activation and extends animal survival[3]. However, expression of mutant SOD1 only in astrocytes is not sufficient to induce disease[39], indicating that astrocyte dysfunction combines with other cellular alterations to accelerate the death of motor neurons.

The consequences of mutant protein expression in oligodendrocytes has been examined using chimeric mice in which oligodendrocytes and motor neurons express mutant SOD1, while all other cells expressed either wild-type or mutant SOD1 (ref. 40). Notably, most of these mice survived substantially longer than mice that expressed SOD1 (G37R) ubiquitously, and did not exhibit motor neuron degeneration at the time of death, suggesting that alterations in cells other than motor neurons and oligodendrocytes are critical for determining disease onset. Nevertheless, we found that selective removal of this mutant protein from oligodendrocyte progenitors markedly slowed disease progression. It is possible that ALS-linked gene mutations render oligodendrocytes more vulnerable to stresses created by abnormalities in other cells, and that oligodendrocyte degeneration is the critical event that triggers motor neuron degeneration. Indeed, oligodendrocyte vulnerability may be exacerbated by the presence of pro-inflammatory cytokines such as interferon-γ[41], which at high levels induces apoptosis of oligodendrocytes[42]. Expression of mutant SOD1 in oligodendrocyte progenitors may also induce long-term changes in gene expression that increase the vulnerability of oligodendrocytes.

Mutations in genes linked to ALS, such as *Sod1* (SOD1), *Tardbp* (TDP-43) and *Fus* (FUS), cause the formation of protein aggregates, often leading to endoplasmic reticulum stress that can induce apoptosis. Ubiquitinated protein aggregates containing TDP-43 have been observed in oligodendrocytes in patients with frontotemporal lobar degeneration[43], and other mutant proteins, such as α-synuclein[44] and tau[45], accumulate in oligodendrocytes in patients with multiple system atrophy and other types of frontotemporal dementia (FTD). These observations raise the possibility that expression of aggregation-prone mutant proteins in oligodendrocytes compromises their ability to provide adequate support to neurons. Selective overexpression in oligodendrocytes of a mutant form of tau (P301L) associated with a human form of FTD (frontotemporal dementia and parkisonism linked to chromosome 17, FTDP-17) leads to formation of filamentous tau$^+$ inclusions in these cells, eventual oligodendrocyte degeneration and reduced myelin[31]. These animals also exhibited impaired axonal transport, muscle atrophy and hind limb weakness, which are suggestive of motor neuron degeneration. We observed that oligodendrocyte degeneration in the spinal cord of ALS mice and demyelination in the brains of ALS patients were prominent in gray matter regions near motor neurons, indicating that oligodendrocytes in these regions are more susceptible to disease-related stresses. Notably, previous studies have shown that oligodendrocytes in the spinal cord gray matter are particularly vulnerable to endoplasmic reticulum stress when proteolipid protein, a component of myelin, is overexpressed[46]. Thus, the regional bias in oligodendrocyte vulnerability may depend more on metabolic demand, which is related to the type of associated neuron, than on the need for myelination.

Although some oligodendrocyte degeneration may be a secondary consequence of motor neuron death in ALS, motor axons represent only a minor portion of myelinated fibers in spinal cord gray matter. Given that each oligodendrocyte in the spinal cord forms on average ~25 internodal segments[47], each with a different axon, it seems likely that there would be sufficient remaining axons to promote oligodendrocyte survival, unless dying motor neurons produce pro-apoptotic signals. Furthermore, enhancing oligodendrogenesis without appropriate target axons to myelinate would appear maladaptive. The increase in ultrastructurally normal axons with immature myelin sheaths in ventral gray matter of end stage *SOD1 (G93A)* mice (**Fig. 6a**) suggests that oligodendrocytes attempt to remyelinate viable axons, rather than simply degenerate as a result of axon loss. Our results also indicate that selective degeneration of motor neurons is not sufficient to enhance the proliferation of NG2$^+$ cells in the spinal cord (**Supplementary Fig. 4**), which is expected to occur if new oligodendrocytes are being formed[17,23,24]. Conversely, degeneration of oligodendrocytes and demyelination are sufficient to induce neuronal apoptosis, as seen after genetically induced oligodendrocyte ablation[25,26] and in multiple sclerosis[48]. Thus, oligodendrocyte loss is expected to have a negative effect on the integrity and survival of motor neurons during the course of disease.

When do oligodendrocytes begin to degenerate in ALS? Although proliferation of NG2$^+$ cells was enhanced well before behavioral onset of disease, their density did not increase, as there was a concomitant increase in the proportion of cells undergoing differentiation. If this increase in oligodendrogenesis compensates for cells that are lost or injured, as would be expected from the maintenance of oligodendrocyte number (**Fig. 2**), then oligodendrocyte degeneration is a very early event in the disease process. Despite the continuous regeneration of oligodendrocytes, the proportion of incompletely myelinated axons increased, myelin levels were reduced and oligodendrocytes failed to express MCT1, indicating that their maturation was impaired. In addition, adult-born oligodendrocytes exhibited morphological characteristics of apoptosis, suggesting that their turnover was accelerated. This expanding cycle of proliferation, differentiation and death in the oligodendrocyte lineage in ALS may accelerate damage to vulnerable motor neurons by consuming resources and triggering reactive changes in other glial cells (**Supplementary Fig. 10**).

The degeneration of oligodendrocytes and impaired maturation of oligodendrocyte progenitors in ALS share similarities to progressive forms of multiple sclerosis, where impaired remyelination following immune-mediated attack of oligodendrocytes leads to neuronal degeneration. Indeed, there is increasing appreciation of gray matter demyelination in multiple sclerosis[49]. Thus, therapeutic approaches that are being developed to treat multiple sclerosis, based on promotion of oligodendrocyte survival or enhancement of oligodendroglial metabolic support to neurons, may be helpful for preventing motor neuron degeneration in ALS.

METHODS

Methods and any associated references are available in the online version of the paper.

Note: Supplementary information is available in the online version of the paper.

ACKNOWLEDGMENTS

We thank N. Ye, I. Srivastava, S. Singh and T. Le for their excellent technical support, M. Pucak for help with Imaris software operation and quantitative analysis, J. Carmen for her contributions to the Cre/lox animal study, and H. Zhang at the Johns Hopkins University School of Public Health FACS core for assistance with NG2$^+$ cell isolation. We thank B. Trapp (Cleveland Clinic Lerner Research Institute) for advice regarding human NG2$^+$ cell staining, R. Dutta (Cleveland Clinic Lerner Research Institute) for advice regarding protein extraction from human tissues and B. Popko (University of Chicago) for providing *Plp1-creER* mice. Human samples were provided by R. Bowser (Barrow Neurological Institute), K. Trevor (SACTL-VA Biorepository Trust), T. Hyde (Lieber Institute for Brain Development and the Johns Hopkins School of Medicine), J. Glass (Emory Alzheimer's Disease Research Center, 5P50AG025688-07), and the Johns Hopkins School of Medicine Department of Neuropathology. We thank E. Mosmiller for helping with patient demographic information. We also thank A. Agarwal and A. Langseth for critical discussions. This work was supported by grants from P^{2}ALS (D.E.B. and J.D.R.), the US National Institutes of Health (NS27036 to D.W.C., NS33958 to J.D.R. and NS051509 to D.E.B.), the ALS Association (4ZMUDE to Y.L.), the Robert Packard Center for ALS Research at Johns Hopkins, and the Brain Science Institute.

AUTHOR CONTRIBUTIONS

S.H.K., Y.L., J.D.R. and D.E.B. designed the experiments. S.H.K. carried out the experiments involving NG2$^+$ cell proliferation, cell fate analysis of NG2$^+$ cells

and oligodendrocytes, and immunohistochemical analysis of oligodendrocyte structure (**Figs. 1–6** and **Supplementary Figs. 1–3** and **5**). Y.L. performed western blot analysis from *SOD1 (G93A)* mice (**Supplementary Fig. 7**) and ALS patients (**Supplementary Fig. 8**), histological analysis of human tissue (**Fig. 7**), analysis of ricin-injected mice (**Supplementary Fig. 4**), and analysis of the *SOD1 (G37R)*–deleted mice (**Fig. 8** and **Supplementary Fig. 9**). M.F. performed the electron microscopic and immunogold analysis (**Fig. 6** and **Supplementary Fig. 6**). I.L. assisted with the ricin injections. D.W.C. provided the *loxSOD1 (G37R)* mice. L.W.O. provided assistance with analysis of the human ALS samples. S.H.K., Y.L., J.D.R. and D.E.B. wrote the manuscript.

COMPETING FINANCIAL INTERESTS

The authors declare no competing financial interests.

1. Clement, A.M. *et al.* Wild-type nonneuronal cells extend survival of SOD1 mutant motor neurons in ALS mice. *Science* **302**, 113–117 (2003).
2. Boillée, S. *et al.* Onset and progression in inherited ALS determined by motor neurons and microglia. *Science* **312**, 1389–1392 (2006).
3. Yamanaka, K. *et al.* Astrocytes as determinants of disease progression in inherited amyotrophic lateral sclerosis. *Nat. Neurosci.* **11**, 251–253 (2008).
4. Ilieva, H., Polymenidou, M. & Cleveland, D.W. Non-cell autonomous toxicity in neurodegenerative disorders: ALS and beyond. *J. Cell Biol.* **187**, 761–772 (2009).
5. Kang, S.H., Fukaya, M., Yang, J.K., Rothstein, J.D. & Bergles, D.E. NG2+ CNS glial progenitors remain committed to the oligodendrocyte lineage in postnatal life and following neurodegeneration. *Neuron* **68**, 668–681 (2010).
6. Magnus, T. *et al.* Adult glial precursor proliferation in mutant SOD1G93A mice. *Glia* **56**, 200–208 (2008).
7. Nave, K.A. Myelination and support of axonal integrity by glia. *Nature* **468**, 244–252 (2010).
8. Nave, K.A. & Trapp, B.D. Axon-glial signaling and the glial support of axon function. *Annu. Rev. Neurosci.* **31**, 535–561 (2008).
9. Lee, Y. *et al.* Oligodendroglia metabolically support axons and contribute to neurodegeneration. *Nature* **487**, 443–448 (2012).
10. Suzuki, A. *et al.* Astrocyte-neuron lactate transport is required for long-term memory formation. *Cell* **144**, 810–823 (2011).
11. Rinholm, J.E. *et al.* Regulation of oligodendrocyte development and myelination by glucose and lactate. *J. Neurosci.* **31**, 538–548 (2011).
12. Niebroj-Dobosz, I., Rafalowska, J., Fidzianska, A., Gadamski, R. & Grieb, P. Myelin composition of spinal cord in a model of amyotrophic lateral sclerosis (ALS) in SOD1G93A transgenic rats. *Folia Neuropathol.* **45**, 236–241 (2007).
13. Cosottini, M. *et al.* Magnetization transfer imaging demonstrates a distributed pattern of microstructural changes of the cerebral cortex in amyotrophic lateral sclerosis. *AJNR Am. J. Neuroradiol.* **32**, 704–708 (2011).
14. Rivers, L.E. *et al.* PDGFRA/NG2 glia generate myelinating oligodendrocytes and piriform projection neurons in adult mice. *Nat. Neurosci.* **11**, 1392–1401 (2008).
15. Zhu, X. *et al.* Age-dependent fate and lineage restriction of single NG2 cells. *Development* **138**, 745–753 (2011).
16. Gurney, M.E. *et al.* Motor neuron degeneration in mice that express a human Cu,Zn superoxide dismutase mutation. *Science* **264**, 1772–1775 (1994).
17. Dal Canto, M.C. & Gurney, M.E. Neuropathological changes in two lines of mice carrying a transgene for mutant human Cu,Zn SOD, and in mice overexpressing wild type human SOD: a model of familial amyotrophic lateral sclerosis (FALS). *Brain Res.* **676**, 25–40 (1995).
18. Woodruff, R.H., Tekki-Kessaris, N., Stiles, C.D., Rowitch, D.H. & Richardson, W.D. Oligodendrocyte development in the spinal cord and telencephalon: common themes and new perspectives. *Int. J. Dev. Neurosci.* **19**, 379–385 (2001).
19. Guo, F. *et al.* Pyramidal neurons are generated from oligodendroglial progenitor cells in adult piriform cortex. *J. Neurosci.* **30**, 12036–12049 (2010).
20. Davalos, D. *et al.* ATP mediates rapid microglial response to local brain injury *in vivo*. *Nat. Neurosci.* **8**, 752–758 (2005).
21. Jamin, N., Junier, M.P., Grannec, G. & Cadusseau, J. Two temporal stages of oligodendroglial response to excitotoxic lesion in the gray matter of the adult rat brain. *Exp. Neurol.* **172**, 17–28 (2001).
22. Wu, Y.J., Tang, Y.F., Xiao, Z.C., Bao, Z.M. & He, B.P. NG2 cells response to axonal alteration in the spinal cord white matter in mice with genetic disruption of neurofilament light subunit expression. *Mol. Neurodegener.* **3**, 18 (2008).
23. Coutts, M., Kong, L.X. & Keirstead, H.S. A model of motor neuron loss: selective deficits after ricin injection. *J. Neurotrauma* **27**, 1333–1342 (2010).
24. Henson, P.M., Bratton, D.L. & Fadok, V.A. Apoptotic cell removal. *Curr. Biol.* **11**, R795–R805 (2001).
25. Locatelli, G. *et al.* Primary oligodendrocyte death does not elicit anti-CNS immunity. *Nat. Neurosci.* **15**, 543–550 (2012).
26. Pohl, H.B. *et al.* Genetically induced adult oligodendrocyte cell death is associated with poor myelin clearance, reduced remyelination, and axonal damage. *J. Neurosci.* **31**, 1069–1080 (2011).
27. Woodruff, R.H., Fruttiger, M., Richardson, W.D. & Franklin, R.J. Platelet-derived growth factor regulates oligodendrocyte progenitor numbers in adult CNS and their response following CNS demyelination. *Mol. Cell Neurosci.* **25**, 252–262 (2004).
28. Chang, A., Nishiyama, A., Peterson, J., Prineas, J. & Trapp, B.D. NG2-positive oligodendrocyte progenitor cells in adult human brain and multiple sclerosis lesions. *J. Neurosci.* **20**, 6404–6412 (2000).
29. Pouly, S., Becher, B., Blain, M. & Antel, J.P. Expression of a homologue of rat NG2 on human microglia. *Glia* **27**, 259–268 (1999).
30. Bu, J., Akhtar, N. & Nishiyama, A. Transient expression of the NG2 proteoglycan by a subpopulation of activated macrophages in an excitotoxic hippocampal lesion. *Glia* **34**, 296–310 (2001).
31. Higuchi, M. *et al.* Axonal degeneration induced by targeted expression of mutant human tau in oligodendrocytes of transgenic mice that model glial tauopathies. *J. Neurosci.* **25**, 9434–9443 (2005).
32. Yazawa, I. *et al.* Mouse model of multiple system atrophy alpha-synuclein expression in oligodendrocytes causes glial and neuronal degeneration. *Neuron* **45**, 847–859 (2005).
33. Horner, P.J., Thallmair, M. & Gage, F.H. Defining the NG2-expressing cell of the adult CNS. *J. Neurocytol.* **31**, 469–480 (2002).
34. Fünfschilling, U. *et al.* Glycolytic oligodendrocytes maintain myelin and long-term axonal integrity. *Nature* **485**, 517–521 (2012).
35. Bruijn, L.I. *et al.* ALS-linked SOD1 mutant G85R mediates damage to astrocytes and promotes rapidly progressive disease with SOD1-containing inclusions. *Neuron* **18**, 327–338 (1997).
36. Pramatarova, A., Laganiere, J., Roussel, J., Brisebois, K. & Rouleau, G.A. Neuron-specific expression of mutant superoxide dismutase 1 in transgenic mice does not lead to motor impairment. *J. Neurosci.* **21**, 3369–3374 (2001).
37. Rothstein, J.D., Van Kammen, M., Levey, A.I., Martin, L.J. & Kuncl, R.W. Selective loss of glial glutamate transporter GLT-1 in amyotrophic lateral sclerosis. *Ann. Neurol.* **38**, 73–84 (1995).
38. Nagai, M. *et al.* Astrocytes expressing ALS-linked mutated SOD1 release factors selectively toxic to motor neurons. *Nat. Neurosci.* **10**, 615–622 (2007).
39. Gong, Y.H., Parsadanian, A.S., Andreeva, A., Snider, W.D. & Elliott, J.L. Restricted expression of G86R Cu/Zn superoxide dismutase in astrocytes results in astrocytosis, but does not cause motoneuron degeneration. *J. Neurosci.* **20**, 660–665 (2000).
40. Yamanaka, K. *et al.* Mutant SOD1 in cell types other than motor neurons and oligodendrocytes accelerates onset of disease in ALS mice. *Proc. Natl. Acad. Sci. USA* **105**, 7594–7599 (2008).
41. Aebischer, J. *et al.* Elevated levels of IFNgamma and LIGHT in the spinal cord of patients with sporadic amyotrophic lateral sclerosis. *Eur. J. Neurol.* **19**, 752–759 (2012).
42. Buntinx, M. *et al.* Cytokine-induced cell death in human oligodendroglial cell lines. I. Synergistic effects of IFN-gamma and TNF-alpha on apoptosis. *J. Neurosci. Res.* **76**, 834–845 (2004).
43. Neumann, M. *et al.* TDP-43-positive white matter pathology in frontotemporal lobar degeneration with ubiquitin-positive inclusions. *J. Neuropathol. Exp. Neurol.* **66**, 177–183 (2007).
44. Tu, P.H. *et al.* Glial cytoplasmic inclusions in white matter oligodendrocytes of multiple system atrophy brains contain insoluble alpha-synuclein. *Ann. Neurol.* **44**, 415–422 (1998).
45. Komori, T. Tau-positive glial inclusions in progressive supranuclear palsy, corticobasal degeneration and Pick's disease. *Brain Pathol.* **9**, 663–679 (1999).
46. Bauer, J. *et al.* Endoplasmic reticulum stress in PLP-overexpressing transgenic rats: gray matter oligodendrocytes are more vulnerable than white matter oligodendrocytes. *J. Neuropathol. Exp. Neurol.* **61**, 12–22 (2002).
47. Chong, S.Y. *et al.* Neurite outgrowth inhibitor Nogo-A establishes spatial segregation and extent of oligodendrocyte myelination. *Proc. Natl. Acad. Sci. USA* **109**, 1299–1304 (2012).
48. Dutta, R. & Trapp, B.D. Pathogenesis of axonal and neuronal damage in multiple sclerosis. *Neurology* **68**, S22–S31 (2007).
49. Rudick, R.A. & Trapp, B.D. Gray-matter injury in multiple sclerosis. *N. Engl. J. Med.* **361**, 1505–1506 (2009).

ONLINE METHODS

Mice. *Pdgfra-creER*[5] and *loxSOD1(G37R)* (ref. 2) mice were generated and described previously. *Plp1-creER*[50] mice were kindly provided by B. Popko (University of Chicago). *SOD1 (G93A)*, *Z/EG*[51], *ROSA26-EYFP*[52] and *ROSA26-mEGFP* (*mT/mG*)[53] mice were purchased from the Jackson Laboratory. *Mobp-EGFP* mice were generated by GENSAT[54] and purchased from the Mutant Mouse Regional Resource Center. All experiments were carried out in strict accordance with protocols approved by the Animal Care and Use Committee at Johns Hopkins University.

BrdU labeling and Cre activity induction. For continuous exposure to BrdU (Sigma), mice were provided with BrdU-containing drinking water (1 mg ml^{-1} supplemented with 1% sucrose), and received additional BrdU injections twice a day (50 mg per kg of body weight, intraperitoneal, at least 8 h apart) for 5 consecutive days. 4HT (Sigma H7904) was administered, 2 mg (to *Plp1-creER; ROSA26-EYFP*) or 4–5 mg (to *Pdgfra-creER; Z/EG* or *Pdgfra-creER; mTmG*) by intraperitoneal injection at either P30 or P60. For the excision of SOD1 (G37R), 4HT was injected to *Pdgfra-creER; loxSOD1(G37R)* mice at P18 (1 mg) and at P30~31 (total 4 mg). Each mouse received up to two injections per day (1 mg per injection), at least 8 h apart.

Ricin injection. After anesthesia with ketamine (120 mg per kg) and xylazine (8 mg per kg, intraperitoneal), the sciatic nerves of P20 mice were exposed and crushed with a fine forcep for 20 s, followed by 1 µl of 1 mg ml^{-1} ricin (Sigma) injection into the nerve in the proximal side of the crush, and 1 µl of phosphate-buffered saline (PBS) in the other side. The mice were killed 1 week later.

Immunohistochemistry. Mice were deeply anesthetized with sodium pentobarbital (100 mg per kg) and perfused transcardially with 4% paraformaldehyde (PFA in 0.1 M phosphate buffer, pH 7.4). Spinal cords were further post-fixed overnight at 4 °C. For immunofluorescence, lumbar spinal cords were stored at 4 °C for more than 36 h in 30% sucrose solution (in PBS, pH 7.4), and then sectioned with a cryostat (35 or 25 µm thick). Immunofluorescence was performed on free-floating sections as described previously[5]. We used primary antibodies to APC (mouse, clone CC1, Calbiochem, OP80,1:50), BrdU (rat, clone BU1/75, Accurate, 1:500), cleaved caspase-3 (rabbit, Cell Signaling, Asp175, 1:500), ChAT (goat, Millipore, AB144P, 1:300), EGFP (goat, Frontier Institute, GFP-Go-Af1480-1, 1:500), EGFP (rabbit, a gift from R. Huganir, Johns Hopkins University, 1:500), GFAP (mouse, clone N206A/8, NeuroMab, 1:500), GFAP (rabbit, DAKO, Z0334,1:1,000), Iba1 (rabbit, Wako, 019-19741, 1:1,000), Ki67 (rabbit, Abcam, ab15580, 1:500), NG2 (guinea pig, Bergles' Lab, 1:4,000), Olig2 (guinea pig, 1:20,000, a gift from B. Novitch, University of California, Los Angeles), Olig2 (rabbit, Millipore, AB9610, 1:500), PDGFαR (rabbit, a gift from W. Stallcup, Burnham Institute, 1:500), SMI32 (mouse, Covance, SMI-32P, 1:1,000) and human SOD1 (rabbit, Rothstein Lab, 1:70). Secondary antibodies were Alexa Fluor 488– (Invitrogen, A-21206 and A-11055, 1:500), Cy3–, or DyLight 647–conjugated donkey $F(ab')_2$ fragments to rabbit (711-166-152, and 712-606-152), goat (705-166-147), mouse (715-166-151 and 715-606-151), rat (712-166-150 and 712-606-153) or guinea pig (706-166-148 and 706-516-148) (Jackson ImmunoResearch). For Olig2, ALDH or APC (CC1) immunostaining, tissue sections were incubated in LAB solution (Polysciences) for 10 min before blocking. For BrdU staining, sections were pre-incubated in 2 N HCl at 37 °C for 30 min, followed by neutralization with 0.1 M sodium borate buffer (pH 8.5) before immunolabeling. DAPI was added during the secondary antibody incubation for most cases. Sections were mounted on slides with ProLong antifade reagent (Invitrogen).

For human tissue histopathological analysis, paraffin-embedded and fresh frozen human primary motor cortex and lumbar spinal cord sections (all 5 µm thick) were used. Sections were deparaffinized in a series of xylene, 100% alcohol, 95% alcohol, 70% alcohol and water, followed by antigen retrieval (boiling in 10 mM citrate buffer at pH 6.0 for 10 min). Sections were incubated with 3% H_2O_2 (vol/vol), blocked with 3% BSA in PBS, and incubated with the primary antibody for 60 min at 20–25 °C or at 4 °C overnight. We used primary antibodies to Iba1 (rabbit, Wako, 019-19741, 1:1,000), MBP (rabbit, Millipore, AB980,1:200) and NG2 (mouse, BD Science, 554275, 1:1,000). Sections were incubated with biotinylated secondary antibodies (Vector Lab), followed by VECTASTAIN Elite ABC reagent according to the manufacture's instruction (Vector Lab) and colorimetrically developed using the 3,3′-diaminobenzidine (DAB) substrate kit (Vector Lab). For double labeling of NG2 and Iba1, mounted fresh frozen sections (5 µm) were fixed with 4% PFA at 20–25 °C for 15 min, incubated with 3% H_2O_2, blocked with 3% BSA (wt/vol), and then incubated with antibody to NG2 at 4 °C overnight. Sections were incubated with HRP-labeled secondary antibody and Renaissance TSA Biotin system (PerkinElmer) according to manufacturer's instructions, and developed with DAB substrate. For Iba1 staining, sections was blocked with the BLOXALL solution (Vector Lab), followed by alkaline phosphatase–conjugated secondary antibody (Promega) and developed with NBT/BCIP substrate (Vector Lab).

Luxol fast blue myelin staining. Tissue sections were stained with 0.1% luxol fast blue solution (vol/vol, Sigma) at 60 °C overnight. Sections were rinsed with 95% ethanol and water, reacted with 1% lithium carbonate solution (wt/vol) and 70% ethanol, followed by rinsing in water. Counter staining with hematoxylin and eiosin was performed as necessary.

Microscopy and cell counting. Mounted slides were imaged using an epifluorescence microscope (Zeiss Axio-imager M1), and Axiovision software (Zeiss), or a confocal laser-scanning microscope (Zeiss LSM 510 Meta) using appropriate excitation and emission filters. A total of 3–5 sections were examined per mouse, and 3–4 mice were analyzed per each data point. Confocal images represent projected stacks of 15–45 images collected at 0.5–1.5-µm steps.

Volume measurement of oligodendrocyte cellular fragments. $EGFP^+$ elements of *Mobp-EGFP* mice that are not associated with Olig2 were quantified using a commercially available three-dimensional analysis package (Imaris, Bitplane). $EGFP^+$ structures were defined by applying an absolute intensity threshold, followed by thresholding for structure size to remove small objects. Identical thresholds were applied to all images. $EGFP^+$ structures that were also associated with Olig2 staining were deleted, as were structures which were positioned at the edge of the imaged field. The volume of $Olig2^-$ $EGFP^+$ was scaled according to total imaged volume.

Electron microscopy. Mice were perfused transcardially with 4% PFA/2.5% glutaraldehyde (vol/vol) in 0.1 M phosphate buffer under deep anesthesia, and brain tissue was isolated and post-fixed for 4 h at 4 °C. Brains were treated with 2% OsO_4 (wt/vol) for 1 h, and washed in water. Samples were incubated in 2% uranyl acetate (wt/vol) for 30 min and dehydrated using 50%, 70%, 90%, 100% ethanol and propylene oxide. Samples were embedded in Epon 812 resin (Ted Pella). Ultrathin sections were obtained using Ultracut UCT (Leica) and stained with 2% uranyl acetate and lead citrate. Electron micrographs were taken with an H-7600 electron microscope (Hitachi). ImageJ was used to measure the diameter of axons and myelin sheath.

For pre-embedding immunoelectron microscopy, 4HT-injected *Pdgfra-creER; ROSA26-mEGFP; SOD1 (G93A)* and *Pdgfra-creER; ROSA26-mEGFP* mice (P60+60) were perfused transcardially with 4% PFA/0.1% glutaraldehyde in 0.1 M phosphate buffer under deep anesthesia. After blocking with 5% normal donkey serum (vol/vol) in PBS, spinal cord sections (50 µm thick) were incubated overnight with rabbit antibody (IgG) to EGFP and then with antibody (IgG) to rabbit conjugated to 1.4-nm gold particles (Nanoprobes). Following silver enhancement (HQ silver, Nanoprobes), sections were osmificated, dehydrated and embedded in Epon 812 resin. Ultrathin sections were prepared with an ultramicrotome (Leica) and stained with 2% uranyl acetate.

Clinical materials. Human autopsy materials, including frozen and paraffin-embedded control and ALS patient cortex and spinal cord tissues, were obtained from the Johns Hopkins University ALS Clinic, Brain Resource Center/Department of Pathology, VA Biorepository Brain Bank. All experiments were performed using motor cortex, cervical and/or lumbar spinal cord tissues. All available demographic information for the ALS and control cases analyzed in this study is presented in **Supplementary Table 1**.

Western blotting. Lumbar spinal cords were collected from control and *SOD1 (G93A)* mice, snap frozen in liquid nitrogen and then stored at –80 °C until use. For human cortex protein analysis, the gray matter and white matter were separated grossly. The tissues were homogenized in RIPA buffer (Thermo) supplemented with proteinase inhibitor (Roche) and phosphatase inhibitor

doi:10.1038/nn.3357

(Calbiochem) on ice. 30 μg of protein was separated on 4–12% gradient Bis-Tris gels (BioRad) or NuPage and transferred to nitrocellulose membranes (BioRad). After blocking with 5% nonfat milk (wt/vol), membranes were probed with primary antibodies at 4 °C overnight, following by HRP-conjugated secondary antibodies, Supersignal Pico detection reagent (Pierce), and then exposed to HyBlot CL autoradiography film (Denville). The intensity for each band was quantified with ImageJ software. We used antibodies to CNPase (mouse, Millipore, MAB326, 1:1,000), MBP (mouse, Millipore, AB980, 1:2,000), PDGFαR (rabbit, Santa Cruz, sc-338, 1:200), GAPDH (rabbit, Cell Signaling, 2118, 1:1,000) and MCT1 (rabbit, Santa Cruz, sc-50325, 1:100).

Analysis of disease progression. For *Pdgfra-creER; loxSOD1(G37R)* mice, the time of disease onset, early disease and end stage were defined as the time when mouse body weight reached the peak, body weight declined to 10% of the maximum weight and paralyzed mice could not right themselves within 20 s when placed on their side respectively, as previously described[2]. The total disease duration was defined as the duration between disease onset and end stage. Mice were weighted once a week when they were 150 d old.

Quantitative PCR determination of transgene excision in NG2$^+$ cells. The brain neural cells from 2-month-old mice (with and without 4HT injection, $n = 3$ each group) were dissociated using Dissociation Kit (P) (Milteny) by following the manufacturer's instructions. Myelin was removed by using Percoll generated gradient. Live cell fraction was collected and the cells were submitted to staining for PDGFαR (1:200, Santa Cruz) followed by Alexa 488–conjugated antibody to rabbit before fluorescence-activated cell sorting (FACS). Dead cells were excluded by propidium iodide staining during sorting using MoFlo MLS high-speed cell sorter (Beckman Coulter) at Johns Hopkins School of Public Health FACS core. Only PDGFαR$^+$ and propidium iodide$^-$ cells were sorted for transgene evaluation. Genomic DNA was extracted by using QIAmp DNA micro kit (Qiagen) following the manufacturer's instructions. qPCR for *SOD1 (G37R)* transgene was performed using the primers and cycler parameters on ABI Plusone cycler as described previously[2].

Statistical analysis. All data are presented as mean ± s.e.m. For multiple groups, data were evaluated by one-way ANOVA and further evaluated with Tukey *post hoc* comparisons. Otherwise, unpaired Student's *t* test was applied. $P < 0.05$ was considered to be statistically significant. The paired Student's *t* test was used to evaluate contralateral and ipsilateral side of cell counts in ricin-injected mouse experiments. Log-rank test was used for survival curve analysis. Mann Whitney test was used for disease duration.

50. Doerflinger, N.H., Macklin, W.B. & Popko, B. Inducible site-specific recombination in myelinating cells. *Genesis* **35**, 63–72 (2003).
51. Novak, A., Guo, C., Yang, W., Nagy, A. & Lobe, C.G. Z/EG, a double reporter mouse line that expresses enhanced green fluorescent protein upon Cre-mediated excision. *Genesis* **28**, 147–155 (2000).
52. Srinivas, S. *et al.* Cre reporter strains produced by targeted insertion of EYFP and ECFP into the ROSA26 locus. *BMC Dev. Biol.* **1**, 4 (2001).
53. Muzumdar, M.D., Tasic, B., Miyamichi, K., Li, L. & Luo, L. A global double-fluorescent Cre reporter mouse. *Genesis* **45**, 593–605 (2007).
54. Gong, S. *et al.* A gene expression atlas of the central nervous system based on bacterial artificial chromosomes. *Nature* **425**, 917–925 (2003).

Review

Cell PRESS

Oligodendroglia: metabolic supporters of axons

Brett M. Morrison, Youngjin Lee, and Jeffrey D. Rothstein

Brain Science Institute, Department of Neurology, Johns Hopkins University, Baltimore, MD 21205, USA

Axons are specialized extensions of neurons that are critical for the organization of the nervous system. To maintain function in axons that often extend some distance from the cell body, specialized mechanisms of energy delivery are likely to be necessary. Over the past decade, greater understanding of human demyelinating diseases and the development of animal models have suggested that oligodendroglia are critical for maintaining the function of axons. In this review, we discuss evidence for the vulnerability of neurons to energy deprivation, the importance of oligodendrocytes for axon function and survival, and recent data suggesting that transfer of energy metabolites from oligodendroglia to axons through monocarboxylate transporter 1 (MCT1) may be critical for the survival of axons. This pathway has important implications both for the basic biology of the nervous system and for human neurological disease. New insights into the role of oligodendroglial biology provide an exciting opportunity for revisions in nervous system biology, understanding myelin-based disorders, and therapeutics development.

Unique vulnerability of neurons

Neurons are specialized cells in the nervous system capable of integrating thousands of inputs (i.e., synaptic afferents) into a single output (i.e., action potential). In long-projection neurons, such as corticospinal tract neurons, spinal motor neurons, and dorsal column sensory neurons, action potentials are transmitted by the axon (see Glossary) for several feet before terminating on another neuron or end organ, such as muscle. Some axons are so extensive that up to 99% of the neuron's cytoplasm is contained within the axon. This unique anatomy of a neuron is the critical component of the emerging field of connectome analysis [i.e., how functional connections between different areas of the central nervous system (CNS) lead to specific behaviors] [1], but may also be a source of unique vulnerability to the neuron. Many of the proteins necessary for axon function, including structural proteins, ion channels, molecular motors, and synaptic vesicle proteins, are translated in the soma and transported into, and in some cases to the end of, axons. Constant metabolic energy is necessary for axonal transport, as well as to maintain the sodium gradient (through Na^+/K^+ ATPases) necessary for action potentials. Together, these features make axons 'energetically expensive' to maintain [2].

Energy for the axon, in the form of ATP, is partly generated from glucose transporters on neuronal cell bodies, but it is likely that local energy is required to maintain axon function along its long course. Access to extracellular glucose is restricted in most long axons by the presence of myelin, a hydrophobic barrier surrounding axons. Myelin, which is formed by oligodendroglia in the CNS and Schwann cells in the peripheral nervous system (PNS), is critical for efficient impulse conduction in the axon. Instead of having to activate channels throughout the axon, the sodium and potassium channels can be focused in discrete regions that lack myelin, termed nodes of Ranvier or juxtaparanodes, respectively [3]. Because up to 99% of the axon's surface area is covered in myelin, only a small percentage of the axon is exposed to the extracellular space, limiting access to glucose and other energetic metabolites in the extracellular space. For this reason, it has been postulated that axons derive some metabolic energy directly from oligodendroglia through their myelin sheaths [4].

Evidence for a local supply of energy to axons came initially from studies of optic nerve explants. *Ex vivo* preparations of optic nerve propagate compound action potentials (CAPs) for several hours after dissection and thus allow sensitive physiological readouts of nerve

Glossary

Axon: specialized component of neurons that electrochemically interconnects brain regions through action potential propagation.
2′,3′-Cyclic-nucleotide 3′-phosphodiesterase (CNP): protein component of myelin with an unclear cellular role, although may be important for intracellular transport.
Demyelination: reduced quantity of myelin covering axons; can be either diffuse or focal.
Juxtaparanode: region adjacent to the paranode in which potassium channels cluster in the axon.
Myelin: multilaminar covering of axons comprising both lipid and protein components.
Node of Ranvier: intermittent gaps in myelin at which voltage-dependent sodium channels cluster in axons.
Oligodendroglia: non-neuronal cells in the CNS that myelinate and support axons.
Paranode: region adjacent to the node of Ranvier in which the myelin sheaths contact the axon.
Proteolipid protein (PLP): most abundant protein component of myelin in the CNS.
Spheroid: focal pathological axon swelling comprising disorganized neurofilaments, microtubules, and transported organelles.

Corresponding author: Rothstein, J.D. (jrothstein@jhmi.edu).
Keywords: MCT1; oligodendroglia; neurodegeneration; myelin; ALS; lactate.

0962-8924/$ – see front matter
 http://dx.doi.org/10.1016/j.tcb.2013.07.007

function under various media conditions [5]. In the absence of glucose, optic nerve explants maintained CAPs for approximately 30 min and irreversible nerve injury can ensue after 60 min. Pretreatment of the nerves with high glucose to induce production of glycogen in resident astrocytes extended the latency for an additional 15 min until CAP failure and prevented much of the permanent nerve injury. CAP failure could also be prevented by lactate administration, which was predictably blocked by lactate transport inhibitors [6,7]. These experiments suggested that astrocytes support neurons by exporting lactate produced from glycogen through MCTs. As detailed below, recent evidence suggests that oligodendroglia are the prominent site of lactate export to neurons, although astrocytes may play a critical role in sustaining energy substrates through their glycogen stores and production of lactate through glycolysis.

Oligodendroglia are critical for axon function/survival

Oligodendroglia are specialized cells in the CNS that wrap axons with myelin. Diseases of oligodendroglia invariably produce some degree of demyelination, which was thought to underlie their clinical signs and symptoms (Box 1). Over the past 10 years, animal studies have demonstrated a critical role for oligodendroglia in the maintenance and long-term survival of axons and neurons and may yield clues to the involvement of oligodendrocytes in neurodegenerative diseases. Multiple transgenic models of oligodendrocyte injury have been investigated, including several with perturbations of proteolipid protein (PLP), 2′,3′-cyclic-nucleotide 3′-phosphodiesterase (CNP) knockout mice, and diphtheria toxin conditional transgenic mice (Table 1). These animal models produce varying degrees of demyelination and progress over different time frames, but all consistently demonstrate axonal pathology. These genes and models of axonal pathology are discussed below.

PLP is the most abundant protein present in myelin. Although its exact function remains unclear, it appears to be important for shuttling some myelin proteins, such as septins and sirtuin 2 [8], from the soma into the myelin sheaths. Several different PLP animal models have been investigated, including naturally occurring point mutations [9–13], PLP1 overexpression rats [14] and mice [15,16], and PLP1 knockout mice [17,18]. It is outside the scope of this review to discuss these in any detail, but many of these animal models demonstrate axon degeneration associated with (e.g., PLP1 point mutations and overexpressor rodents) or without (e.g., PLP1 null mice) demyelination and in some cases axon degeneration has been directly linked to decreased axonal transport [16,17]. The exact mechanism of axon degeneration in these mice is unknown, although it may involve abnormal trafficking of critical oligodendroglial mRNA or proteins, possible including metabolic transporters, because numerous myelin proteins are reduced or absent in these animal models.

A second oligodendroglia gene that can lead to axonal injury is CNP. CNP is an RNA-binding protein that may function to promote intracellular RNA transport by binding RNA to tubulin [19]. CNP null mice develop CNS pathology reflecting degeneration of either axons or oligodendroglia, including spheroids and myelin ovoids, probably from failure of axonal transport and disruption of structural components of the paranode, and later exhibit muscle atrophy, weight loss, hydrocephalus, and premature death [20–22]. Interestingly, these mice do not have demyelination at ages when the axon degeneration is prominent. The etiology of axon degeneration is unclear, but given the disrupted paranodal architecture it is likely to involve failure of oligodendrocytes to interact with axons. Although the pathology of CNP null mice is similar to that of PLP1 disrupted mice, the mechanism of degeneration must be different because double knockout mice develop increased axonal degeneration compared with either null mouse alone [22]. Thus, disruption of oligodendroglial proteins with different cellular functions such as PLP1 and CNP can lead to a common phenotype of severe disruption of axon function and integrity.

Recent studies have also investigated the impact of acute death of oligodendroglia on neuron function and survival. Oligodendroglial cell death was induced by crossing a conditionally targeting diphtheria toxin to PLP-CreER mice [23] or by treating with diphtheria toxin mice in which the oligodendroglia had been sensitized by selectively expressing diphtheria toxin receptor within them [24,25]. In these models, the diphtheria toxin led to rapid and selective oligodendroglial death via blockade of protein synthesis. Although the clinical severity differed between the mice, one model developed rapid spastic paralysis and died within 3 weeks [25], another developed motor deficits, tremor, and ataxia without early death [23], and the third model developed tremor and gait abnormalities only [24]; all models of oligodendroglial death produced severe axonal injury characterized by accumulation of non-phosphorylated neurofilaments and amyloid precursor proteins [25].

Box 1. Oligodendroglial dysfunction in human disease

The diseases most directly associated with oligodendroglial injury are multiple sclerosis (MS) and inherited leukodystrophies. MS is an autoimmune disease most commonly characterized by relapsing–remitting neurological symptoms and signs. Patients frequently have multiple 'neurological events' characterized by subacute, progressive development of weakness, numbness, or vision loss that frequently improves (i.e., remits) to some degree. These events reflect new focal areas of demyelination in the CNS that reduce the efficiency of action potentials. Over time, the myelin is repaired and the symptoms remit. Importantly, however, most patients eventually reach a progressive stage of the disease in which the symptoms do not remit and autopsies of MS patients show not only demyelination but also significant axon injury and neuron loss [57]. A second group of oligodendroglial diseases are inherited leukodystrophies, including Pelizaeus–Merzbacher disease (PMD) produced by mutations in the PLP1 gene, Pelizaeus–Merzbacher-like disease (PMLD) produced by mutations in Cx47, and adrenoleukodystrophy due to mutations in a peroxisomal enzyme necessary for degrading very long-chain fatty acids. In addition to oligodendroglial injury and demyelination, these diseases also produce varying degrees of axon injury that ultimately lead to the most disabling neurological symptoms [58–61].

These human diseases suggest a role for oligodendroglia in supporting axons; however, all of these diseases also cause demyelination and most produce secondary inflammation. Due to this, it is unknown whether the axon injury is a direct result of oligodendrocyte injury or secondary to downstream events. For this reason, transgenic mice have been studied in which the impact of oligodendrocyte injury can be separated from demyelination and inflammation.

Table 1. Pathology and mechanism of axon injury in multiple rodent models and human diseases involving oligodendrocytes

Rodent model or human disease	Mechanism	Oligodendroglial/myelin pathology	Axon pathology	Refs
PLP1 mutant mice (jimpy/rumpshaker)	PLP1 point mutations	Demyelination Variable oligodendroglial injury	Mild (jimpy)	[11–13]
PLP1 null mice	PLP1 null	Normal	Spheroids Slow transport	[17,18]
PLP1 overexpressor mice	PLP1 overexpression	Demyelination	Spheroids Slow transport	[16]
CNP null	CNP null	Grossly normal Subtle ultrastructural deficits	Spheroids Severe and early	[20–22]
Diphtheria toxin mice	Oligodendroglial death	Oligodendroglial loss Variable demyelination	Spheroids Abnormal nodes	[23–25]
PMD	PLP1 duplications/mutations	Oligodendroglial loss Demyelination	Spheroids	[58–60]
PMLD	Cx47 mutations	Demyelination	Spheroids	[61]

Although some of these mice exhibited abnormalities in myelin composition, overall myelination was not affected, suggesting that axonal injury is not due to demyelination [25]. Additionally, axon injury is not dependent on the secondary immune reaction, because it persisted after crossing to an immunodeficient line of mice [23]. These studies demonstrate that oligodendroglia themselves, and not just components of myelin, are critical for maintaining axons.

Taken together, these animal models strongly suggest that perturbation of oligodendroglia cause axon injury, at least partly through disruption of axon transport, as reflected by the altered morphology and axonal inclusions (e.g., spheroids, multivesicular bodies), which are dependent on normal axonal transport. The exact mechanism by which this occurs is unknown, but another recurring theme from the animal models is that oligodendroglial intracellular trafficking often appears to be disrupted. Perhaps oligodendroglial support of axonal transport is dependent on one or more molecules in the myelin sheath and failed trafficking to the myelin sheath leads to axonal pathology. Although there are several possible myelin proteins that may play a role in supporting axons, recent data suggest that transporters for monocarboxylates are critical for maintaining axon integrity. Failure of these transporters to be expressed in oligodendroglia would reduce the availability of local metabolic energy to the axon [26,27], potentially impacting energy-dependent processes in the axon such as axonal transport [4,28].

MCT1 is critical transporter for axon support by lactate

MCTs are extracellular membrane channels that transport lactate, pyruvate, and ketone bodies, along with protons, down their concentration gradient across membranes (see [29] for a review). Based on sequence homology, 14 members have been identified, although only MCT1, 2, and 4 localize to the CNS and cotransport monocarboxylates and protons. Transport can be enhanced by decreasing pH or increasing substrate concentration, as would be expected for passive diffusion [30]. In the CNS, MCT1 is expressed predominately in oligodendroglia and a few specific neuronal populations [27,31], although it may be present in much smaller amounts in astrocytes and endothelial cells [32,33]. MCT2 is expressed primarily in neurons [34–36] and MCT4 in astrocytes [35,36]. The cellular distribution and physiological properties of MCTs led to the lactate shuttle hypothesis [34]. In this hypothesized mechanism for energy transfer between cells, a heavily glycolytic (i.e., nonoxidative) cell produces large amounts of pyruvate that is converted to lactate and transported extracellularly down its concentration gradient through specific MCTs. The extracellular lactate is then transported into cells dependent on oxidative metabolism by other MCTs, converted to pyruvate, and then used in the Krebs cycle to produce ATP. This cellular interdependence is hypothesized to occur between astrocytes and neurons (i.e., astrocyte–neuron lactate shuttle) [37]. Recently published work has modified this hypothesis by showing that oligodendroglia are critical intermediaries for lactate transport to neurons [26,27].

Downregulation of MCT1, which is present almost exclusively within oligodendroglia in the CNS, resulted in axon injury and/or neuron loss *in vitro* and *in vivo* (Figure 1) [27]. Treatment of spinal cord organotypic cultures with antisense oligonucleotides or a specific pharmacological inhibitor of MCT1 (MCT1i) led to motor neuron loss, although they required prolonged treatment. Motor as well as other neuron loss was accelerated by incubating the sections in glucose-free media. Glucose deprivation makes neurons completely dependent on lactate as a source of metabolic energy and neuron loss following treatment with MCT1i was immediate. Importantly, loss or blockade of MCT1 was not toxic to oligodendroglia *in vitro* and neuron death was prevented by adding exogenous lactate. These *in vitro* experiments support the hypothesis that failed lactate release from oligodendroglia, not blockage of uptake and oligodendroglial energy failure, was responsible for neuron loss and provided mechanistic support for several experiments *in vivo* demonstrating the neurotoxicity of MCT1 attenuation.

In each of the *in vivo* experiments (Figure 1), MCT1 expression was attenuated either globally [i.e., MCT1 heterozygous null mice or lentiviral constructs expressing short hairpin RNA (shRNA) driven by nonspecific promoters] or selectively within oligodendroglia (i.e., cell-specific promoters or Cre-expressing transgenic mice) [27]. In all of these studies, downregulation of MCT1 resulted in axon degeneration. Furthermore, when injected focally into the spinal cord, MCT1 shRNA caused not only axon degeneration but also motor neuron loss. Together, these experiments confirmed the findings observed *in vitro* that downregulation of MCT1 produces axonal degeneration and, in some cases, neuron loss.

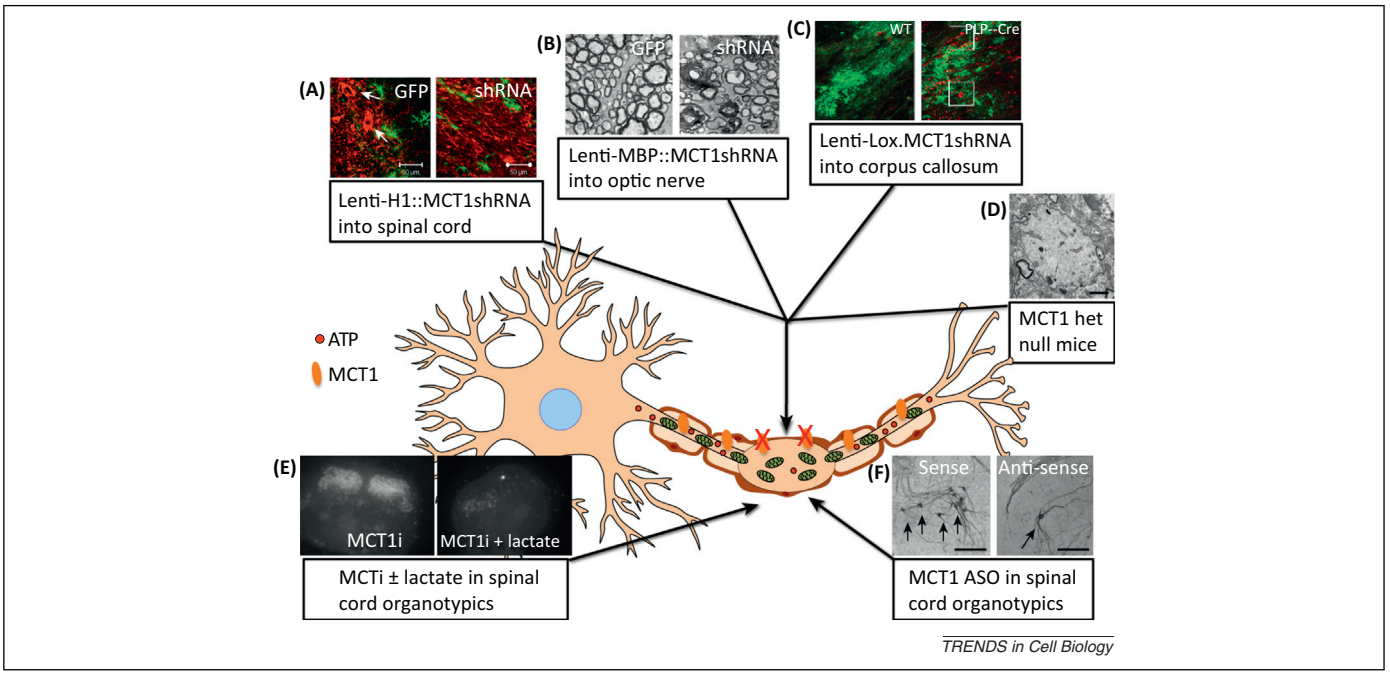

Figure 1. Multiple manipulations that attenuate monocarboxylate transporter 1 (MCT1) in rodent models **(A–D)** or spinal cord organotypic cultures **(E,F)** produce motor neuron cell death (A,F) (arrows indicate motor neurons), spinal neuron death (E) (propidium iodide), or axon injury (B–D).

Given its known role as a transporter of lactate and its localization in the myelin sheaths surrounding axons [31], these studies suggested for the first time that oligodendroglial MCT1 is a key transporter of energy metabolites to axons and that attenuation of MCT1 produces axon pathology due to local energy failure within the axon. A limitation to these studies, however, is that lactate flux is never measured directly – rather, it is inferred by indirect measurements of axonal injury – and loss of MCT1 could potentially cause axon degeneration through other mechanisms. Further support for a role for lactate came from transgenic experiments in which oligodendroglial mitochondria were selectively targeted by mutations in cytochrome oxidase [26]. In the CNS, no pathology was seen even at 9 months of age, probably due to stable mitochondria produced before conditional expression of cytochrome oxidase mutations, but brain lactate measured by magnetic resonance spectroscopy was increased in mice under isoflurane anesthesia. Alterations in brain lactate are likely to result from increased export of lactate from oligodendroglia forced to utilize nonoxidative metabolism due to mitochondrial mutations. Interestingly, the levels of lactate rapidly returned to that of controls after discontinuing anesthesia, possibly due to rapid uptake by neurons/axons. Although this study makes several assumptions about metabolic activity in anesthetized neurons and oligodendroglia (i.e., reduced metabolic activity in neurons but not in oligodendroglia), it provides further support for a direct role of oligodendroglia in the supply of lactate to axons.

In aggregate, these recent studies provide strong evidence for a new role of oligodendroglia in direct energy-substrate support of axons (Figure 2). However, there are several issues raised by these studies that need to be further addressed, including the role of astrocytes in energy supply to neurons, whether MCT1 on oligodendroglia is an exporter or importer of lactate, and whether lactate is truly the critical energetic molecule for direct energy supply to axons.

Astrocytes: possible link between oligodendroglia and nutrient supply

Although these aforementioned studies provide strong evidence for the role of oligodendroglia in directly supplying energy support to axons, alternative cells including astrocytes could also be directly or indirectly involved in supplying energy to neurons. There is a substantial literature on astrocytes supplying lactate to neurons (see [38,39] for recent reviews). Much of the early literature is based on isolated cultures and therefore may not be reflective of *in vivo* physiology, because expression of these transporters is known to change under culture conditions [27]; however several recent studies have investigated the role of lactate and astrocytes *in vivo*. These experiments, including studies in ischemia [40], lactate utilization by functional imaging studies [41], and memory function [42,43], demonstrate that lactate is critical for neuronal energy supply *in vivo* and that neurodegeneration or neuronal dysfunction results from interfering with this pathway. In both studies of memory function, an important role for the astrocyte was indirectly implicated due to dependence on glycogen utilization, which is almost exclusively present within astrocytes in the CNS [44]. None of these studies *in vivo* proves, however, that the supply of lactate to neurons is directly from astrocytes, because none of the modifications was astrocyte specific. By combining results obtained from both astrocyte and oligodendroglial studies, it is possible that astrocytes transfer energy metabolites directly to oligodendroglia, which in turn supports neurons/axons.

Oligodendroglia make direct connections with astrocytes in the form of gap junctions (Figure 3). These gap junctions comprise two oligodendroglial proteins, connexin

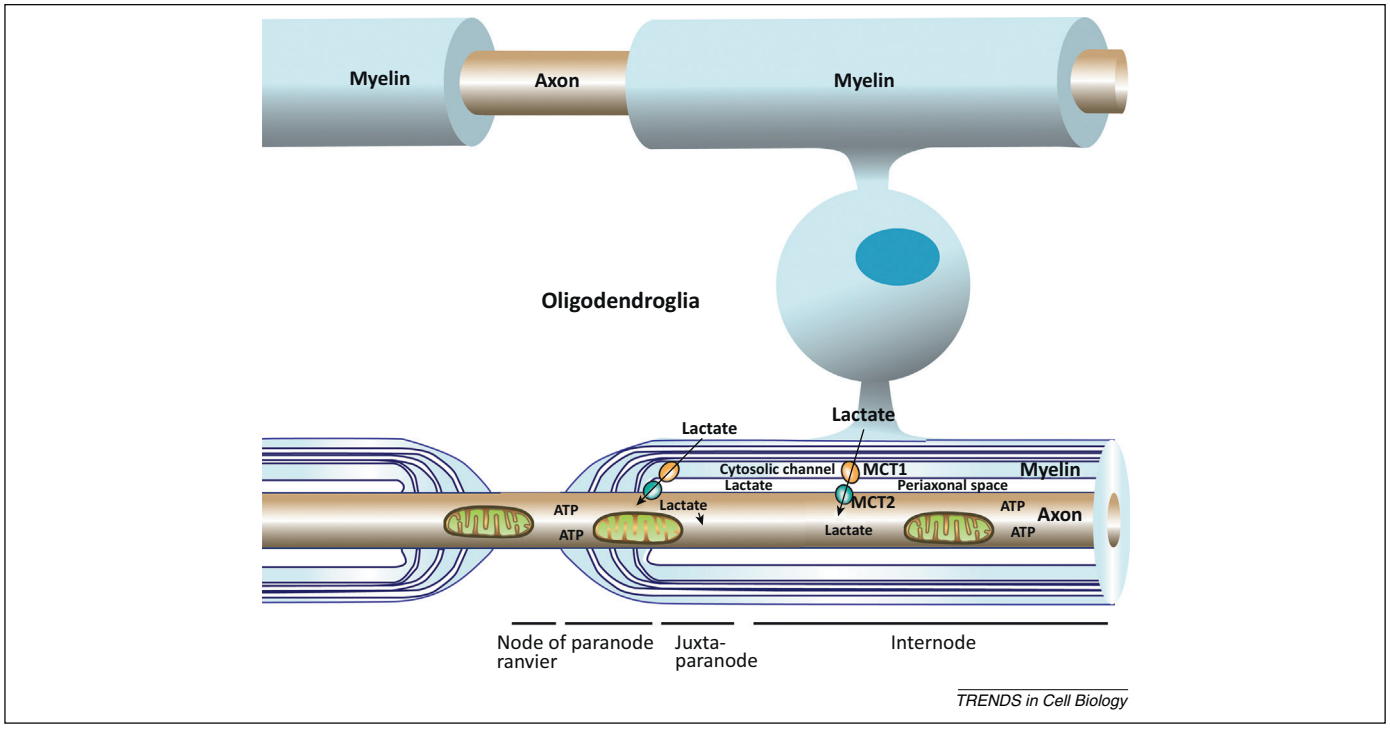

Figure 2. Schematic of oligodendroglia and axonal monocarboxylate transporters. Oligodendroglia transport lactate, or other monocarboxylates, to the periaxonal space through monocarboxylate transporter 1 (MCT1). From this space, lactate can be taken up into axons by MCT2, converted to pyruvate by lactate dehydrogenase, and imported into mitochondria for oxidative phosphorylation and the subsequent generation of ATP.

32 (Cx32) and 47 (Cx47), that form heteromeric channels with astrocyte connexin 30 (Cx30) and 43 (Cx43), respectively [45]. These connexins appear to be important for oligodendroglial (and probably Schwann cell) function because mutations of Cx32 produce Charcot–Marie–Tooth disease type 1X (CMT1X), an inherited peripheral neuropathy [46], and Cx47 produces Pelizaeus–Merzbacher-like disease (PMLD), a severe childhood-onset leukodystrophy characterized by nystagmus, ataxia, and spasticity [47]. Transgenic mice null for both Cx32 and Cx47 exhibit profound CNS demyelination, axonal injury, tremors, seizures, and premature death by 2 months of age [48]. In addition, Cx47 and Cx30 double null mice, in which gap junctions between oligodendroglia and astrocytes are effectively disconnected, also develop myelin pathology and motor impairments and die by 3 months of age [49]. Although the function of astrocyte–oligodendrocyte gap junctions is not well clarified, they are capable of transporting energy metabolites such as glucose [50] and presumably could also transport lactate. Although speculative at this point, transport of lactate from highly glycolytic astrocytes to oligodendroglia through gap junctions could provide some of the energy substrates shuttled into the periaxonal space by oligodendroglial MCT1. If demonstrated experimentally, this hypothesized metabolic connection between astrocytes, oligodendroglia, and axons would explain prior studies showing the critical nature of both astrocytes and oligodendroglia in the support of axons. Ultimately, these findings may help to support the astrocyte–neuron lactate shuttle model by extending it to include oligodendroglia as critical intermediaries for at least some of the lactate supply to neurons.

Directionality of lactate transport

The directionality of lactate transport through MCT1 in oligodendrocytes is critical for understanding their function. As importers of lactate, oligodendrocytes are likely to use lactate for their own energetic needs. If, indeed, they export lactate, they are likely to be supporting the metabolic needs of other cells. Determining the direction of transport *in vivo* is difficult experimentally. MCTs are bidirectional transporters, with the direction of transport being determined by the relative intracellular and extracellular concentrations of substrates (i.e., lactate and hydrogen ions). Thus far, lactate transport has been measured only *in vitro*, where directionality is determined by the components of the media. Although excellent *in vitro* tools for measuring lactate transport are available, there is no sensitive tool for measuring lactate transport *in vivo*. Nevertheless, several lines of indirect evidence support the conclusion that oligodendroglia are generally exporters, not importers, of lactate [27]. First, it was found that exogenous lactate completely prevented neuron loss in organotypic cultures produced by blocking oligodendroglia MCT1 transporters, presumably by substituting for the lactate unable to be released from oligodendroglia due to the MCT1 inhibitor [27]. Second, oligodendroglial death was not seen *in vitro* or *in vivo* after attenuation of MCT1 [27]. Third, MCT1 is predominantly localized to the myelin sheath around CNS axons, as would be expected for an exporter of lactate to axons, and not to the cell body [27]. Fourth, as described above, selective mitochondrial deficits in oligodendroglia that enhance lactate production within oligodendroglia lead to increased extracellular lactate when neuronal function is suppressed by an anesthetic [26]. Of course, lactate may also be imported into

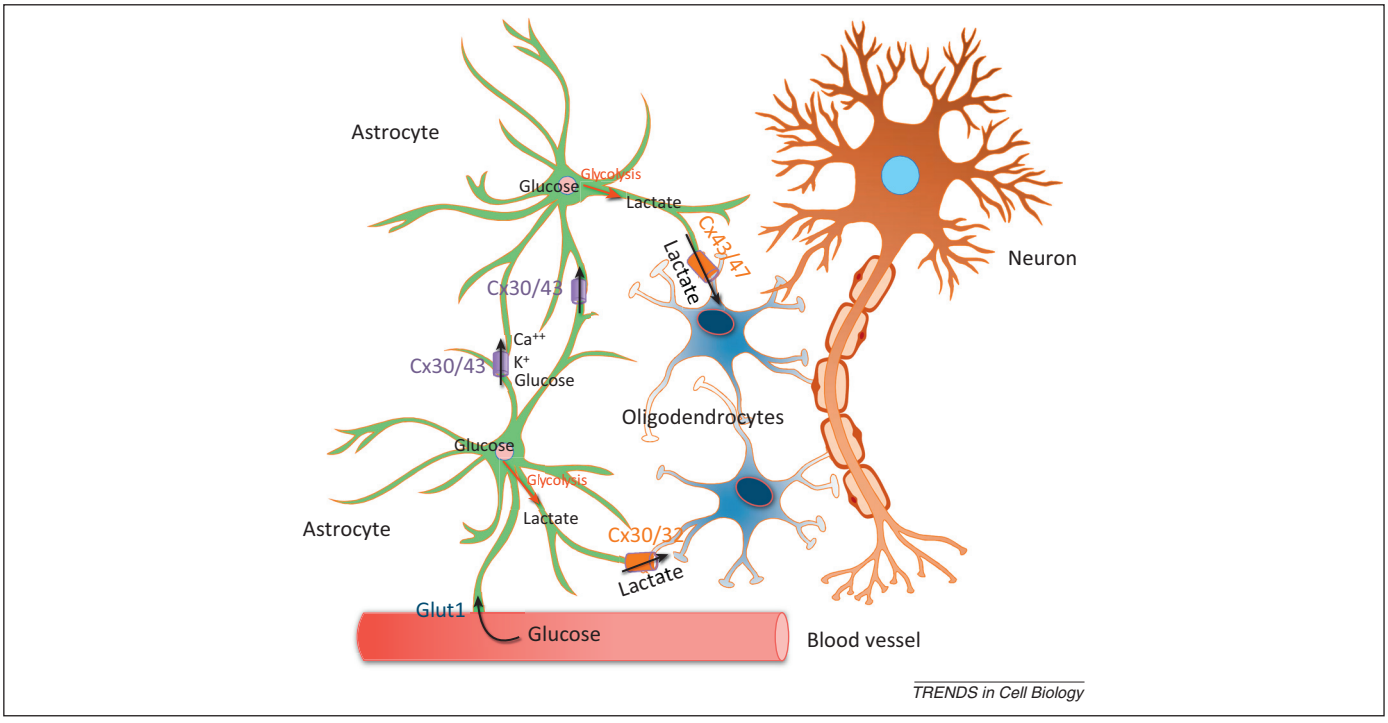

Figure 3. Astrocytes and oligodendroglia form a syncytium connected together by gap junctions formed by specific connexin molecules. Although just a hypothesis, lactate may transport from astrocytes to oligodendroglia through gap junctions before being used as axonal energy.

oligodendroglia, through MCT1 or another mechanism, and contribute to the production of myelin, as has been shown in dissociated [51] and cortical slice [31] cultures, but attenuation of MCT1 does not appear to cause neuron or axon degeneration through this mechanism.

Alternative oligodendroglia-based energy sources

The final issue raised by these studies is whether the energy metabolite transported by oligodendroglia MCT1 is lactate. Most of the discussion of alternative energy sources to glucose centers around lactate, but MCTs can also transport pyruvate and ketone bodies such as β-hydroxybutyrate and acetone. Indeed, ketone bodies and pyruvate can also be produced by astrocytes and thus contribute to the supply of energy to neurons (see [52] for a review). Ketone bodies are produced by astrocytes from fatty acids, particularly when glucose supply is limited, and can readily be used for energy by neurons. Ketone body production is dependent on the supply of fatty acids, not glycogen, and therefore is not responsible for glycogen-dependent memory function, as detailed previously [42,43]. Pyruvate could also function as an alternative source of energy in neurons. It is produced in the brain by astrocytes and, unlike ketone bodies, is a product of glycogenolysis. It can be rapidly utilized by neurons as an energy source *in vitro*, although a role *in vivo* remains to be shown. The disadvantage of pyruvate is not to neurons, but rather to the producing astrocyte. To perpetuate glycolysis, NAD^+ must be regenerated. In the setting of oxidative metabolism, this is accomplished by mitochondria; however, in nonoxidative metabolism, NADH is oxidized to NAD^+ as pyruvate is metabolized to lactate. Despite this, it is possible that astrocytes oxidize NADH by an alternative pathway and pyruvate may to some extent be an important energetic molecule in neurons. In summary, astrocytes are capable of producing numerous energy intermediaries that can be transported through MCTs and each may be used under different metabolic conditions. Blocking MCT1 reduces transport of all of these intermediaries and therefore does not delineate which are critical for support of axons.

Potential implications for disease

In addition to being critical for understanding basic cell biology, the recent discovery that oligodendroglia supply energy directly to axons through MCTs also has possible ramifications for human disease. Deficits in axonal energy, such as mitochondrial failure, have been implicated in Alzheimer's disease, Parkinson's disease, Huntington's disease, hereditary spastic paraplegia, and amyotrophic lateral sclerosis (ALS). All of these adult-onset neurodegenerative diseases demonstrate 'dying-back' neuropathy, suggesting early failure of axon function. In most of these diseases (or, more specifically, in cellular or animal models of these diseases), axon transport has been directly shown to be deficient, and in others axon pathology was prominent, indirectly implicating failure of axon transport (see [53] for a review). Although deficits in axon transport do not necessarily result from energy failure and could be due to damage to molecular motors, tubulin scaffolding, or other factors, it is intriguing that energy failure may play a role in this diverse group of diseases. Although general defects in axon transport or early pathology to axons indirectly implicates energy pathways in axons, there is more direct evidence for this role in ALS.

ALS is a progressive neurodegenerative disease characterized pathologically by the loss of both upper and lower motor neurons. Despite the importance of motor neuron

Box 2. Outstanding questions

- How do oligodendroglia obtain sufficient glucose and/or lactate for transport to axons?
- Does a connexin-based network of oligodendroglia and astroglia underlie this metabolic support?
- Are the MCT1 transporter in oligodendroglia (and other metabolic transporters) and the MCT2 transporter in axons concentrated to certain regions of the myelin sheath and axolemma (e.g., paranodal regions) where energy demands in the axon might be greatest?
- Are there ways to enhance MCT-based transport in oligodendroglia or axons that could be protective and thereby therapeutic?

loss to the development of symptoms, recent work has suggested that glia, including astrocytes, microglia, and, recently, oligodendroglia [54–56], contribute to the death of motor neurons. In two recent publications, oligodendroglia were found to degenerate in mutant SOD1 transgenic mice, a model of ALS, and although replaced by differentiation of oligodendroglial precursor cells (OPCs) appear to be dysfunctional [55,56]. Although the full scope of this dysfunction is unknown, oligodendroglia in the ventral spinal cord of SOD1 transgenic mice and in motor cortex from patients with ALS were both deficient in MCT1 [27]. Additionally, removing the toxic mutation in SOD1 from OPCs, and subsequently from newly generated oligodendroglia, resulted in marked attenuation of disease progression [56]. Given the deleterious effects of reducing oligodendroglial MCT1 on motor neurons [27], these results suggest that reduced expression of MCT1 in oligodendroglia is one mechanism contributing to motor neuron degeneration in ALS. Further work evaluating mechanisms to protect oligodendroglia or increase MCT1 transport activity in models of ALS should shed further light on the importance of oligodendroglial MCT1 in ALS.

Concluding remarks

Oligodendroglia have increasingly been recognized as important contributors to axon function and survival. Several human diseases of oligodendroglia produce axon injury, as do numerous mouse models, but until recently the mechanism by which oligodendroglia support axons was unknown. Recently published studies have shown that oligodendroglia express MCTs and disruption of these transporters leads to axon injury and neuronal death, suggesting that supply of energy metabolites to axons in the form of lactate (or possibly ketone bodies and pyruvate) is a critical function of oligodendroglia *in vivo*. Further work is necessary to determine whether oligodendroglia support axons through other mechanisms, as well as the importance of these transporters in diseases affecting oligodendroglia (Box 2).

References

1 Bargmann, C.I. and Marder, E. (2013) From the connectome to brain function. *Nat. Methods* 10, 483–490
2 Nave, K.A. (2010) Myelination and the trophic support of long axons. *Nat. Rev. Neurosci.* 11, 275–283
3 Dupree, J.L. *et al.* (1999) Axo-glial interactions regulate the localization of axonal paranodal proteins. *J. Cell Biol.* 147, 1145–1152
4 Nave, K.A. (2010) Myelination and support of axonal integrity by glia. *Nature* 468, 244–252
5 Stys, P.K. *et al.* (1991) Compound action potential of nerve recorded by suction electrode: a theoretical and experimental analysis. *Brain Res.* 546, 18–32
6 Wender, R. *et al.* (2000) Astrocytic glycogen influences axon function and survival during glucose deprivation in central white matter. *J. Neurosci.* 20, 6804–6810
7 Tekkok, S.B. *et al.* (2005) Transfer of glycogen-derived lactate from astrocytes to axons via specific monocarboxylate transporters supports mouse optic nerve activity. *J. Neurosci. Res.* 81, 644–652
8 Werner, H.B. *et al.* (2007) Proteolipid protein is required for transport of sirtuin 2 into CNS myelin. *J. Neurosci.* 27, 7717–7730
9 Sidman, R.L. *et al.* (1964) Mutant mice (quaking and jimpy) with deficient myelination in the central nervous system. *Science* 144, 309–311
10 Griffiths, I.R. *et al.* (1981) Shaking pups: a disorder of central myelination in the Spaniel dog. Part 1. Clinical, genetic and light-microscopical observations. *J. Neurol. Sci.* 50, 423–433
11 Schneider, A. *et al.* (1992) Uncoupling of hypomyelination and glial cell death by a mutation in the proteolipid protein gene. *Nature* 358, 758–761
12 Gotow, T. *et al.* (1999) Abnormal expression of neurofilament proteins in dysmyelinating axons located in the central nervous system of jimpy mutant mice. *Eur. J. Neurosci.* 11, 3893–3903
13 Al-Saktawi, K. *et al.* (2003) Genetic background determines phenotypic severity of the Plp rumpshaker mutation. *J. Neurosci. Res.* 72, 12–24
14 Mayer, J.A. *et al.* (2011) Characterization of a PLP-overexpressing transgenic rat, a model for the connatal form of Pelizaeus–Merzbacher disease. *Neurobiol. Dis.* 44, 231–238
15 Karim, S.A. *et al.* (2007) PLP overexpression perturbs myelin protein composition and myelination in a mouse model of Pelizaeus–Merzbacher disease. *Glia* 55, 341–351
16 Edgar, J.M. *et al.* (2010) Demyelination and axonal preservation in a transgenic mouse model of Pelizaeus–Merzbacher disease. *EMBO Mol. Med.* 2, 42–50
17 Edgar, J.M. *et al.* (2004) Oligodendroglial modulation of fast axonal transport in a mouse model of hereditary spastic paraplegia. *J. Cell Biol.* 166, 121–131
18 Griffiths, I. *et al.* (1998) Axonal swellings and degeneration in mice lacking the major proteolipid of myelin. *Science* 280, 1610–1613
19 Gravel, M. *et al.* (2009) 2′,3′-Cyclic nucleotide 3′-phosphodiesterase: a novel RNA-binding protein that inhibits protein synthesis. *J. Neurosci. Res.* 87, 1069–1079
20 Lappe-Siefke, C. *et al.* (2003) Disruption of Cnp1 uncouples oligodendroglial functions in axonal support and myelination. *Nat. Genet.* 33, 366–374
21 Rasband, M.N. *et al.* (2005) CNP is required for maintenance of axon-glia interactions at nodes of Ranvier in the CNS. *Glia* 50, 86–90
22 Edgar, J.M. *et al.* (2009) Early ultrastructural defects of axons and axon-glia junctions in mice lacking expression of Cnp1. *Glia* 57, 1815–1824
23 Pohl, H.B. *et al.* (2011) Genetically induced adult oligodendrocyte cell death is associated with poor myelin clearance, reduced remyelination, and axonal damage. *J. Neurosci.* 31, 1069–1080
24 Ghosh, A. *et al.* (2011) Targeted ablation of oligodendrocytes triggers axonal damage. *PLoS ONE* 6, e22735
25 Oluich, L.J. *et al.* (2012) Targeted ablation of oligodendrocytes induces axonal pathology independent of overt demyelination. *J. Neurosci.* 32, 8317–8330
26 Funfschilling, U. *et al.* (2012) Glycolytic oligodendrocytes maintain myelin and long-term axonal integrity. *Nature* 485, 517–521
27 Lee, Y. *et al.* (2012) Oligodendroglia metabolically support axons and contribute to neurodegeneration. *Nature* 487, 443–448
28 Nave, K.A. and Trapp, B.D. (2008) Axon-glial signaling and the glial support of axon function. *Annu. Rev. Neurosci.* 31, 535–561
29 Pierre, K. and Pellerin, L. (2005) Monocarboxylate transporters in the central nervous system: distribution, regulation and function. *J. Neurochem.* 94, 1–14
30 Garcia, C.K. *et al.* (1994) cDNA cloning of the human monocarboxylate transporter 1 and chromosomal localization of the SLC16A1 locus to 1p13.2-p12. *Genomics* 23, 500–503
31 Rinholm, J.E. *et al.* (2011) Regulation of oligodendrocyte development and myelination by glucose and lactate. *J. Neurosci.* 31, 538–548

32 Hanu, R. *et al.* (2000) Monocarboxylic acid transporters, MCT1 and MCT2, in cortical astrocytes in vitro and in vivo. *Am. J. Physiol. Cell Physiol.* 278, C921–C930
33 Pellerin, L. *et al.* (1998) Expression of monocarboxylate transporter mRNAs in mouse brain: support for a distinct role of lactate as an energy substrate for the neonatal vs. adult brain. *Proc. Natl. Acad. Sci. U.S.A.* 95, 3990–3995
34 Pellerin, L. *et al.* (1998) Evidence supporting the existence of an activity-dependent astrocyte–neuron lactate shuttle. *Dev. Neurosci.* 20, 291–299
35 Bergersen, L. *et al.* (2002) Immunogold cytochemistry identifies specialized membrane domains for monocarboxylate transport in the central nervous system. *Neurochem. Res.* 27, 89–96
36 Rafiki, A. *et al.* (2003) Highly differential expression of the monocarboxylate transporters MCT2 and MCT4 in the developing rat brain. *Neuroscience* 122, 677–688
37 Magistretti, P.J. and Pellerin, L. (2000) The astrocyte-mediated coupling between synaptic activity and energy metabolism operates through volume transmission. *Prog. Brain Res.* 125, 229–240
38 Belanger, M. *et al.* (2011) Brain energy metabolism: focus on astrocyte-neuron metabolic cooperation. *Cell Metab.* 14, 724–738
39 Pellerin, L. and Magistretti, P.J. (2012) Sweet sixteen for ANLS. *J. Cereb. Blood Flow Metab.* 32, 1152–1166
40 Schurr, A. *et al.* (2001) Blockade of lactate transport exacerbates delayed neuronal damage in a rat model of cerebral ischemia. *Brain Res.* 895, 268–272
41 Wyss, M.T. *et al.* (2011) In vivo evidence for lactate as a neuronal energy source. *J. Neurosci.* 31, 7477–7485
42 Suzuki, A. *et al.* (2011) Astrocyte–neuron lactate transport is required for long-term memory formation. *Cell* 144, 810–823
43 Newman, L.A. *et al.* (2011) Lactate produced by glycogenolysis in astrocytes regulates memory processing. *PLoS ONE* 6, e28427
44 Brown, A.M. *et al.* (2004) Energy transfer from astrocytes to axons: the role of CNS glycogen. *Neurochem. Int.* 45, 529–536
45 Orthmann-Murphy, J.L. *et al.* (2007) Two distinct heterotypic channels mediate gap junction coupling between astrocyte and oligodendrocyte connexins. *J. Neurosci.* 27, 13949–13957
46 Kleopa, K.A. and Scherer, S.S. (2006) Molecular genetics of X-linked Charcot–Marie–Tooth disease. *Neuromol. Med.* 8, 107–122
47 Uhlenberg, B. *et al.* (2004) Mutations in the gene encoding gap junction protein alpha 12 (connexin 46.6) cause Pelizaeus–Merzbacher-like disease. *Am. J. Hum. Genet.* 75, 251–260
48 Menichella, D.M. *et al.* (2003) Connexins are critical for normal myelination in the CNS. *J. Neurosci.* 23, 5963–5973
49 Tress, O. *et al.* (2012) Panglial gap junctional communication is essential for maintenance of myelin in the CNS. *J. Neurosci.* 32, 7499–7518
50 Rouach, N. *et al.* (2008) Astroglial metabolic networks sustain hippocampal synaptic transmission. *Science* 322, 1551–1555
51 Sanchez-Abarca, L.I. *et al.* (2001) Oligodendrocytes use lactate as a source of energy and as a precursor of lipids. *Glia* 36, 321–329
52 Guzmán, M. and Blázquez, C. (2004) Ketone body synthesis in the brain: possible neuroprotective effects. *Prostaglandins Leukot. Essent. Fatty Acids* 70, 287–292
53 Morfini, G.A. *et al.* (2009) Axonal transport defects in neurodegenerative diseases. *J. Neurosci.* 29, 12776–12786
54 Kang, S.H. *et al.* (2010) $NG2^+$ CNS glial progenitors remain committed to the oligodendrocyte lineage in postnatal life and following neurodegeneration. *Neuron* 68, 668–681
55 Philips, T. *et al.* (2013) Oligodendrocyte dysfunction in the pathogenesis of amyotrophic lateral sclerosis. *Brain* 136, 471–482
56 Kang, S.H. *et al.* (2013) Degeneration and impaired regeneration of gray matter oligodendrocytes in amyotrophic lateral sclerosis. *Nat. Neurosci.* 16, 571–579
57 Haines, J.D. *et al.* (2011) Axonal damage in multiple sclerosis. *Mt. Sinai J. Med.* 78, 231–243
58 Garbern, J.Y. *et al.* (2002) Patients lacking the major CNS myelin protein, proteolipid protein 1, develop length-dependent axonal degeneration in the absence of demyelination and inflammation. *Brain* 125, 551–561
59 Mar, S. and Noetzel, M. (2010) Axonal damage in leukodystrophies. *Pediatr. Neurol.* 42, 239–242
60 Hobson, G.M. and Garbern, J.Y. (2012) Pelizaeus–Merzbacher disease, Pelizaeus–Merzbacher-like disease 1, and related hypomyelinating disorders. *Semin. Neurol.* 32, 62–67
61 Abrams, C.K. and Scherer, S.S. (2012) Gap junctions in inherited human disorders of the central nervous system. *Biochim. Biophys. Acta* 1818, 2030–2047